Submission for the examination of PhD

Interactions between Activation and Repolarisation in Predisposition Towards Cardiac Arrhythmia

by

Malcolm Charles Finlay

B.A. (Oxon.) B.M. B.Ch., M.R.C.P.

University College London 2014

Declaration

I, Malcolm Charles Finlay confirm that the work presented in this thesis is my own. Where information has been derived from other sources, I confirm that this has been indicated in the thesis.

Abstract of Thesis

The lethal cardiac arrhythmias ventricular fibrillation (VF) and ventricular tachycardia (VT) are a leading cause of death in heart disease. We hypothesised that dynamic activation and repolarisation interactions will vary according to autonomic tone and the nature of the myocardial substrate as affected by disease states. This hypothesis was tested in a series of human and murine experiments.

Incorporation of data from human electrophysiological studies into a linear computer model was able to predict activation dynamics of sequential extrastimuli. This served as a validation of the concept of dynamic interactions between activation and repolarisation in man.

A human model of mental stress demonstrated that activation and repolarisation dynamics are altered by intrinsic autonomic stimulation. Specifically, a reduction in activation potential duration and an increase in dispersion of repolarisation occurred at short coupling intervals during stress. A weak increase in conduction velocity and excitability was also observed.

Patients with early-stage arrhythmogenic right ventricular cardiomyopathy (ARVC) were seen to exhibit conduction changes prior to the onset of structural disease. This was used to determine potential diagnostic criteria based on surface ECG correlates of intracardiac observations. These criteria are able to distinguish early ARVC from benign right ventricular outflow tract tachycardia.

Finally, the mechanism of modulation of tissue level activation dynamics were further studied using a novel thin-tissue slice murine model. Conduction velocity and excitability were modulated by both sympathetic and parasympathetic stimuli,

parasympathetic modulation is demonstrated to be dependent on the $G\alpha_{i2}$ regulatory pathway at the tissue level. The tissue slice method provides a novel tissue-level platform for the study of cardiac electrophysiology in genetically modified mice.

In conclusion, this work demonstrates that modulations of activation and repolarisation dynamics are seen in pro-arrhythmic states, specifically in sympathetically active states and in arrhythmogenic right ventricular cardiomyopathy.

Acknowledgements

My principal academic thanks for the completion of this project go to my primary supervisor, Pier Lambiase. He has been encouraging, supportive and a great mentor over my years as his student. Thanks also to Professor Andy Tinker, for welcoming me into the lab and introducing me to experimental bench work and animal studies. My gratitude also goes to Professor Taggart, it has been a privilege to work in the company of a giant of cardiac electrophysiology and I hope to be able to continue to contribute towards his body of work.

Thanks to Professor Schilling, Dr Simon Sporton and Dr Mark Earley, who stand out as true inspirations and mentors. Thank you for keeping me real. Also Prof McKenna, your support and encouragement lifted me through a difficult time and encouraged me to pursue the causes of arrhythmia. My humble gratitude also to the members of Pier's and Prof Tinker's group who have been so helpful, practically as well as intellectually: Justine Amato, Steve Harman, Muriel Nobles, Qadeer Aziz, Jem Lane, Lorna Forrest and Sonia Sebastian *et al*. *Merci* to my clinical and research electrophysiology colleagues, especially: Jack McCready, Ross Hunter, Richard Ang, Niall Campbell, Aaisha Opel, Vivienne Ezzatt, Gopi G, Matthew Lovell, Syed Ashan, Ed Duncan, Glyn Thomas and all the others too numerous to mention. Thank you to the clinical lab staff, without whom nothing would have been done.

I need to thank the engineers that have been such a help, support and good fun. Lei Xu, Michele Orini, Ben Hanson and Adrien Deschargens. Thanks. You were right. Matlab *is* awesome.

Thanks to the Wellcome Trust for believing in me and in my project.

Gràcies a Bet, la meva dona. Molts gràcies per tota la seva ajuda, l'amor i el support d'aquests anys. T'estimo per tot. Un peton molts molts grand. Thank you to my sons Tomas and Liam for not playing "delete everything" on my computer whilst I've been doing this. I'm the luckiest guy alive with the three of you.

Mum, Dad. To answer your question: *this* is what I've been doing on my computer. I love you both, thank you for everything. Sazzie!-) yeahyeahyeah!

Finally, Great-Uncle Alex. I finally have a Christmas present for you…

Dedication

In memory of Akhil, who let me go do EP.

Table of Contents

Table of Figures

Published Work derived from thesis

Pubmed-listed papers

Finlay, M.C., Xu, L., Taggart, P., Hanson, B. & Lambiase, P.D. (2013b) Bridging the gap between computation and clinical biology: validation of cable theory in humans. *Front Physiol*, **4**, 213.

Gomes, J., Finlay, M., Ahmed, A.K., Ciaccio, E.J., Asimaki, A., Saffitz, J.E., Quarta, G., Nobles, M., Syrris, P., Chaubey, S., McKenna, W.J., Tinker, A. & Lambiase, P.D. (2012) Electrophysiological abnormalities precede overt structural changes in arrhythmogenic right ventricular cardiomyopathy due to mutations in desmoplakin-A combined murine and human study. *Eur Heart J*, **33**, 1942-1953.

Papers in preparation

Finlay, M.C., Ahmed, A., Sugre, A., Bhar-Amato, J., Quarta, G., Pantazis, A., Ciaccio, E., Syrris, P., Ben-Simon, R., Chow, A., Lowe, M., Segal, O., McKenna,W., & Lambiase, P.D. Dynamic Activation and Repolarisation Differences in Early Arrhythmic Right Ventricular Cardiomyopathy Versus Benign Outflow Tract Tachycardia. *Accepted to PLOS One 2014.*

Finlay, M.C., Lambiase, P.D., Zisos, K., Ben-Simon, R., Xu, L. & Taggart, P. Pro-arrhythmic electrophysiological changes induced by conscious mental stress: first direct measurement in man. *In preparation*

Meeting Abstracts

Finlay M, B Lim, J McCready, L Xu, S Ahsan, A Gopalamurugan, A Chow, M Lowe, O Segal, E Rowland, & Lambiase, P.D. (2012) When is an electrogram fractionated?: Inconsistencies between automated algorithms in the identification of fractionation. (Abstracts from the 2012 Boston AF Symposium). *Journal of Cardiovascular Electrophysiology*, **23**, 677-686.

Finlay, M.C., Ahmed, A., Barr-Amato, J., Butcher, C., Segal, X.J., O., Lowe, M., Simon, R., Chow, A., McKenna, W., Pantazis, A. & Lambiase, P.D. (2011) Dynamic conduction and repolarization changes can help distinguish between arrhythmic right ventricular cardiomyopathy and benign right ventricular outflow tract tachycardia MODERATED POSTERS, SESSION 2, HRC 2011. *Europace*, **13**, iv16-iv19.

Finlay, M.C., Lambiase, P.D., Zisos, K., Ben-Simon, R., Xu, L. & Taggart, P. (2012) Pro-arrhythmic electrophysiological changes induced by conscious mental stress: first direct measurement in man; ABSTRACTS FOR ORAL PRESENTATION, SESSION 1. *Europace*, **14**, iv4-iv8.

Finlay, M.C., Xu, L., Nobles, M., Lane, J., Lowe, M., Ben-Simon, R., Bhar-Amato, J., Hussain, Q., Sebastian, S., Taggart, P., Tinker, A. & Lambiase, P.D. (2013a) Effects of mental stress on cardiac electrophysiology: a parallel human & murine study POSTER SESSION 2, HRC 2013. *Europace*, **15**, iv31-iv35.

Malcolm Finlay, Ahmed, A., Alan Sugre, Justine Bhar-Amato, Giovanni Quarta, Antonis Pantazis, Edward Ciaccio, Petros Syrris, Ron Ben-Simon, Anthony Chow, Martin Lowe, Oliver Segal, William McKenna, & Lambiase, P.D. (2012a) Differentiation Of Concealed Arrhythmogenic Right Ventricular Cardiomyopathy From

Benign Right Ventricular Outflow Tract Ectopy- From Endocardial Mapping To Dynamic Surface ECG Markers. *J Interv Card Electrophysiol*, **36**,

Finlay, M.C., Ahmed, A., Barr-Amato, J., Quarta, G., Xu, L, Ben-Simon, R., Segal, O., Lowe, M., McKenna, W., Chow, A., & Lambiase, P.D. (2012b) Dynamic Changes In Activation And Repolarisation Distinguish Early Arrhythmic Right Ventricular Cardiomyopathy From Benign Outflow Tract Tachycardia: Insights From Non-contact Mapping And Computational Analysis. *Heart rhythm : the official journal of the Heart Rhythm Society Heart rhythm : the official journal of the Heart Rhythm Society Heart Rhythm*, **9**, S292-S328.

Bhar-Amato, J., Jie, X., Finlay, M., Chaubey, S., Xu, L., Nunn, L., Chow, A., Segal, O., Simon, R., Lowe, M., Rowland, E. & Lambiase, P. (2012) Autonomic modulation in brugada syndrome: mapping conduction and repolarisation changes in the epicardium and endocardium (YOUNG INVESTIGATORS COMPETITION). *Europace*, **14**, iv1-iv3.

C Butcher, M. Finlay, WL Yao, M Lowe, O Segal, R Ben-Simon, E Rowland, A Chow, P Lambiase (2011) Long-term follow up post-elective, outflow tract ventricular tachycardia ectopy ablation. (ECAS 2011 Special Issue). *J Interv Card Electrophysiol,* **30**, 87-198.

Chapter 1 Introduction

1.1 General Introduction

Cardiac arrhythmia claims over 70,000 lives per year in the UK, and roughly 300,000 in the USA. The majority of these deaths are due to ventricular fibrillation (VF) or ventricular tachycardia (VT) (Papadakis et al., 2009; Zheng et al., 2001), the majority of which occur in the context of acute cardiac ischemia. A smaller proportion are as a result of inherited conditions, which can occur in people seemingly in peak physical condition. The death of an athlete or young person from cardiac arrhythmia carries an impact over and above that conveyed by mortality statistics alone.

Acute treatments for fibrillation exist. Direct current cardioversion is highly effective at restoring normal cardiac rhythm, and the introduction of the implantable cardioverter-defibrillator (ICD) stands as one of the major advances in clinical cardiology over the last 30 years (Moss et al., 1996; AVID investigators, 1997; Buxton et al., 1999; Moss et al., 2002). Medical treatments aiming to prevent the occurrence of ventricular arrhythmia have been universally disappointing however. Both the CAST trial (Moss et al., 1998) and the SWORD trial (Waldo et al., 1996) were stopped early after interim analyses showed excess of deaths in the antiarrhythmic assignment. Similarly, the sudden cardiac death in heart failure (SCD-HeFT) trial showed amiodarone to be equivalent to placebo and inferior to ICD therapy in preventing death for patients with heart failure (Bardy et al., 2005). Only beta-receptor blockade has shown a defined benefit in preventing sudden death in randomized clinical trials (Hjalmarson et al., 2000). These findings highlight our lack of understanding of the mechanism and causes of ventricular arrhythmias.

The increased appreciation of severe complications associated with long term ICD implantation, i.e. device infection (Tolosana et al., 2009; Moore et al., 2009) and

inappropriate therapy delivery (Sakhuja et al., 2009; Duncan et al., 2010), brings the imperfections in our assessments of patient risk into focus. Risk stratification tools developed to predict a cardiac electrical event have resorted to using a general assessment of contractile function (left ventricular ejection fraction) as the best predictor of arrhythmic risk, well illustrated by the multicentre automated defibrillator implantation trial (MADIT, Moss et al., 1996). Direct, patient specific investigation of cardiac electrophysiology has generally been disappointing in aiding this risk stratification, and this paradox underlines the lack of understanding of the genesis of ventricular arrhythmia in clinical practice (Cutler and Rosenbaum, 2009; Selvaraj et al., 2007; Gold et al., 2008). Specifically, the VT stimulation study has been shown repeatedly to have little or no useful clinical role in clinical risk stratification (Moss et al., 1996; Buxton et al., 1999).

Although a number of surface markers have been proposed, it appears that dynamic markers of electrical function show the greatest promise for risk stratification. This indicates that interrogation of conduction and repolarisation kinetics is likely to yield predictive arrhythmic markers (Verrier et al., 2011). Recent work from André Ng's group in Leicester has highlighted dynamic changes in the paced ECG as a predictor of VT risk in patients with cardioverter defibrillators who underwent electrophysiological studies (Nicolson et al., 2012). Such work demonstrates the importance of dynamically induced heterogeneities in cardiac electrophysiology in arrhythmogenisis, and could be a clinically useful approach to risk stratification in patients at risk of cardiac arrhythmia. Further validation of this specific test is required in larger prospective cohorts before its adoption into clinical use. A more fundamental assessment of what this index actually represents at the myocardial tissue substrate level is also required.

The classic understanding of arrhythmia generation first arose from the work of Mines, who established the concept of re-entry as the basis of cardiac arrhythmia (Mines, 1914). A century of investigation has expanded on potential mechanisms of arrhythmia to describe in detail triggered activity and the various manifestations of circus movement re-entry, including spiral rotors, figure-of-eight re-entry and leading circle re-entry, where no anatomical boundary was required for arrhythmia to manifest.

Such basic and theoretical studies have provided a wealth of data indicating mechanisms by which a stable cardiac conduction can degenerate into the self-perpetuating & chaotic rhythm of VF (Watanabe et al., 2001; Pastore et al., 1999, Circulation, 99, 1385-1394). These generally involve the interplay of two conditions: a change in the cycle length or coupling interval of cardiac activation, and heterogeneity in the electrophysiological properties of the conducting tissue (Gilmour et al., 2007). Though a large body of work has concentrated on the ability of sustained, raised heart rates, to induce unstable beat-to-beat variations in repolarisation times (T-wave alternans), the common clinical observation is that of only one or two extrasystoles as the trigger of ventricular arrhythmias. Common to both of these modes of arrhythmia induction is the concept of interactions between activation and repolarisation, which may ultimately lead to block of a wave of activation when that activation wave impinges on the repolarisation of a previous beat (Bernus et al., 2002; Zaitsev et al., 2003). This mechanism of "functional block" can cause the transition from orderly activation to chaotic re-entry, the hallmark of VF (Chow et al., 2004). The process of functional block disturbing a homogeneous conduction wavefront is termed *wavebreak* and is discussed in detail below.

There remains a gap in understanding between basic cellular electrophysiology and the clinical phenomena of cardiac arrhythmia (Pandit, 2010). A particular question exists as to the temporal promotion of clinical arrhythmia, i.e. why should an individual develop a specific arrhythmia at a particular time? In some cases a systemic upset can be pinpointed as being responsible for predilection to arrhythmia e.g. thyroid dysfunction, drug treatment or myocardial ischaemia. In many clinical arrhythmias no specific major structural or functional change is ever identified coincident with the onset of arrhythmia. This can be highlighted in the occurrence of inherited arrhythmia syndromes. Individuals may carry a propensity to arrhythmia throughout their entire childhood and early adult life, yet this only becomes manifest at a specific time. e.g. J-point elevation before onset of VF in early repolarisation syndromes.

The autonomic nervous system is a prime suspect in the transient changes of the excitable properties of cardiac tissue accounting for the apparent randomness of events. Detailing how it may modulate activation and repolarisation properties (thereby promoting or supressing clinical arrhythmia) is a key challenge of arrhythmia research. The autonomic effects of mental stress on cardiac electrophysiology are discussed in detail later in this chapter.

The presented work attempts to translate basic measurements of cardiac electrophysiology to clinical arrhythmias, concentrating on tissue-level electrophysiology of the heart.

1.2 Chapter Aims

Cardiac electrophysiology and arrhythmia must be understood in context. In this chapter the basic tenants of cardiac electrophysiology will be introduced, and activation and repolarisation interactions reviewed with emphasis on their dynamics and modulation. Furthermore, the concepts of mental stress provoked arrhythmia and arrhythmogenic right ventricular cardiomyopathy will be presented as potential pro-arrhythmic states.

1.3 Normal cardiac electrophysiology

The cardiac action potential, first described in the 1880s (Burdon-Sanderson, 1880), is fundamental for our understanding of the electrical function of the heart. Its distinctive spike-and-plateau shape implies its function; the sharp activation allowing rapid conduction and activation, the lengthy plateau activating intracellular calcium release, which in turn allows contraction of cardiac muscle (Grant, 2009). The ionic basis of the cardiac action potential was first described in the seminal work of Hodgkin and Huxley, and a basic model has been refined over decades to include a multitude of channels (Noble, 1962; Noble, 2007). Nonetheless, an appreciation of a simple model of the cardiac action potential is an important pre-requisite for further detailed appreciation of cell-to-cell, tissue and organ functioning.

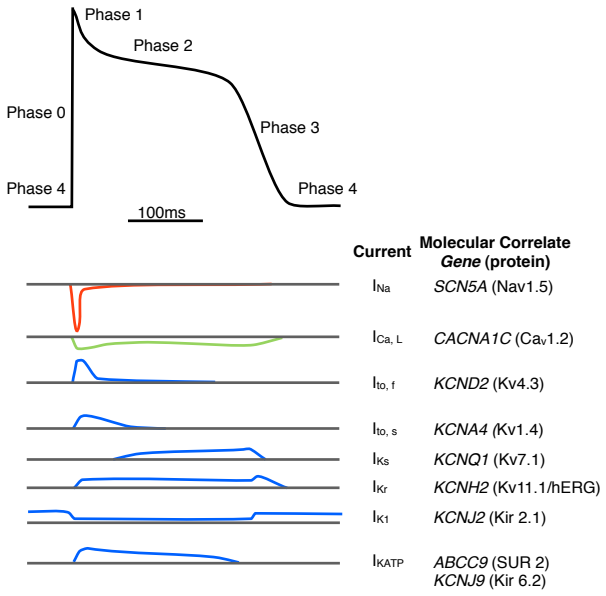

Figure 1-1 Currents contributing to the normal cardiac ventricular action potential in humans

Currents are shown with their molecular correlates. Red indicates sodium current, green calcium and blue potassium currents. There is a far greater heterogeneity in repolarising currents than in depolarising or plateau currents. Molecular correlates are given as: principal gene (principal pore forming protein (Redrawn and adapted from Pond and Nerbonne, 2001; Gray et al., 2013).

The ionic currents and their molecular correlates are summarised in Figure 1-1. In the resting, non-exited, state, the cardiac cell membrane maintains a voltage gradient of around -70mV by actions of the Na^+-K^+ and Na^+-Ca^{++} ion exchange currents (Pond and Narbonne, 2001). A minor depolarization of the membrane triggers a rapid depolarization of the cardiac cell. This depolarization (phase 0) of the cardiac action potential is governed by the fast sodium current, flowing through the Nav1.5 voltage-gated sodium channel. A rapid influx of Na^+ ions arrives into the cell down a steep concentration gradient, causing membrane depolarization, and subsequent hyperpolarization to around +20mV. The rapid increase in sodium concentration in turn produces conformational change on sarcolemmal calcium channels and allows calcium release into the cell. The rising intracellular calcium concentration itself further triggers opening of calcium channels on the sarcoplasmic reticulum. This positive feedback loop is termed calcium-induced calcium release.

The continued rise in the intracellular calcium concentration is maintained for up to 200ms and is responsible for the continued depolarization of the cardiac cell. The opening of slowly activating outward potassium currents allows membrane repolarisation and restoration of the resting membrane potential. This restoration of the membrane potential signals the end of cellular refractoriness, and the cell will once again respond to electrical stimuli (Pond and Nerbonne, 2001; Noble, 2007). Stimuli occurring prior to the full restoration of the resting membrane potential may still excite an action potential, but increasingly greater stimuli are required. Eventually a prematurity occurs where absolute refractoriness is reached.

This general and simplistic model of cardiac cellular electrophysiology serves as an introduction to the ionic model of cardiac cellular activation. The action potential

varies between species, between cardiac chambers and is even distinct between cell layers in vitro (though the *in-vivo* significance of this can be debated). Importantly, the profile of the cardiac action potential is dynamic. Variations in ionic currents causing changes in action potential morphology. The action potential can thus be changed not only by extreme insults, such as cellular ischemia or disturbances in cellular ionic environment, but also by physiological changes, such as autonomic tone and cardiac rate (Kuo and Surawicz, 1976).

The very specific adaptation to heart rate by cardiac cells is termed "restitution" (Elzinga et al., 1981), and deserves detailed consideration.

1.4 Cardiac Action Potential Duration (APD) Restitution, adaptation and conduction velocity restitution

The cardiac action potential tends to shorten in response to a decrease in coupling interval of successive beats. Specifically, action potential duration (APD) restitution can be defined as a shortening of the APD in response to a decrease in the diastolic interval (DI) preceding that activation. A slower rate-dependence shortening, termed adaptation, may occur as a steady state cycle length is reduced (Taggart et al., 2003). The functional effects of APD restitution and adaptation can be discussed in terms of molecular mechanisms, arrhythmic (or anti-arrhythmic) effects and functional adjustment of the myocyte to increases in heart rate. Furthermore, slowing of conduction velocities occurs at very short diastolic intervals, observed in response to short coupling intervals (Figure 1-2).

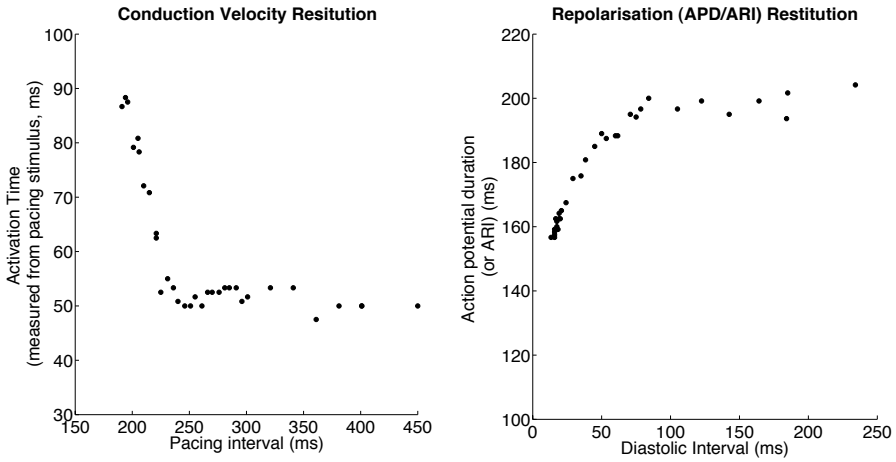

Figure 1-2 Conduction velocity restitution and Action Potential Resitution

Typical activation time and action potential duration (APD) responses to decreases in coupling interval are shown. APD responses are conventionally displayed as a function of local diastolic interval (i.e. time since repolarisation of prior excitation), whereas activation time responses are best displayed as a function of pacing interval (a.k.a. coupling interval, stimulus interval). The activation repolarisation interval (ARI, time between local activation and local repolarisation determined from the unipolar electrogram) is often used as a surrogate for APD.

1.4.1 The molecular basis of APD restitution and adaptation

Initially APD restitution was described in isolated cat papillary muscle (Moore et al., 1965), followed by dog (Toyoshima et al., 1981), guinea pig (Laurita et al., 1996), mouse and human cardiac tissue. The ionic basis of cardiac restitution has been determined from experimental and computational studies, principally in guinea pig and canine myocytes, and human cellular computation models. At long coupling intervals, the majority of respolaristaion currents are through the IKr channel. The I_{Ks} (slow inward rectifying potassium) current appears to contribute very little to the repolarisation time course in the resting state at slow heart rates but its contribution increases at higher rates.

Markov modelling has revealed how the I_{Ks} channel may contribute to cardiac restitution and adaptation (Silva and Rudy, 2005, Decker et al., 2009). I_{Ks} consists of four pore forming KCNQ1 subunits, which associate with the KCNE single transmemrane regulatory unit. Each of these subunits can exist in an active, inactive or deep-inactive state, thus a total of 17 different channel states can exist. The transition from a deep-inactive to inactive state is slow, whereas the time course of opening from an inactive state is rapid. Zones can be grouped into two inactive zones depending whether a voltage sensor exists in the deep-inactive state, as well as the channel open zone. In Zone 2, at least one channel subunit must transfer to the inactive state from the deep-inactive to allow channel opening to occur, whereas in Zone 1 all voltage sensors are in the inactive state. Thus a channel in Zone 1 is able to rapidly open, whereas those in Zone 2 have to make at least one slow voltage sensor to transition to an inactive state before they are able to open.

This provides an elegant model of how the contribution of IKs to repolarisation can increase at short coupling intervals. During adaptation (i.e. at sustained short coupling intervals), there is accumulation of channels in Zone 1. As these are able to rapidly open, a "repolarisation reserve" of channels in state Zone 1 builds up, and the action potential shortens.

Action potential restitution can be seen as being due to a similar, albeit transient, increase in I_{Ks} at short coupling intervals. At long coupling intervals, almost all I_{Ks} channels exist in the deep inactive state at the start of the action potential. I_{Ks} will transition to the inactive state with each action potential, but the long diastolic intervaI between activations allows the channels to fall back to the deep inactive state. I_{Ks} thus contributes very little to the overall repolarisation current in the long steady state. A close-coupled S_2 beat will activate the cell prior to the full transition of I_{Ks} to deep-inactive Zone 2 states, the proportion of channels in Zone 1 will still be elevated as a consequence of the previous activation. The more premature the S_2, the greater the proportion of channels available in Zone 1 to rapidly open, and hence the greater the contribution to repolarisation from I_{Ks}. The net consequence is a greater repolarising current and a shorter action potential.

A “repolarisation reserve” becomes present as the cell membrane returns to the resting potential, ensuring an action potential arising after a subsequent premature stimulation will be shorter than one at steady state (Figure 1-3; Silva and Rudy, 2005).

Accomodation may be seen as a separate but related phenomenon. It is observed that action potential duration does not reach a steady state following a change in constant pacing cycle length immediately, but requires several minutes before stabilisation. This phenomenon has not been fully explored at the molecular level, but changes in

intracellular ionic concentrations, particularly of intracellular Na^+, may play a key role. At short constant diastolic intervals, the Na^+-Ca^{++} exchanger is unable to extrude all the Ca^{2+} entering the cytoplasm through the L-type calcium channel. Steady-state low intracellular Ca^{2+} is not preserved, and increasing intracellular Ca^{2+} directly inhibits the L-type calcium channel by Ca^{2+}-dependent inactivation. This prevents further increase of intracellular Ca^{2+} and Ca^{2+} efflux through the Na^+-Ca^{++} exchanger acting in forward-mode, is increased.

There is a consequent increase in intracellular Na^+. As a result, the Na^+-K^+ exchanger is unable to extrude all the intracellular Na^+ entering the cell during phase 0 of the action potential. The secondary effects on intracellular Na^+ from increasing intracellular Ca^{2+} compound this & the combined result is an increase in intracellular Na^+. Such an increase in intracellular sodium ions in turn promotes an increase in repolarising Na^+-K^+ exchange currents, shortening the action potential and shifting the restitution curve to shorter APDs (Silva and Rudy, 2005). Furthermore, a shift in the steady state equilibrium of rectifying potassium channels, including I_{Ks} and I_{Kr}, is predicted to occur, allowing a shorter action potential to persist (O'Hara et al., 2011).

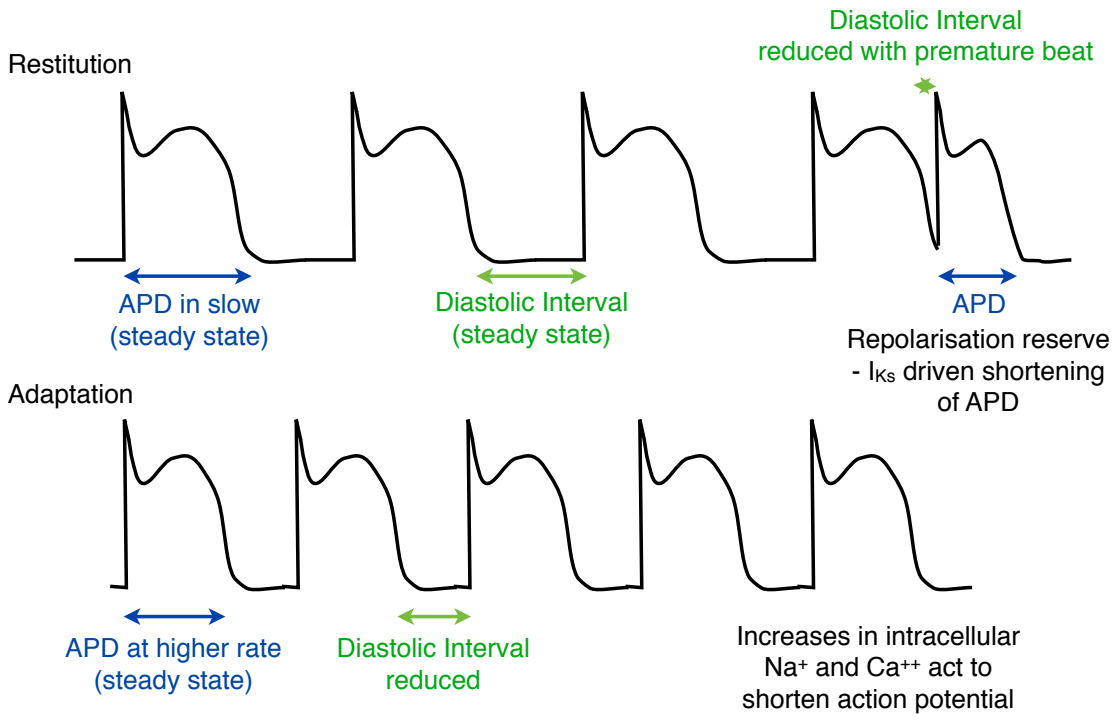

Figure 1-3 Restitution and Adaptation

A schematic illustration of action potential restitution and adaptation is shown. In restitution, a reduction in the diastolic interval results in a change in the APD of the subsequent activation. Adaptation can be represented as a steady state phenomenon, where increases in intracellular sodium and calcium ions act to shorten the action potential.

1.4.2 Wavebreak and the generation of cardiac arrhythmia

The genesis of re-entrant chaotic cardiac arrhythmia (in contrast to spontaneous focal arrhythmia e.g. ventricular ectopy) can be understood through the concept of *wavebreak* (Weiss et al., 2005). Cardiac excitation can be considered as a wave of excitation proceeding through tissue, the wavefront corresponding to the upstroke of the cardiac action potential and the waveback to repolarisation. As the wave of excitation propagates through cardiac tissue, the wavefront and waveback never come into contact under normal circumstances. However, tissue heterogeneity (either functional or fixed) can allow the wavefront of one wave to touch the waveback of the preceding wave, the so-called “wavebreak”. If the entire excitation wave is thus extinguished, no arrhythmia

will occur. On the other hand if the wavebreak is localised, a wavefront of excitation can curl around the loose end of the wavebreak and re-enter previously excited, but now no longer refractory, tissue (Cabo et al., 1994). The point at which this occurs can signify either an anatomical obstacle (e.g. scar) or functional heterogeneity in the tissue. This re-entry in normal tissue is termed a *rotor*. Alessi and colleagues first described these rotors as spiral waves in atrial tissue (Allessie et al., 1973), 3D scroll waves were later demonstrated in fibrillating ventricular tissue (Davidenko et al., 1992).

The wavebreak as an index event in the onset of fibrillation is generally accepted, but the mechanisms of maintenance of fibrillation remain contentious. The mother rotor hypothesis places a circus re-entry principal spiral or scroll wave as the driving phenomena in fibrillation, with subsequent wavebreaks occurring as epiphenomena in regions unable to support rapid activations from the principal rotor. An alternative interpretation is termed the multiple wavelet hypothesis, where on going wavebreaks continue to drive chaotic fibrillatory activity.

Both of these interpretations of arrhythmia require heterogeneity in cardiac electrophysiology in order to establish, either a fixed or functional (induced) heterogeneity.

1.4.3 Cardiac restitution and arrhythmia

Initially electrical restitution was described as being important in governing the contractile force generated following a premature beat (Kruta and Braveny, 1963). Interest in restitution properties grew as it became apparent that restitution could also be critical in explaining induction of heterogeneity in tissue that appeared homogenous during steady state activation. One manifestation of this is the conversion from stable to unstable APD alternans at short coupling intervals (Weiss et al., 2005). Indeed, half a

century ago, Nolasco and Dahlen proposed a theoretical model predicting that APD restitution slopes of >1 would produce unstable responses to rapid cardiac stimuli, cumulating in APD alternans (Nolasco and Dahlen, 1968). This concept has been further refined via mathematical biodomain models, in one and two dimensions (Clayton and Taggart, 2005). Even heterogeneity in restitution properties alone has been shown to be sufficient to enable fibrillation to be induced by 2 premature stimuli, at least in theoretical models (Clayton and Taggart, 2005). Restitution properties became an attractive site for targeting pharmaceutical agents, and Garfinkel and colleagues showed that flattening the APD restitution curve with bretylium suppressed spiral wave break up and prevented VF in an animal model (Weiss et al., 2002).

But the measurement of APD restitution slope as a lone measure for risk prediction has been singularly unsuccessful, some recent data in animal models even points to steeper APD restitution in hearts resistant to VF induction (Osadchii et al., 2010). Little has been published linking the extensive theoretical and basic understanding of restitution to VF induction in the clinical context, despite extensive theoretical investigations into the mechanisms of ventricular fibrillation (Lambiase et al., 2009; Chow et al., 2004).

Of course, the fact that discrepancies exist in the understanding of relationships between restitution (a cellular-level phenomenon) and risk of fibrillation (a tissue-level phenomenon) can be understood as cardiac cells do not exist in isolation, but within their tissue and organ: each cell is connected to its neighbours both structurally and electrically. The principal intra-cellular structural connection is the desmosome, a transmembrane multipler of proteins, which enables strong anchoring of intracellular structural components with those of the neighbouring cell (Gallicano et al., 1998; Saffitz et al., 2010). Closely associated with this are the freely porous gap junctions, so called because of their distinctive electron-microscopic appearance. These junctions

consist of hexamers of connexon proteins, allowing the unimpeded passage of small ions, and hence electrical signalling and the action potential, from cell to cell. Indeed, so closely are the gap-junctions and the desmosome thought to associate, that the concept of a connexosome has arisen. Likewise, recent evidence suggests that ion-channels, particularly the Nav1.5 channel, is also associated with this membrane multipler and the interactions between the different membrane constituents may be functionally relevant (Rizzo et al., 2012). Whatever the exact interactions on the atomic scale, though, it is apparent that the intracellular connections in the normal myocardium allow exquisite coupling of the cellular components to form a functional tissue syncytium.

It is tempting to assume that conduction velocity through such syncytial tissue would be dictated principally by cell-coupling (King et al., 2012). If this were the case, marked reductions in connexin expression would be expected to markedly reduce conduction velocity. This does not appear to be true, indeed marked conduction slowing only becomes apparent if connexin levels are reduced >90% in the murine heart (van Rijen et al., 2004). However, reductions in sodium channel function do significantly reduce conduction velocities, both in experimental models (Stein et al., 2011) and in disease of the sodium channel (such as Brugada syndrome, Lambiase et al., 2009). Furthermore, interactions between the sodium channel and Cx43 exist, these interactions may account for conduction velocity reductions in very low-levels of Cx43 (Jansen et al., 2012). Action potential propagation along the cell membranes in a continuous manner, more than conduction from cell to cell, would thus appear to be the key determinant of cardiac conduction velocity (King et al., 2013).

1.4.4 Conduction Velocity Restitution

Many theoretical assessments of reentry with VF induction assume a homogeneous conduction velocity (CV) in tissue (Xie et al., 2004; Paz et al., 2006; Gilmour et al., 2007; ten Tusscher and Panfilov, 2006). Yet the key electrophysiological phenomena associated with clinical and experimental arrhythmogenisis, be it organized or chaotic, is that of slow conduction. Conduction velocity also undergoes restitution at short coupling intervals. Termed CV restitution (but previously a.k.a. / analogous to: dispersion curve, activation restitution), this is only apparent at much shorter coupling intervals than APD restitution. Relatively little direct data exist on the contribution of CV restitution to induction of arrhythmia, and its manifestations have been overlooked in many theoretical models. Nonetheless, we can hypothesise several ionic and cellular mechanisms by which conduction velocity may be decreased at very short coupling intervals.

As is seen in APD restitution, at short DIs, intracellular Na^+ increases as a result of inadequate extrusion via the Na^+-K^+ exchanger and as a sequelae of intracellular Ca^{2+} increase. At very short coupling intervals, intracellular Na^+ could be high enough to reduce the velocity of the action potential upstroke by reducing the transmembrane Na^+ gradient and thereby slow conduction velocity. Sodium channels exists in several states, Markov models predict that at short coupling intervals fewer of them will have cycled through the conformational changes necessary to return them to a resting state. Thus at short DIs, membrane sodium channel availability will be reduced (O'Hara et al., 2011).

Locational cycling of channels and pores may also contribute to conduction slowing at short diastolic intervals. Though active at the cell membrane, the Nav1.5 protein and the Connexin proteins exist in a state of equilibrium with subcellular apparatus (Hallaq et al., 2006). It is possible, but as yet unproven, that altering the membrane locational

equilibrium of either of these proteins will reduce cellular conductivity or excitability.

1.5 The autonomic nervous system and cardiac electrophysiology

Powerful direct and indirect evidence points to the role of modulation of autonomic tone in arrhythmogenisis, and the effects of the autonomic nervous system on cardiac conduction. The reduction of cardiac arrhythmic death by beta-blockade during myocardial infarction (MI) is the most widely known of these data, and is best illustrated by the one-third risk-reduction in arrhythmic death in MI patients who were taking a beta-blocker in the CAST trial (Moss et al., 1989). Similarly, a significantly decreased mortality was observed in those patients taking beta-blockers in the Multicenter Unsustained Tachycardia Trial (MUST, Buxton et al., 1999) and in the Metoprolol CR/XL Randomised Intervention Trial in Congestive Heart Failure (MERIT-HF, Hjalmarson et al., 2000). Despite the concerns that a treatment bias may confound some beta-blockade trial results (beta-blockade may have been withheld from some of the sickest patients over fears regarding their modest negative-inotropic effects), pharmacological inhibition of cardiac beta-receptors is a mainstay of current antiarrhythmic therapy (Zipes et al., 2006; Ellison, 2002).

The multi-tiered contribution of autonomic tone to cardiac arrhythmia onset is illustrated by numerous striking observations of increased arrhythmia frequency coincident with major psychological stress. These include earthquakes (Voridis et al., 1983; Trichopoulos et al., 1983; Leor et al., 1996; Lampert et al., 2000; Huang et al., 2001), missile (or threatened missile) attack (Meisel et al., 1991) and in the 9-11 World Trade Centre attacks (Shedd et al., 2004, Steinberg et al. 2004). Eye-catching associations have also been made with the phenomenon of voodoo death (Samuels, 2007; Lester, 2009) and as an explanation for increased arrhythmic events during world

cup football supporters (Wilbert-Lampen et al., 2008). More controlled data have showed ICD shocks to be associated with mental stress (Lampert et al., 2005).

Controlled laboratory experiments have solidified these associations. This work has been pioneered by Lampert and coworkers at Yale, Connecticut. In a series of elegant studies, mental stress was induced using a standardized series of psychometric tests, including mental arithmetic (reverse serial sevens with harsh encouragement) and anger recall (Lampert et al., 1994; Lampert et al., 2000; Lampert et al., 2002; Stopper et al., 2007; Lampert et al., 2007; Lampert et al., 2009; Lampert, 2010; Abisse et al., 2011). This series of works has examined the physiological effects on the 12-lead ECG and T-wave in particular of patients at risk of arrhythmia. Furthermore, they have documented increased frequencies of ICD discharges/therapies during periods of intense stress in ischaemic heart disease patients (e.g. Steinberg et al., 2004). A history of stressful life events prolonged mental stress has also been associated with arrhythmia burden in Long-QT syndrome patients (Hintsa et al., 2010). Previous works have also documented increased arrhythmogenicity in animal models during induced stress (Verrier & Lown, 1984; Lown, 1977, 1978, Parker et al., 1987, Parker et al., 1990).

The effects of sympathomimetic agents on direct cardiac electrophysiology have been investigated. The principal effects of sympathetic stimulation by pharmacological intervention include a reduction in action potential duration and steepening of the APD restitution curve. This has been observed in both animal and human studies (Taggart et al., 2009; Taggart et al., 2003; Ng et al., 2007; Mantravadi et al., 2007). Animal work has also described cardiac electrophysiological effects of direct vagal stimulation, notably the reduction in arrhythmic thresholds during parasympathetic stimulation (e.g. Myers et al., 1974).

Direct experimental evidence derived from human work has been limited, though. It has been hypothesized that mental stress can contribute to arrhythmia by increasing heterogeneities of repolarisation and activation (or conduction velocity) throughout the heart (Kop et al., 2004; Toivonen et al., 1997; Kovach et al., 2001). These effects may thus amplify pre-existing heterogeneity, for example, due to ischemic heart disease or cardiomyopathy. But it is important to note that these observations have been derived from the surface electrocardiogram, rather than action potential or electrogram measurements. Few descriptions of the electrophysiological effects of intrinsic autonomic stimulation exist at the cardiac tissue level in humans.

Mental stress induced arrhythmia is not a simple case of increased sympathetic drive. Rather, the sympathetic and parasympathetic axes appear to work in unison to optimise physiology to the perceived requirements of both bodily homeostasis and higher-level neuronal inputs.

1.5.1 Autonomic effects on cellular electrophysiology

It is clear then that the autonomic nervous system has critical modulatory effects on cardiac electrophysiology. The consequences of sympathetic stimulation on cellular repolarisation have been extensively described (e.g. van der Hayden et al. 2005). In the ventricle, sympathetic stimulation predominantly acts via the β_1 receptor. This seven-transmembrane domain G-protein coupled receptor protein exerts its affects via the $G\alpha_s$ subunit's activation of adenyl-cyclase. The subsequent rise in intracellular cyclic adenosine monophosphate (cAMP) enables cAMP-dependent Protein Kinase A (PKA), which exerts intracellular effect via a multitude of phosphorylation events. Furthermore, resulting increases in calcium transients can increase Calmodulin Protein Kinase 2 (CaMKII) activity, and a direct mechanism in its upregulation may also be active but

this is controversial (Grimm and Brown, 2010). Downstream consequences of phosphorylation events include increasing the calcium transients that underpin the sympathetic inotropic response. The shortening of the action potential and the steepening of the APD restitution curve observed with sympathetic can be principally explained by an increase in I_{Ks}, phosphorylation of the KCNQ1 protein (at position Ser27), leading to current upregulation (Kurowara et al., 2009; Silva and Rudy, 2005).

The sympathetic effects on conduction are less well characterised. Only a single study has examined the effects of isoprenaline on conduction velocities, canine Purkinje fibres were isolated and conduction velocities measured in this pseudo-1D-model (Cragun et al., 1997). Sympathomimetic stimulation increased the conduction velocity and excitability of this tissue.

On the other hand, a large body of work has examined calcium-driven excitability in response to sympathetic stimulation. This has predominantly concentrated on examination of calcium related phenomena of automaticity, sparks and after depolarisations (Pogwizd et al., 2001; Desantiago et al., 2012; Myles et al., 2012).

Several major questions remain regarding the mechanisms of autonomic-promoted arrhythmias, particular in the mechanistic translation of known cellular phenomena to clinical arrhythmia. There has not been a description of differential regional responses to autonomic stimulation; indeed even the differences between atria and ventricle in electrophysiological responses to autonomic stimulation are not fully described. The extent to which laboratory-observed cellular phenomena act in the *in vivo* human heart have not been established, nor has there been a convincing connection between cellular phenomena and the development of clinical arrhythmia.

1.6 Electrophysiology-based risk prediction

Attempts at establishing effective clinical risk prediction for cardiac ventricular arrhythmias based on electrical criteria have met with limited success. Early descriptions of the benefits of ventricular stimulation protocols at risk stratification have not been substantiated in the contemporary era (Wellens et al.,1972; Grimm et al., 1998). The transient effects of the autonomic nervous system on cardiac electrophysiology is well established, and a wealth of evidence connects the development of VF with raised sympathetic tone in ischaemic heart disease, and increased parasympathetic tone in several inherited cardiac arrhythmias (Lampert et al., 2000; Rashba et al., 2002; Hintsa et al., 2010; Volders et al., 2010). Variations in autonomic tone thus appear critical in providing the milieu in which an arrhythmia may occur, and the artificial environment in which VT stimulation protocols have traditionally occurred (i.e. in the catheter laboratory under conscious sedation) would be expected to be significantly different from that occurring in everyday life.

Another postulated reason for failure of risk stratification is the reliance of the surface 12-lead ECG for establishing normality of cardiac conduction, yet the dynamic nature of ECG abnormalities has been established in observational studies (Quarta et al., 2010; Sy et al., 2011; Schwartz and Crotti, 2011; Antzelevitch and Yan, 2010). Examination of the underlying cardiac electrophysiology of such conditions with invasive techniques may reveal marked abnormalities of electrophysiological behaviour that are not apparent at rest. In these cases, such patients may never even have been recruited into studies assessing more complex risk predictive strategies.

Several endeavours at risk stratification have used more subtle and elegant assessments of cardiac electrophysiology, aiming for a continuous risk stratification rather than

binary outcome. Samaurez developed an invasive technique by which fractionation of electrograms during pacing was assessed (Saumarez et al., 1995b; Saumarez et al., 1995a; Saumarez and Grace, 2000; Saumarez et al., 2003; Saumarez, 2009). Unlike the VT stimulation protocol, the responses to premature stimuli over several cardiac sites were assessed in a continuous manner. Both fractionation and electrogram delay were assessed, and a computerized algorithm was used to define a measure to be compared to cutoff. This was shown to be predictive of future cardiac arrhythmia events in a population with hypertrophic cardiomyopathy. This technique was assessed in a randomized trial, and appeared to show efficacy in risk prediction (Saumarez et al., 2008). The conclusions from this trial were disputed, however, as this technique failed to match more conservative, non-invasive, risk predictors and was underpowered for sudden death events (Elliott and Spiro, 2009).

Microvolt T-wave alternans testing refers to a beat-to-beat variation in T-wave amplitude during cardiac exercise testing. T-wave alternans has been observed to occur more frequently in patients at risk of cardiac ventricular arrhythmia in several key studies (Bloomfield et al., 2004; Paz et al., 2006; Gold et al., 2008; van der Avoort et al., 2009; Costantini et al., 2009). However, a consensus has not been reached on how T-wave alternans testing should be used in clinical risk stratification (Cutler et al., 2009).

The most common risk-stratification tool employed in clinical practice involves both an assessment of ventricular function and observation of the resting ECG. A combination of abnormal ventricular conduction (usually a reduced LV ejection fraction measured by echocardiography) and conduction disturbance (a prolonged QRS duration) has been shown to be associated with a markedly increased risk of sudden cardiac death. These criteria (supported by numerous clinical trials e.g. Bardy et al., 2005; Moss et al., 2002; Moss et al., 1996) have formed the basis of primary-prevention ICD implantation

guidelines worldwide (Epistein et al., 2008). But this strategy remains far from perfect; the majority of patients who will be eligible for ICD implantation under these criteria do not have their lives saved by their implant. Similarly, when absolute numbers are considered, many more patients who fall outside of these guidelines will die of ventricular arrhythmia than those included (Al-Khatib et al., 2011).

It is incorrect to dismiss the low ejection fraction as a purely empirical marker of arrhythmic risk; several mechanistic strands can link poorly functioning muscle with predisposition to arrhythmia (reviewed in Nattel et al. 2009). First, myocardial scar and fibrosis reduce pump function and form lines of conduction block that can act as substrate for re-entrant arrhythmia. Second, calcium handling is known to be impaired in adaptations to heart failure. This can be either as a primary or secondary phenomenon, and lead to further decreased calcium sensitivity of tissues and increased calcium transients. Third, heart failure is associated with a breakdown in the syncytial conductive nature of heart muscle. Increased anisotropy and preferential conduction slowing may be a powerful substrate for arrhythmia.

With the exception of epinephrine testing for Long QT syndrome (Vyas et al., 2006), none of the clinically employed arrhythmia-risk strategies routinely take changes in electrophysiology during autonomic stress into account during their assessment. This is perhaps unsurprising; there is little contemporary data regarding underlying *in vivo* electrophysiological changes that may be induced by autonomic stimuli, and detailed *in vivo* electrophysiological responses to non-pharmacological autonomic stimuli have not been studied. Yet the increased susceptibility to arrhythmia during autonomic stress is well recognised, and is used as a routine clinical tool in the electrophysiology laboratory to promote arrhythmia (Brownstein et al., 1998).

1.7 One dimensional modelling incorporating CV restitution

A further step is required to complete the translation of basic understanding of dynamic activation/repolarisation interactions to clinical arrhythmia, i.e. the tissue characteristics and consequences of modulation of these responses must be defined. The development of complex computational models has enabled tissue-level sequelae to be examined in situations where experimental validation or measurement may be very difficult.

The contribution of CV restitution to instabilities in cardiac conduction was first explored following Alain Vinet's theoretical questioning: *"Imagine this hypothetical experiment: A circulating wave of excitation is set up in a thin ring of tissue. As time passes you reduce very slowly the length of the ring. Which kind of dynamic will you observe: a) if the excitable tissue is nerve-like (no electrical restitution, i.e. APD is constant); and b) if the excitable tissue is cardiac-like (electrical restitution present)?"* (Gilmour and Chialvo, 1999). This line of reasoning cumulated in Courtemanche's (1993) theoretical assertion whereby the effect of CV restitution was included in a linear-ring model predicting instabilities resulting from CV/APD restitution interactions.

Further progress on examining the electrical properties via a single-fibre model was made by the groups of Fenton, Cherry, Gilmour, Garfinkle and Weiss over the subsequent decades (Watanabe et al., 2001; Cherry and Fenton, 2004; Cherry and Fenton, 2007; Fenton et al., 2009; Weiss et al., 2010). Much of this has centred on the assertion that functional block is a necessary condition, but not necessarily sufficient, for chaotic re-entry and the initiation of VF to occur (Weiss et al., 2000; Qu et al., 2000b; Garfinkel et al., 2000; Qu et al., 2000a; Xie et al., 2002; Weiss et al., 2002). Otani and Fox developed this framework to demonstrate that functional block can occur through heterogeneities induced by sequential extrastimuli in otherwise homogeneous

tissue (Fox et al., 2003; Otani, 2007; Gilmour et al., 2007; Siso-Nadal et al., 2008). This work provided an avenue by which these theoretical models could be tested *in vivo*. The validation work of Gelzer and colleagues (2008) incorporated data from canine myocardial restitution into a single-fibre model, and used this model to predict whether or not VF would be induced with a series of long-short coupling interval extrastimuli. Here, a head-meets-tail phenomenon causing function block was taken to be a surrogate of the first stage of wavebreak. It was assumed that if functional block occured, a reentrant (and chaotic) arrhythmia (i.e. VF) would follow. This work was repeated in a canine cardiomyopathy model with success, implying relevance to human disease (Gelzer et al., 2011).

It is tempting to postulate that an application of Gelzer's technique to patients could aid risk stratification, an *in silico* assessment of cardiac arrhythmic risk could be performed based on patient-specific electrophysiological data. This is a proposition that will be examined in this thesis.

1.8 Arrhythmogenic cardiomyopathy as an example of electrical phenotype

Our discussions regarding the generation of arrhythmia have focused on the interactions between activation and repolarisation, particular the dynamic interactions that may lead to wavefront collision, wavebreak and ventricular arrhythmia. The most common underlying cause of arrhythmia in human ventricles is myocardial ischemia, which remains an important public health problem. It is relatively straightforward to explain the onset of arrhythmia in the ischaemic myocardium by virtue of the large heterogeneities in conduction and repolarisation induced; this would clearly form substrate for arrhythmogenisis (Gilmour et al., 2007; Coronel et al., 2009).

Still, several important conditions are also associated with life-threatening arrhythmias without such overt structural disease. These include Brugada syndrome, the association of abnormal surface ECG patterns (saddle-shaped ST elevation in the precordial chest leads) with ventricular arrhythmia, and arrhythmogenic right ventricular cardiomyopathy. Our group has extensively studied Brugada syndrome. Slow conduction, particularly in the right ventricle and right ventricular outflow tract has been shown to be present and represents a clear substrate for arrhythmia (Lambiase et al., 2009; Morita et al., 2008).

Arrhythmogenic right ventricular cardiomyopathy has emerged over the last 20 years as an important cause of sudden arrhythmic death, and is the commonest cause of sudden deaths in competitive athletes in Italy. It was first characterized in the later stages of disease, where the hallmark of fibrofatty replacement of cardiomyocytes in the right ventricle is established (Marcus et al., 2010). Yet it is increasingly recognised that

ventricular arrhythmia can be the initial presentation, manifesting as sudden death in the absence of significant structural heart disease (Thiene et al., 1988a). Recent advances in genetics have established ARVC as a disease of cardiac cell adhesion; mutations in desmosomal proteins are primarily associated with the condition. To date, mutations in seven desmosomal and five extra-desmosomal proteins have been described (Basso et al., 2012, Table 1-1). Interestingly, the extra-desmosomal mutations appear to have distinct phenotypes. Diagnosis of ARVC remains complex, partially because of the subtly of early phenotypes.

Recently, consensus diagnostic criteria have been updated and modified (Marcus et al., 2010). A major change has been the inclusion of new genetic markers of disease. These enable confirmation of diagnosis more frequently, and even in the absence of structural disease. Patients who have confirmed ARVC but who lack major structural features of the condition present an ideal opportunity to study activation and repolarisation dynamics in people at risk of arrhythmia.

Benign right ventricular outflow tract tachycardia or ectopy (benign RVOT ectopy) is a benign condition characterized by frequent unifocal ectopic beats arising from the right ventricular outflow tract in the absence of structural heart disease. This condition is difficult to differentiate from the early stages of ARVC, yet patients have ostensibly structurally normal hearts and it is clear they do not develop progressive ventricular disease (Morady et al., 1990; Tsai et al., 1997). We thus have two conditions that are overtly very similar, both with ventricular ectopy as a major feature, but patients with ARVC appear at increased risk of arrhythmic death. We hypothesized that investigation of activation repolarisation interactions would enable differentiation of these conditions,

and may explain increased arrhythmogenicity in patients with ARVC as opposed to benign RVOT ectopy.

Reference	Gene	Chromosome locus	Protein	Mode of inheritance	Comment
Desmosomal genes					
McKoy et al. (2000)	JUP	17q21	Junction plakoglobin	AR*	Cardiocutaneous syndrome
Asimaki et al. (2007)	JUP	17q21	Junction plakoglobin	AD	None
Norgett et al. (2000)	DSP	6p24	Desmoplakin	AR‡	Cardiocutaneous syndrome
Rampazzo et al. (2002)	DSP	6p24	Desmoplakin	AD	None
Gerull et al. (2004)	PKP2	12p11	Plakophilin-2	AD, AR	None
Pilichou et al. (2006)	DSG2	18q12	Desmoglein-2	AD	None
Syrris et al. (2006b)	DSC2	18q12	Desmocollin-2	AD, AR	None
Extradesmosomal genes					
Tiso et al. (2001)	RYR2	1q42–q43	Ryanodine receptor 2	AD	CPVT (AC phenocopy)
Beffagna et al. (2005)	TGF B3	14q23–q24	Transforming growth factor β3	AD	Pathogenic or modifier?
Merner et al. (2008)	TMEM43	3p25	Transmembrane protein 43 (protein LUMA)	AD	None
van Tintelen et al. (2009)	DES	2q35	Desmin	AD	Overlap syndrome (DC and HC phenotype, early conduction disease)
Taylor et al. (2011)	TTN	2q31	Titin	AD	Overlap syndrome (early conduction disease, AF)

Table 1-1 Genes associated with ARVC

Genes currently known to be associated with ARVC are shown. *Naxos disease. ‡Carvajal disease. Abbreviations: AC, arrhythmogenic cardiomyopathy; AD, autosomal dominant; AF, atrial fibrillation; AR, autosomal recessive; CPVT, catecholaminergic polymorphic ventricular tachycardia; DC, dilated cardiomyopathy; HC, hypertrophic cardiomyopathy. Adapted from (Basso et al., 2012).

1.9 Conclusion and Key hypotheses

1.9.1 Conclusion

Cardiac risk prediction is currently imperfect, and a great deal of this can be subscribed to our incomplete understanding of basic mechanisms of arrhythmia, particularly at a tissue level.

A major determinant of the unpredictability of arrhythmia initiation appears to be autonomic tone, which has defined effects on cardiac cellular repolarisation. Other abnormalities may exist in patients with predispositions to ventricular arrhythmia. In early ARVC, where sympathetic stimulation is associated with arrhythmia in patients with otherwise structural hearts, the dynamics of repolarisation may be significantly different from normal individuals.

1.9.2 Hypothesis

This work addresses the following major hypothesis:

Modulation of dynamic activation and repolarisation interactions varies according to the level autonomic tone (parasympathetic/sympathetic balance) and the nature of the myocardial substrate.

This hypothesis has been addressed by a series of experiments on conscious humans and murine cardiac tissue. Signal analysis techniques have been developed in order to acquire and analyse recorded data. One-dimensional cell-fibre models have been used to allow further understanding of observed phenomena, and as a validation of experimental techniques and measurements. The normal human electrophysiological responses to conscious stimuli (mental stress) are defined. A murine cardiac tissue slice

technique was developed in order to investigate the relative contribution of the sympathetic and parasympathetic stimuli to stress-induced arrhythmias. Finally, these concepts have been applied to a disease-condition characterised by predisposition to ventricular arrhythmia (early ARVC), and contrasted this to both normal patients and patients with benign right ventricular outflow tract ectopy.

This thesis will detail:

- Principal signal analysis methods,
- Activation-repolarisation interaction measurements in humans,
- Modelling of activation-repolarisation interactions based on human endocardial recordings
- Modulation of dynamic activation-repolarisation by mental stress
- Activation-repolarisation interaction in disease,
- Surface ECG correlates of intracardiac activation-repolarisation interactions
- Examination of intracellular mechanisms by which modulation of dynamic activation-repolarisation may occur

Chapter 2 Methods

2.1 Cardiac signal analysis

2.1.1 Introduction

Any investigation into cardiac electrophysiology relies on the measurement of electrical potentials from the cardiac tissue. Though it is possible to directly measure the cardiac action potential from single cells *in vitro* by means of a sharp electrode (the cellular patch clamp), this technique is not possible with current technology *in vivo*. *In vivo* cardiac electrophysiology thus relies upon measurement of extracellular potentials. Potential differences are measured between two electrodes. Both electrodes may contact with cardiac tissue, the bipolar signal thus generated is referred to as the *biopolar electrogram*. This is often used in clinical cardiac electrophysiology coupled with high-pass filtering, as it gives a clear inscription of local activation timing as an activation wavefront passes across the electrodes. The *unipolar electrogram* refers to a signal produced where only one of the poles is in contact with cardiac tissue, the reference anode is either distant (e.g. in the inferior vena cava) or is a mathematical mean of surface potentials acquired from the ECG limb leads (Wilsons' central terminal) (Potse et al., 2009). The unipole thus actually represents a widely-spaced bipole, but with only the cathode in contact with cardiac tissue.

The cardiac unipolar EGM is infrequently used in clinical electrophysiology as analysis of timepoints relating to local phenomena are less easily discernable than in the bipolar electrogram. Less filtering is usually applied to unipolar signals, enabling a clear T-wave to be visualized. The unipolar EGM thus has an advantage of potentially allowing both local activation and repolarisation timings to be determined.

Theoretical work provides clear assessments of how local activation can be related to the unipolar EGM (Wyatt RF, 1981; Steinhaus, 1989; Haws and Lux, 1990). As a

cardiac wavefront approaches and passes a cathode electrode, that electrodes potential will undergo a very rapid change. But as the cathode is referenced to a distant anode, the summed result is that the greatest negative change in cardiac potential occurs as the wavefront passes. This can be expressed mathematically as:

Local activation time = dV/dT_{min}

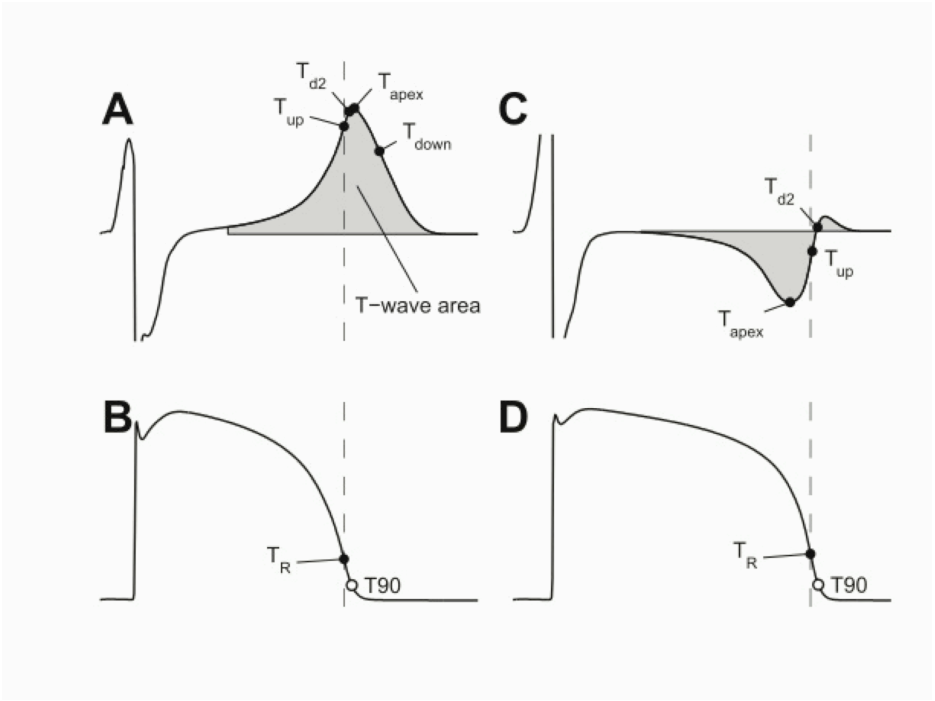

Figure 2-1 The relation of the Unipolar T-wave to the underlying action potential

The unipolar T-wave (A & C) can be related to the underlying action potential (B & D) in early (A & B) and late (C & D) activating sites. Several different differential points have been examined theoretically, T_{up} , the sharpest upstroke of the T-wave, provides a good approximation of APD_{90} the end of the action potential.

This theory is well validated in both theoretical and biological models as well as in clinical practice (Potse et al., 2009). The assessment of a precise local activation time to the intracardiac electrode gives a theoretical advantage over the bipolar EGM, though providing an easy-to-interpret visual signal, the precise onset of activation is harder to pinpoint, as deflection in the signal is seen with any potential difference between the two electrodes.

More controversial is the assessment of local repolarisation time with the unipolar electrogram. The unipolar T-wave relates to the repolarisation phase of the cardiac action potential. Its interpretation is harder and less clear-cut than that of the activation inflection. The unipolar T-wave represents a lower frequency phenomenon and the instantaneous local repolarisation current is thus small. When this is superimposed onto the far-field electrogram (representing repolarisation of the entire heart) interpretation can be challenging. However, it is generally accepted that the best approximation to the local repolarisation time is given by the most positive upstroke of the T-wave (Figure 2-1, Potse et al., 2007).

This has been validated against the "gold standard" for measurement of intracardiac action potentials, the sharp monophasic action-potential (MAP) catheter (Franz et al., 1987). It is worthwhile considering the technique of action potential recording in-vivo. The MAP electrode (also known as a Franz catheter) uses a sharp central electrode as a reference anode surrounded by a ring cathode. An injury current, i.e. a fixed cell depolarization, is created when the catheter is pressed against the myocardial wall, and the potential difference between this and the surrounding tissue allows a waveform similar to a transmembrane action potential to be visualized. Unlike the action potential of Hodgkin and Huxley (which describes the action potential across a membrane of a single cell), this waveform is created by the summed potentials of the extracellular field of a small area of tissue referenced against an "intracardiac" potential, which appears as a fixed potential reference. From this AP waveform it is easy to determine both activation and repolarisation timings. But several practical considerations are serious drawbacks to the routine employment of this technique in intracardiac investigations.

- Only single point APs can be acquired with this catheter. Separate catheters are required if APs are to be assessed simultaneously at multiple sites.

- The signals achieved are highly dependent on pressure applied, and the resulting waveforms are transient. This is due to the tissue damage caused by the sharp anodal electrode. Initially a robust injury current is obtained, but after several minutes these currents equalize and the AP wans. AP-type signals can be restored by application of transient further pressure to the catheter. This causes further tissue injury and restores a fixed electrical reference. But the transitory nature of directly acquired AP signals reduces the utility of these catheters for acquisition of APs under varying conditions.
- The Franz catheters themselves are difficult to obtain, and we have found them unwieldy in clinical use. Although no complications from their use have been reported, the sharp electrode certainly has the potential to cause cardiac perforation. This adds to the reticence regarding their employment for research, the caution they entreat further reduces the chances of completing data acquisition during research involving a clinical case.

These shortcomings of the MAP technique inspired efforts in derivation of local repolarisation times from unipolar electrograms (Wyatt RF, 1981). Again, initially derived from theory but later validated in vivo, the Wyatt or classical technique essentially takes the same theory used for determining the activation time, i.e. the rate of change of electrical potentials being greatest as a repolarisation passes the cathode (Potse et al., 2007; Potse et al., 2009). As the potential change during repolarisation is reversed though, the most positive differential of the repolarisation wave is taken as the point of local repolarisation i.e. dV/dT_{max}.

This technique has been put under intense scrutiny, with validation for contact measurements both in mathematical, in-vivo and extensively in-vitro (Yue et al., 2004; Yue, 2006; Yue, 2007). The derivation of repolarisation times from unipolar

measurements is very much more convenient in the clinical setting than using MAP catheter recordings. Multiple electrode sites can be recorded simultaneously, and unipolar EGMs are stable over time thus allowing recordings under different conditions can be compared to one another. Unipolar EGMs can be derived from almost any standard clinical electrophysiological catheter. The most appropriate catheter for each patient and recording site can be chosen allowing a high success in recording from targeted sites.

As with any indirect technique, there remain some weaknesses associated with derivation of timings of activation and repolarisation from the unipolar EGM. Foremost, the repolarisation time is highly correlated to the dV/dT_{max} of the unipolar T wave. Yet repolarisation time tends to be underestimated if the t-wave is positive. Thus the activation-repolarisation index (ARI), for the positive T-wave tends to be slightly shorter than the action-potential duration (APD), measured from the action potential upstroke of phase 0 to 90% repolarisation voltage (APD_{90}). The negative T-wave appears unaffected by this phenomenon, thus any comparisons between ARIs derived from unipolar EGMs with different T-wave morphology should be accompanied by an in-depth appreciation of this snag. Nonetheless, as long as T-wave morphology remains constant, changes and relative changes between electrograms can reasonably be compared.

We used unfiltered, unipolar signals for clinical data acquisition during our clinical work.

2.1.2 Signal analysis

Large quantities of data were acquired during clinical studies. Each patient typically had around 30 electrodes from which data was analysed for activation and repolarisation

times following each paced drive train and premature stimulus. It was immediately apparent that semi-automated software was a requirement for data processing.

A series of customized software scripts was written to run within Matlab (The Mathworks Inc., MA, USA). These allowed a multi-staged workflow (Figure 2-2) :

- Import of electrogram data from ASCII format, and display
- Automatic recognition of paced stimuli, and calculation of exact stimuli timing
- Automatic selection of penultimate drive train and premature stimuli, and export of these electrogram segments for further analysis
- Analysis of selected segments for activation time, repolarisation time and electrogram morphology (according to the classical (Wyatt) method)
- Review of all raw electrogram data, checking for outliers, erroneous calculations and allowing manual override correction of misallocated points.
- Export of data to a standardized format that could be further analysed statistically with other scripts or other software packages (e.g. R).

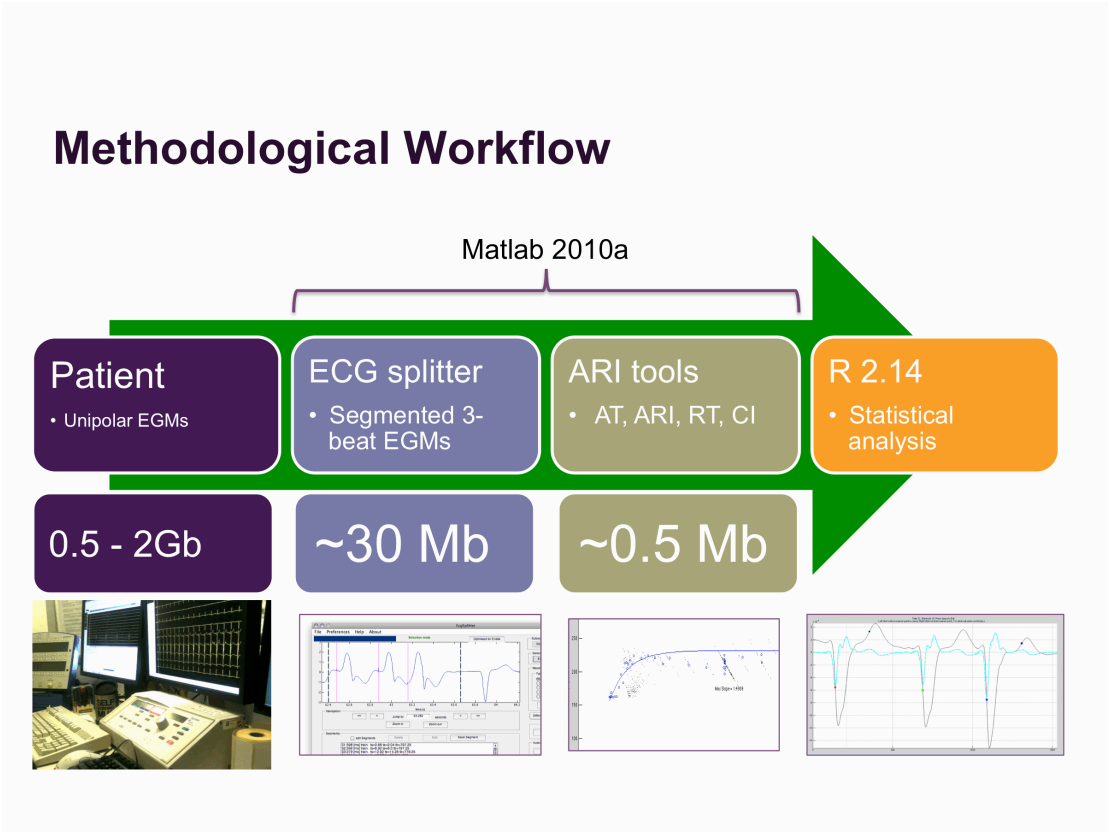

Figure 2-2 Methodological workflow for signal analysis

This chapter will summarise the function and operation of each section of script in turn. Where other authors and co-authors have contributed to each script is acknowledged.

2.1.2.1 Import of electrogram data

The Ensite (St Jude Medical, MN, USA) or Labsystem Pro (Bard Inc, MN, USA) systems were used for all clinical studies. Each system allows the export of ECG, electrogram and pacing data to text formats (ASCII). Matlab scripts were written allowing the import of this data, and recognition of the recording frequency of the data. An individual workflow script was required for each iteration of the software export. This became a technical issue with the Ensite system, during the course of the research study five separate updates to the export formats were made by St Jude Medical. Each required a new import script to enable full compatibility. After import, electrogram or ECG data was held in random access memory (RAM) by the microcomputer as a

common variable, which could be displayed as a signal on screen. Though the import scripts were able to operate as generic functions within Matlab, for practical purposes they were integrated into the "ECG splitter" program. The ECG splitter was developed from a signal analysis graphical user interface (GUI, wave_inspector.m) created by David Western, UCL.

2.1.2.2 Automatic recognition of paced stimuli and calculation of exact stimuli timing

ECG splitter is a simple graphical user interface (GUI) allowing import, analysis and export of signals exported from a commercial electrophysiology system. Our adaptations allowed recognition of pacing spikes (either by examining the time differential of signal, or signal magnitude), QRS complexes (an original function of wave_inspector) as well as functionality involving filtering and selection of electrogram channel for analysis.

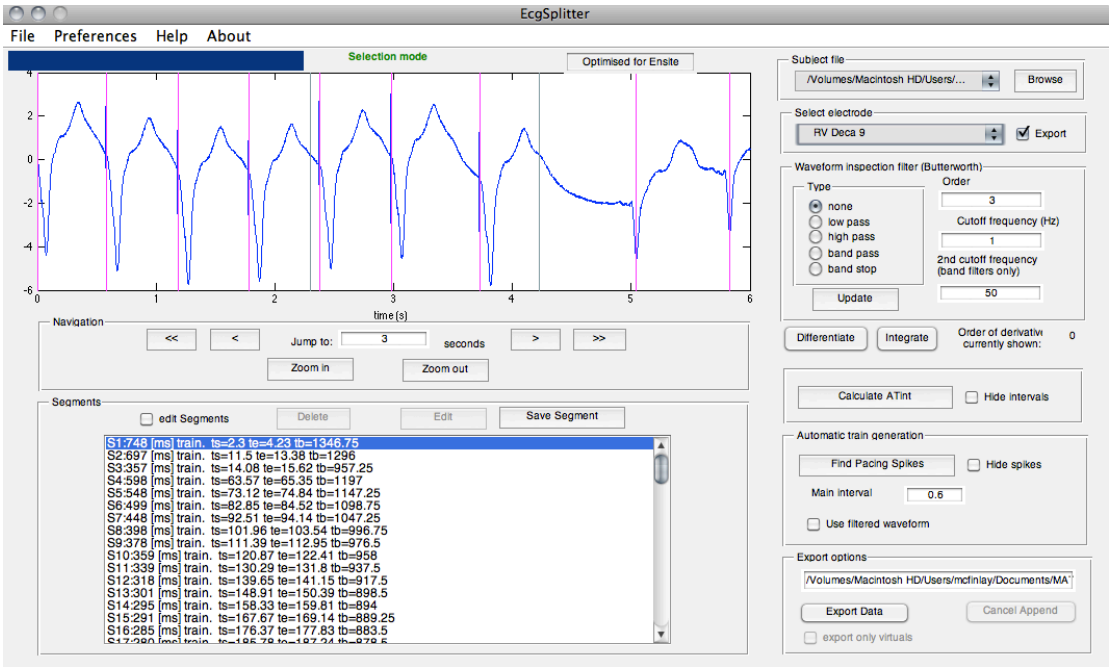

Figure 2-2-3: The ECGSplitter GUI window

The EcgSplitter allows automatic import of electrogram data from .txt or .csv files. Pink lines show positions of automatically detected pacing spikes. The lower window shows automatically detected timing intervals and positions. The control panel on the right allows filtering, selection of electrode to examine and several elements of legacy functionality, including the ability to calculate activation time intervals.

2.1.2.3 Automatic selection of penultimate drive train and premature stimuli, and export of these electrogram segments for further analysis

A key adaptation was the automatic recognition of the final 3 complexes in an S1S2 pacing protocol drivetrain. After inputting the drive train constant, the script was able to recognize the final beats of a drivetrain, and select these for export. These "snippets" of the large electrogram data could then be checked for accuracy, before exporting as a variable structure, named "Curve". As well as including the electrogram data, this structure variable included information on drive train, signal frequency, electrode names and locations and pacing stimulus timings. The Curve variable was then saved in a user-defined location.

2.1.2.4 Analysis of selected segments for activation time & repolarisation time (according to the classical (Wyatt) method)

Working with the assistance of Vadim Kositsky, I adapted a series of scripts originally written by Ben Hanson, UCL, to automate analysis of the Curve data. Dubbed ARI_tools, these scripts were initially developed to analyse ARI and DI interactions from manually selected ultimate 3 beats from S1S2 protocols. Initial versions of these scripts simply allowed analysis of Ensite data. We developed these tools to allow determination of activation and repolarisation, and to determine interactions with coupling intervals of stimuli, rather than just the local responses to DI changes.

These changes ultimately required the rewriting of analytic scripts, though the workflow structure remained similar to Dr Hanson's original.

Thus far, all signals had been processed in an unfiltered manner as much as was possible. For accurate determination of activation and repolarisation times, filtering

was necessary to remove artefact. A high pass filter of 0.1Hz was employed for all signals to remove baseline wander. A Savitzky-Golay FIR smoothing filter was applied to minimise high-frequency noise. A 15ms sample window with 1st degree polynomial fitting was used. This filtering technique applies a local polynomial regression to the signal, with the advantage that local maxima, minima and width of signal features tend to be maintained, without adjusting of the time course (i.e. highly non-destructive). This filtering technique is ideally suited to intracardiac signal analysis, where preservation of both precise time course and signal features is required.

The controversy regarding differential methods of analysing the unipolar electrogram for repolarisation highlighted shortcomings in the alternative method as a reliable indicator of repolarisation times. Although absolute values of repolarisation determined with the Wyatt method may be underestimated in the positive T-wave (especially when non-contact mapping is employed), this method of selecting the sharpest upstroke of the T-wave as the point of local repolarisation appears robust at determining the dynamics of repolarisation. We used the long-established and well-validated Wyatt method throughout the analysis presented.

Selection of the window in which to analyse the T-wave is problematic. Automatic signal analysis is often poor at determining activation times and repolarisation times because of the dependence of "windowing" on the signal. We wrestled with this problem in many iterations of our tool, attempting complex analytics to determine the boundaries within which activation and repolarisation would lie. This allowed the computer algorithm to select the time differential of just the region of interest in the electrogram signal. Unfortunately, biological signals rarely conform to the ideals that signal analytic scripts seek; invariably some signals were contaminated by noise, rendering selection of activation and repolarisation timings inaccurate. Furthermore,

determination of repolarisation time depended completely on accurate measurement of the time point of activation (given by most negative dV/dT on the unipolar electrogram).

Therefore a manual script was instituted enabling selection of windows in which to search for repolarisation and activation times. "Windowing" is performed by selecting the start of the T-wave on the *shortest coupled* S2 beat (restitution theory indicates that the short coupled beats should have the shortest repolarisation time), and the end of the T-wave from a drive train beat (which should have relatively long repolarisation times). Generous windows were allowed to ensure that very early repolarisation times were not missed. Activation windows are selected with the *latest* activation being the end of the activation QRS signal on the *shortest coupled* S2 beat (again, which should display most latency or delay in activation) and the *earliest* activation being the earliest activation during steady state pacing (essentially just following the pacing spike). Windowing is performed separately for electrograms from each chamber (e.g. Right ventricle, Left ventricle, Epicardium).

This approach allowed reliable and reproducible determination of activation (using dV/dT min of QRS) and repolarisation (using dV/dT max of T-wave) times.

2.1.2.5 Review of electrogram data

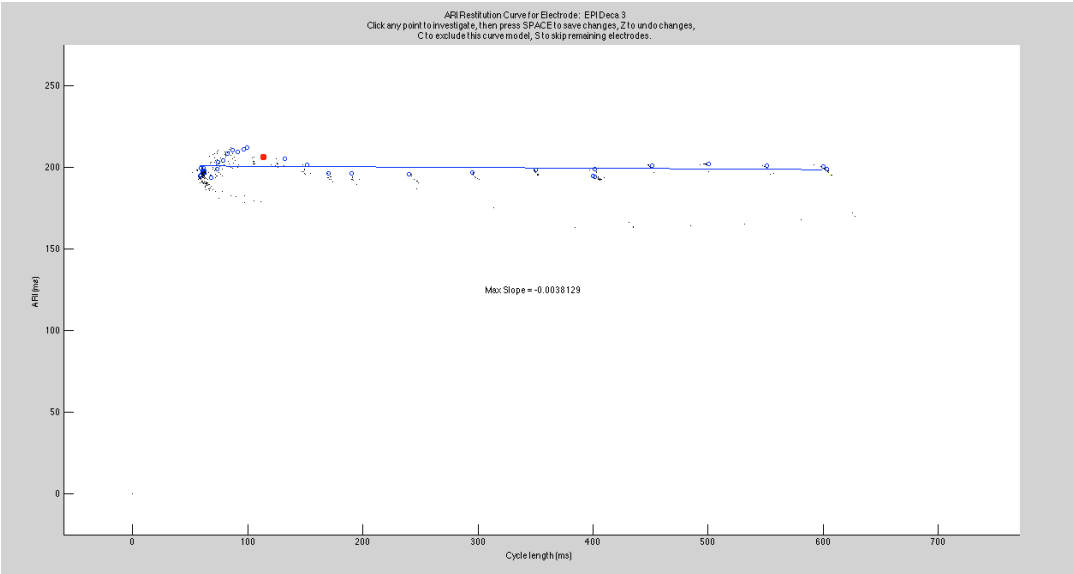

Figure 2-4 Representation of ARI-DI restitution curve for data checking

Calculated ARI-DIs are displayed as blue circles. The red circle shows a selected point (see Figure 2-5).

Following analysis of all electrograms, ARItools displays series of plots of ARI against DI for each and every electrode (Figure 2-4). This allows quick determination of outlier points visually. Clicking on a point brings up a window displaying original data and the differentiated data (Figure 2-5). At this point a data point can be either deleted or moved to a correct manual position. In extreme cases, for example where poor electrogram quality prevented clear determination of activation or repolarisation times, data from entire electrodes can be deleted at once. Similarly if a single S_1S_2 series was anomalous, all data from that coupling interval could be removed at this point e.g. when an ectopic activation fused with paced data. Such manual checking provided a robust method of checking electrograms analysis for inaccuracies or artefacts, whilst reducing operator bias (data acquisition remained primarily automatic).

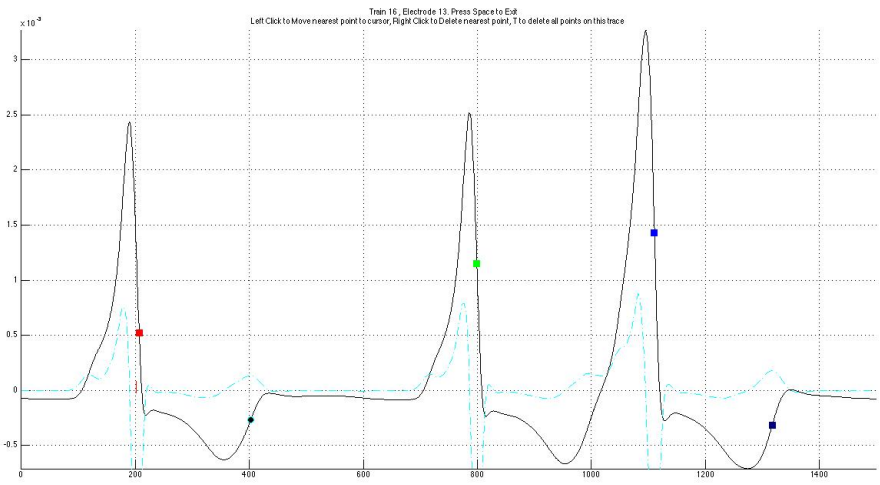

Figure 2-5 Raw Electrogram data with selection of inflection points

Coloured dots represent activation and repolarisation times as selected by the automatic algorithm. These can be adjusted with the computer mouse. The light blue interrupted line represents the time differential of the electrogram; this assists in visual selection of electrogram points.

2.1.2.6 Export of data.

Finally, ARItools offers a GUI script that saves all calculated values from its analysis to a single structure variable. This export function allows data to be added to a previously saved variable, essentially allowing build up of large database of analysis results, with raw data staying intact. These can be interrogated and exported in various formats by other scripts to allow statistical analysis. We exported scripts to .csv format, this could be read by a wide variety of statistical programmes, including Excel (Microsoft, WA, USA) & R (Team R, Vienna, Austria).

2.1.3 Sinus rhythm analysis

2.1.3.1 Import & analysis of sinus rhythm electrograms

ECGSplitter has functionality to allow user-determined selection and export of electrogram

segments, not just those automatically selected at the end of a pacing drive train. If sinus beats are selected, these can be passed onto a curve structure and analysed in a similar way to signals from paced drive trains, including activation, repolarisation and fractionation of signals.

2.1.3.2 Import & analysis of surface electrogram signals

The 12-lead electrocardiogram (ECG) is the most common investigation for cardiac abnormalities, and is formed by body surface potentials resulting from cardiac activation. 12-lead ECGs were recorded throughout all mapping studies performed, and these can be examined for changes concurrent to changes observed in intracardiac signals. Thus we hypothesized that our simultaneous recordings would allow correlations of surface ECG changes arising from intracardiac phenomena.

12 lead ECG data was imported in a similar manner to the intracardiac electrograms. Analysis was performed semi-automatically, with manual windowing for determining T wave parameters, but manual selection of P-QRS-T timepoints.

2.1.4 Fractionation analysis

Fractionation of intracardiac signals has been proposed as a sign of myocardial disarray, if there is heterogeneity of wavefront propagation at a point, several variations in the QRS time course may be inscribed on the electrogram. These variations may be quantified by counting the peaks on the mathematical differentiation of the unipolar electrogram. The resulting trace can be held as equivalent to the bipolar electrogram, though of course the latter represents a spatial differential rather than a time differential.

We sought to quantify this during our analysis, particularly during studies regarding arrhythmogenic cardiomyopathy. A script incorporating fractionation determination

was incorporated into ARItools. The time differential of the unipolar electrogram was examined from just following the stimulus artefact to 100ms following the local activation time. Signal peaks of absolute amplitude greater than 0.6 times maximal absolute of the differentiated, filtered signal were counted, and this total was given as the signal fractionation index (Figure 2-6).

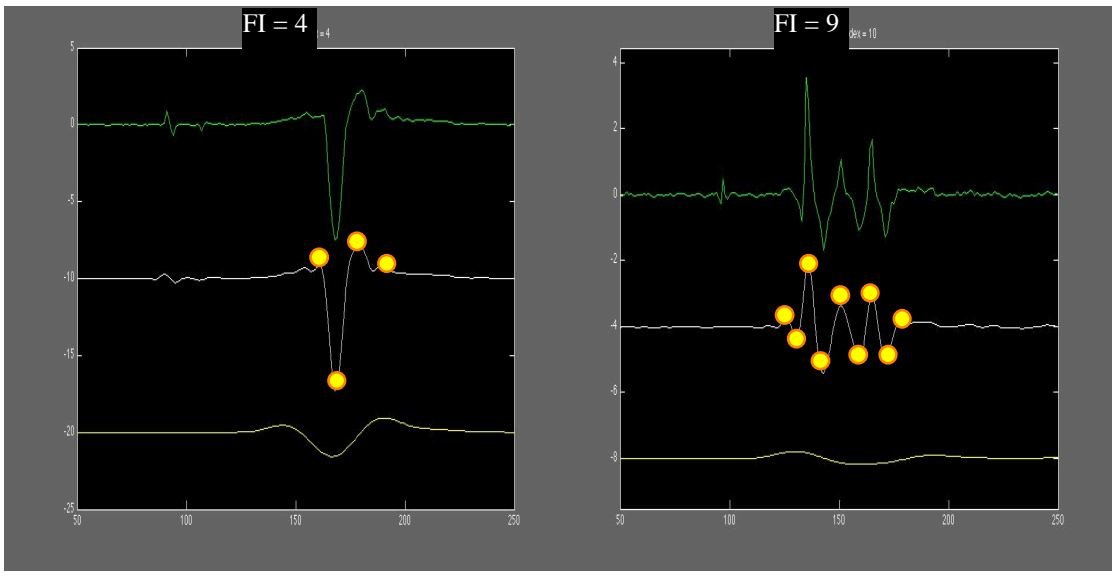

Figure 2-6 Examples of fractionated electrograms

Examples of Fractionation testing. The first electrogram is clean, and has a Fractionation Index (FI) of 4, the electrogram displayed on the right has multiple sharp components on filtered & unfiltered signals, and has an FI of 9.

2.2 Modelling of 1D conduction

2.2.1 One-dimensional conduction model and CV restitution modelling

A novel method of conduction velocity restitution quantification from biologically acquired data using a linear cell fibre model was derived by Lei Xu (UCL). This is given in detail below.

Arbitrary length of cells of 0.1mm was used for model derivation. Each cell within a fibre was assumed to have homogenous CV and APD restitution properties. Both of these factors were described by exponential functions.

If the length of a tissue unit (e.g. a myocyte) is assumed as Δx, and the conduction velocity within tissue as CV, the activation time and repolarisation time of a cell x_i can be calculated as:

Activation time: $$AT_n(x_i) = AT_n(x_{i-1}) + \frac{\Delta x}{CV_n(x_i)}$$ Equation 1

Repolarisation time: $$RT_n(x_i) = AT_n(x_i) + ARI_n(x_i)$$ Equation 2

Where: AT and RT are the activation time and repolarisation time; ARI is the activation recovery interval; n is the number of beat.

Hence, the activation time and recovery time at cell x_i can be expressed as:

$$AT_n(x_i) = AT_n(x_0) + \sum_{j=0}^{i} \frac{\Delta x}{CV_n(x_j)}$$ Equation 3

$$RT_n(x_i) = AT_n(x_0) + \sum_{j=0}^{i} \frac{\Delta x}{CV_n(x_j)} + ARI_n(x_i)$$ Equation 4

Where: x_0 represents the site of stimulation.

Thus the period between activation n and activation n+1 for site x_i can be calculated as:

$$AT_{n+1}(x_i) - AT_n(x_i) = AT_{n+1}(x_0) - AT_{n+1}(x_0) + \sum_{j=0}^{i} \left(\frac{\Delta x}{CV_{n+1}(x_i)} - \frac{\Delta x}{CV_n(x_i)} \right)$$ Equation 5

Here, the period between activation n and activation n+1 for site x_0 equals to the coupling interval CI_{n+1}() applied at site x_0

$$AT_{n+1}(x_0) - AT_n(x_0) = CI_{n+1}$$ Equation 6

The period between activation n and activation n+1 for site x_i can also be calculated as:

$$AT_{n+1}(x_i) - AT_n(x_i) = ARI_n(x_i) + DI_{n+1}(x_i)$$ Equation 7

Combining equation 5, 6, and 7, the basic equation for one-dimensional conduction model can be expressed as:

$$DI_{n+1}(x_i) = CI_{n+1} + \sum_{j=0}^{i} \left(\frac{\Delta x}{CV_{n+1}(x_j)} - \frac{\Delta x}{CV_n(x_j)} \right) - ARI_n(x_i)$$ Equation 8

The conduction velocity $CV(x_i)$ is assumed to be a function of its preceding diastolic interval (DI):

$$CV(x_i) = CV_{SS} - B_{CV} \cdot e^{C_{CV} \cdot DI}$$ Equation 9

where CV_{SS} is the steady-state conduction velocity, a constant defined to be 0.72 (Fox,

2002); B_{CV} and C_{CV} are two constants determining the steepness of CV restitution curve.

Referring to the experimental data, $DI_{n+1}(x_i)$ is the diastolic interval of premature beat S_2, ARI_n is the ARI of the steady-state activation following S1 $ARI_n = ARI_{SS}()$, CI_{n+1} is the S_1S_2 coupling interval. These three parameters were directly obtained from experimental data. $CV_n(x_i)$ is the conduction velocity of a steady-state activation, i.e. is equal to CV_{SS}.

For each investigated site, the activation conduction pathway from the pacing site to the investigated site was assumed to be an independent one-dimensional conduction pathway with uniform restitution properties. From the experimental data, an assumed length of the conduction pathway (given the assumed steady state conduction velocity) can be calculated by the product of steady-state conduction velocity and the steady-state conduction time, $AT_{SS}(x_i)$, from the pacing site to the investigated site:

$$L(x_i) = CV_{SS} \cdot AT_{SS}(x_i) \qquad \text{Equation 10}$$

Hence, the number of cells included in the conduction pathway is $i = \frac{L(x_i)}{\Delta x}$.

Equation 8 can be rearranged into the following form, which allows its solution using experimental data:

$$DI_{S2}(x_i) + ARI_{SS}(x_i) - CI_{S2} + AT_{SS}(x_i) = \sum_{j=0}^{i} \frac{\Delta x}{CV_{S2}(x_j)} \qquad \text{Equation 11}$$

All the dynamics in the left hand side of equation 11 are those obtained from experimental data. For each investigated site, the one-dimensional conduction model and CV restitution model can be fitted with its dynamics from experimental data. An iterative approach was taken, adjusting B_{CV} and C_{CV} in equation 9, and a minimum least-squares error method was employed to select optimum parameters.

2.2.2 Incorporation of patient data into one dimensional models

Data acquired from patient studies was applied to the model, and a separate (and independent) model was created for each electrode site. ARI and conduction velocity restitution was modelled using a mono-exponential equation of the form specified in equation 13.

A standard value of 0.72ms^{-1} was assumed as baseline conduction velocity, changing this absolute value by ±0.2ms did not significantly affect derived CV dynamics. Despite model fitting being computationally intense, the use of simplified exponential dynamics allowed modern desktop machines to derive CV parameters reasonably quickly. For a typical patient, 100-2000 cells were included, depending on the distance of the conduction pathway. For example, if the steady-state conduction time was 100ms at the investigated site, assuming the steady-state conduction velocity to be 0.72 ms^{-1} and cell length to be 100μm, the number of cells included in the conduction model was 720.

Conduction velocity restitution "fitting" was performed by a recursive method. Similar conduction velocity restitution and repolarisation parameters were assumed along the entire conduction path, multiple different exponential restitution parameters (of the form given in equation 13) were tried and simulated along the conduction path. These were automatically adjusted according to closeness of fit, and the simulation repeated until the best fit of the measured activation times with simulation was achieved. Each

recursive cycle thus calculated activation and repolarisation along the entire conduction path, and the conduction velocity parameters were adjusted accordingly. A least-squares fit method was used running within the Matlab environment.

Validation of our method was performed in two ways, comparison with ionic cellular model system and comparison with experimentally acquired patient data.

Once both ARI and CV restitution parameters had been derived from patient data, the cell fibre model was used to predict conduction dynamics of a second extrastimuli (S_3) introduced following a short S_1S_2 coupling interval. Modelling of sequential beats was only attempted if the r^2 for fitting to S_2 data was >0.7 at that electrode site, and sites where electrograms were of poor quality were excluded. Activation times following the S_3 beat (obtained experimentally) were quantitatively compared to those obtained from the cell fibre model.

2.2.3 Comparing the exponential model of repolarisation dynamics against data ionic cellular simulation

At short S_2S_3 coupling intervals, the QRS complex of the unipolar electrogram following an S_3 can widen to fuse with the repolarisation complex. This precludes using unipolar electrograms to validate our simple model for prediction of repolarisation times. We thus performed preliminary validation of our model for prediction of S_3 repolarisation times against data taken from an ionic cellular model. The ion channel model is obtained from ten Tusscher et al. (2009) from their studies of human ventricular tissue.

The ten Tusscher human ventricular ionic model includes 16 types of currents, and 30 ionic gate variables. It is practically impossible with current technology to obtain detailed information of each type of ion current or gate variables on an individual

patient. However, the experimental data provides information on key cellular properties such as APD, activation time, and repolarisation time. These three interdependent properties were fitted with the restitution models, which are then used to simulate interactions of activation and repolarisation.

The ten Tusscher human ventricular model can be summarised in a general form below (the forward Euler method was used to integrate the model):

$$\frac{\partial V}{\partial t} = -\frac{I_{ion} + I_{stim}}{C_m} \qquad \text{Equation 12}$$

Where: V is voltage,

t is time,

I_{ion} is the sum of all transmembrane ionic currents,

I_{stim} is the stimulus current,

C_m is cell capacitance per unit surface area.

Action potential duration (APD) is defined to be action potential duration at 90% repolarisation (APD_{90}).

Diastolic interval (DI) equals to the coupling interval of S2 minus APD from steady-state beat (APD_{ss}).

The form of exponential model tested against data acquired from the ionic cellular model was:

$$APD = APD_{SS} - B \cdot e^{C \cdot DI} \qquad \text{Equation 13}$$

The pacing protocols applied to ion channel model were the same as those used

clinically (i.e. a sequential extrastimulus study). Data acquired from the ion channel model was compared against S_3 repolarisation times modelled using our simple exponential-based approach.

2.3 Human studies

2.3.1 Introduction

Human electrophysiological studies were first performed in the 1960s (Damato et al., 1969; Scherlag et al., 1969; Goldreyer and Bigger, 1971). Several concurrent developments in cardiac therapy, namely cardiac pacing, angiography (and fluoroscopy) and the development of high-sensitivity recording equipment allowed the recording of cardiac potentials from humans using catheters placed via the venous system. These early innovations enabled the first detailed descriptions of human electrophysiology, and were rapidly followed by development of mapping technologies during the late 1990s into the early 21st century. These depended on advances in computation and electronic recording as well as new manufacturing techniques and innovations, enabling the production and use of multipolar recording catheters.

2.3.1.1 Non-contact mapping

Non-contact mapping, (Ensite System) was developed in the late 1990s as a method of calculating electrograms on the entire cardiac chamber wall from far-field signals (St. Jude Medical, MN, USA) (Schilling et al., 1998). In brief, a specialized balloon catheter is advanced via the femoral veins to the heart and placed within the chamber of interest (e.g. right ventricular outflow tract). The catheter has 64 electrodes laser-etched into splines surrounding a fluid-filled balloon that may be inflated or deflated (Figure 3-1). This balloon prevents clots forming amongst the metal splines within the blood pool. When deployed inside the heart, far field signals received by these 64 electrodes can be used to reconstruct "virtual" electrograms projected onto the cardiac wall. This requires knowledge of the specific anatomy in which the device is deployed. This anatomy is created by a steerable ablation or mapping catheter, moved by the operator within the

cardiac chamber. High frequency electrical impedance changes are used to track the motion of the mapping catheter relative to the Ensite balloon within 3D space, and by moving the catheter around the chamber, the limits of its motion, and hence the chamber endocardial location can be determined. This is displayed as a 3D image on a computer console, and "virtual" electrogram data projected upon it.

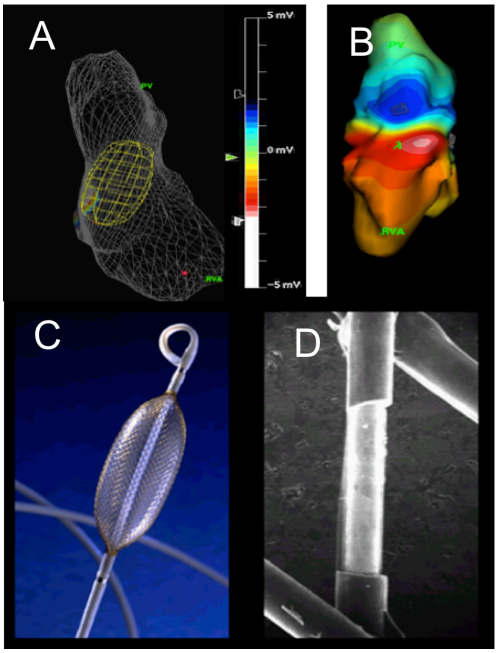

Figure 2-7 The Non Contact Array

The non-contact array is illustrated. Panel A shows a computer display of the array within a 3-D cardiac geometry, panel B shown the non-contact isochronal map typical for clinical display on the Ensite system. Panel C illustrates the physical appearance of the non-contact array when deployed (from St. Jude literature). Panel D shown an electromicrograph of a single electrode from the array. From St Jude literature, MN, USA.

2.3.1.2 Advantages and disadvantages of non-contact mapping

Non-contact mapping offers the possibility of high-density simultaneous measurement of electrical activity throughout a heart chamber. However, it has several disadvantages that limited its usefulness for our studies. First, the current iteration of the non-contact mapping balloon catheter is unwieldy and is often difficult to place. The procedure requires expert knowledge & experience of the Ensite system and is often lengthy,

requiring sedation. This technique was not appropriate for mental stress studies, , where sedation must be minimised. Placement in the RVOT is usually possible though, thus it was suitable for comparisons involving right ventricular outflow tract tachycardia/ectopy (RVOTE) and arrhythmogenic right ventricular cardiomyopathy (ARVC) (Lambiase et al., 2004; Yue et al., 2005).

Second, the quality of the derived virtual electrograms is limited, especially in dilated chambers. Initial validation of activation and repolarisation concentrated on the ventricular chambers, but later studies highlighted the inability of non-contact mapping to reliably resolve signals from chambers with an internal dimensions exceeding >5.5 cms (Abrams et al., 2007). We concentrated our use in ventricles with normal internal dimensions.

Finally, a huge amount of data can be generated from each study, considering the >3000 virtual electrograms possible. Analysis of all data was unfeasibly lengthy. We selected four columns consisting of six virtual electrodes, covering apex, mid-ventricle and base. These 24 electrode locations gave excellent coverage of the entire endocardial surface without overwhelming data.

This chapter will describe the basic methods we have employed in collection of human electrophysiological data, namely contact and non-contact mapping.

2.3.2 Cardiac Electrophysiological Studies

2.3.2.1 Catheter placement and clinical studies

Human contact-mapping electrophysiological studies were performed by Dr. Malcolm Finlay (author), with assistance and supervision from Dr Pier Lambiase, Dr Ron Ben Simon, Dr Martin Lowe, Dr Syed Ashan, Dr Gopi Gopalarugan and Dr Edward Rowland. Studies were performed in patients undergoing cardiac electrophysiological

studies with a view to diagnosis and ablation of supraventricular tachycardia. All gave prior informed consent. Studies were performed under minimal conscious sedation with local anaesthetic (lignocaine 1%) or with local anaesthetic only (mental stress studies) in the post-absorptive state. Antidysrhythmic drugs were discontinued for 5 days prior to the study. The study protocols had local ethics committee approval (UCL REC no. 10/H0715/19) and conformed to the standards set by the Declaration of Helsinki.

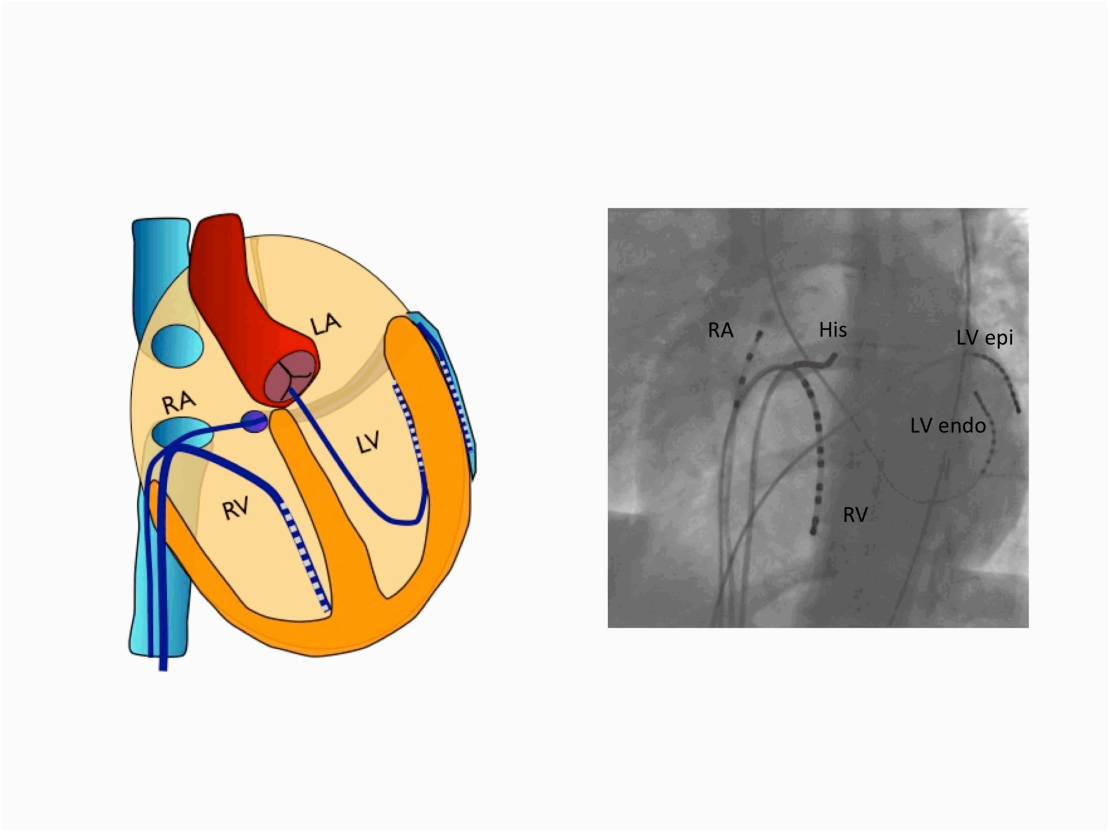

Figure 2-8 Catheter positions for in-vivo studies

Schematic (left) and x-ray fluoroscopy (right) catheter positions are shown. RA: Right Atrium, LA: Left Atrium, RV: Right Ventricle, LV: Left Ventricle, epi: epicardial, endo: endocardial.

Catheters were placed via venous sheaths (6F to 8F), with 4F arterial access (LV retrograde catheter, Figure 2-8). All patients received 5000 units of unfractionated heparin. Decapolar catheters were placed in an epicardial coronary vein via the coronary sinus, at the RV apex and retrogradely within the LV cavity adjacent to the epicardial catheter (St Jude Pathfinder). X-ray fluoroscopy was used to guide catheter electrode

placement. A reference anodal electrode was placed in the inferior vena cava. Further catheters were placed according to clinical requirements. Electrograms were digitized and recorded at 1000Hz (Bard Clearsign, Mn, USA, Figure 2-2). If no arrhythmia was initiated by ventricular pacing during the initial clinical study, restitution studies were performed prior to further clinical testing. Surface 12 lead ECGs were recorded throughout the study. Oxygen saturations were measured continuously using pulse oximetry & blood pressure was measured non-invasively at 5-minute intervals.

Following the clinical procedure, venous and arterial sheaths were removed and haemostasis achieved with manual pressure.

2.3.2.2 Non-contact array mapping

Non-contact mapping was performed by Dr Pier Lambiase, UCL, with assistance from Dr Akbar Ahmed, Dr Justine Bhar-Amato, Dr Martin Lowe, Dr Anthony Chow, Dr Ron Ben Simon and Dr Malcolm Finlay (author). The Ensite catheter was placed via a 9F sheath in the left femoral vein into the right ventricular outflow tract under fluoroscopic guidance. Patients were formally anticoagulated during non-contact mapping procedures, with an activated clotting time (ACT) kept between 250 and 300 with boluses of unfractionated heparin. The non-contact mapping balloon was inflated and signals checked for consistency across all 64 electrodes. A mapping catheter was introduced from the right femoral vein and placed in the right heart and connected to the Ensite system. Movement of the catheter around the bounds of the right ventricle allowed the creation of a 3D endocardial geometry on the Ensite console. This was orientated correctly using fluoroscopy. Recording was commenced and a restitution protocol performed.

2.3.2.3 Restitution Pacing Protocol

A restitution study was conducted using programmed electrical stimulation (PES). Following 3 minutes of steady state pacing at the RV apex at a cycle length of 600ms, a drivetrain of 10 beats was followed by an extrastimulus (S_2). The S_1S_2 interval was decremented by 20ms to 300ms, thereafter in 5ms intervals until ERP was reached. The ERP was found by increasing CIs by 8ms and then decrementing by further 2ms intervals. In patients undergoing second extrastimuli (S_3) studies, the S_2 extrastimulus was set at 10ms above the observed refractory period, and an S_3 was delivered at CIs progressively decrementing to a minimum of 180ms. In patients undergoing studies involving mental stress or pharmaceutical agents, restitution pacing studies were repeated during mental stress or drug administration.

2.3.2.4 Mental stress studies

I performed all mental stress studies. PES was performed during an active relaxation protocol, and again during mental stress in the manner described by Burg et al. (1993). During active relaxation, subjects were asked to think of a situation that they found subjectively relaxing, and were asked to imagine themselves being in that situation. Lab lighting was turned down to a minimum and quiet kept amongst staff. Gentle prompts in a clam & reassuring manner were used to encourage the subject's active memory of the situation.

Mental stress was induced in two forms, mental arithmetic with harsh encouragement and anger recall. Data is presented from that which provoked the greatest stress response. Lab lighting was returned to full during the stress protocol. Mental arithmetic involved subtraction of serial 7s from a four-digit number. Harsh encouragement was given according to maintain subjects interest and concentration. During anger recall,

subjects were asked to remember a recent situation that made them angry. They were asked to relive that situation, and tell the investigator as if describing that situation later that same day to a close friend. The investigator then attempted to mildly provoke further reaction with mild awkward questioning. Subjective stress was recorded on a Likert scale for each protocol, which has been shown to accurately correlate with physiological measures of stress (Callister et al., 1992). Intrinsic heart rate and serum catecholamine levels were taken as objective measures of stress response. 10mls of blood was extracted from the left femoral vein midway through each protocol. Samples were rapidly cooled to 4ºC on ice, centrifuged at 10000rpm for 2mins. Plasma was snap frozen and stored at -70ºC. Presented comparisons are for peak stress compared to relaxation for each patient.

2.3.2.5 Pharmacological Studies

PES restitution protocols were performed at baseline and following administration of ajmaline 50mg (5mg/ml) into a central vein via a femoral sheath. Periods of sinus rhythm were recorded between drive trains enabling comparison of sinus rhythm activation.

2.3.2.6 Data export

At the end of the case, data was exported to text format for analysis using standard export tools. Data was saved in anonymised files on an encrypted external hard drives.

2.3.3 Human Genotyping

Dr Giovanni Quarta & Dr Syrris (UCL) carried out human genotyping. 10ml whole blood samples were obtained from ARVC patients and family members. Genomic DNA was extracted using a commercially available DNA extraction kit (QIAamp DNA

Blood mini kit, Qiagen). Index cases were part of a larger patient cohort comprehensively screened for mutations in desmoplakin, plakoglobin, plakophilin-2, desmoglein-2 and desmocollin-2. Primer pairs for DSP exons were designed in flanking intronic sequences and are available from Dr Syrris. Polymerase chain reaction (PCR) amplification and direct sequencing on an ABI 3130 Genetic Analyser were performed using standard protocols (Syrris et al., 2007; Syrris et al., 2006a; Syrris et al., 2006b). A total of 300 unrelated healthy, ethnically matched Caucasian volunteers served as controls.

2.4 Murine Genotyping and Electrophysiology

2.4.1 The transgenic mouse and methodology of electrical phenotyping

Cardiovascular biology has been revolutionized by transgenic technology, which has enabled investigators to determine exact molecular mechanisms and pathways. Prior to the development of transgenic murine models, "classical" physiology had sought to determine the cause of disease largely using combinations of surgery and pharmacology, techniques that often introduced important co-founders to results & required caution in translation of results. Technological advancements now allow researchers to modify genes quickly and with great accuracy, enabling the study of specific aspects of cardiovascular physiology and biology (Bockamp et al., 2002). Several transgenic strategies exist. These include the integration of transgenes by pro-nuclear injection, but the targeting of specific genes through homologous recombination in pluripotent embryonic stem (ES) cells has allowed the murine model to come to the forefront of transgenic mammalian research (Shuldiner, 1996). Gene targeting is performed in ES cells *in vitro*; these cells are then reintroduced into blastocysts, thus creating chimeric embryos (Figure 2-9). The resulting mice, with introduced mutations into their germline, can be used as founders, and the engineered defect is transmitted into subsequent progeny. The mouse is ideally suited to these techniques owing to its transgenic versatility, fast reproduction rates and large litters.

A

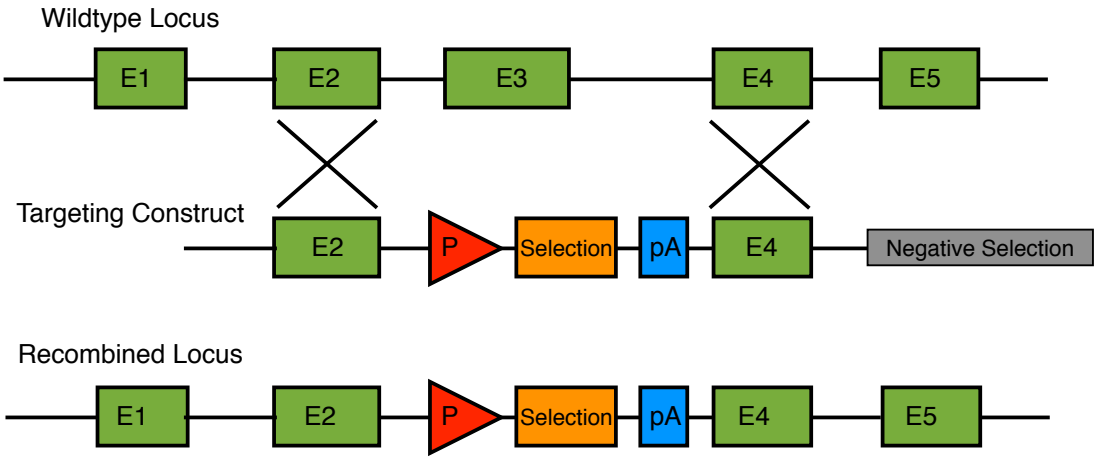
Wildtype Locus
E1
E2
E3
E4
E5
Targeting Construct
E2
P
Selection
pA
E4
Negative Selection
Recombined Locus
E1
E2
P
Selection
pA
E4
E5

B

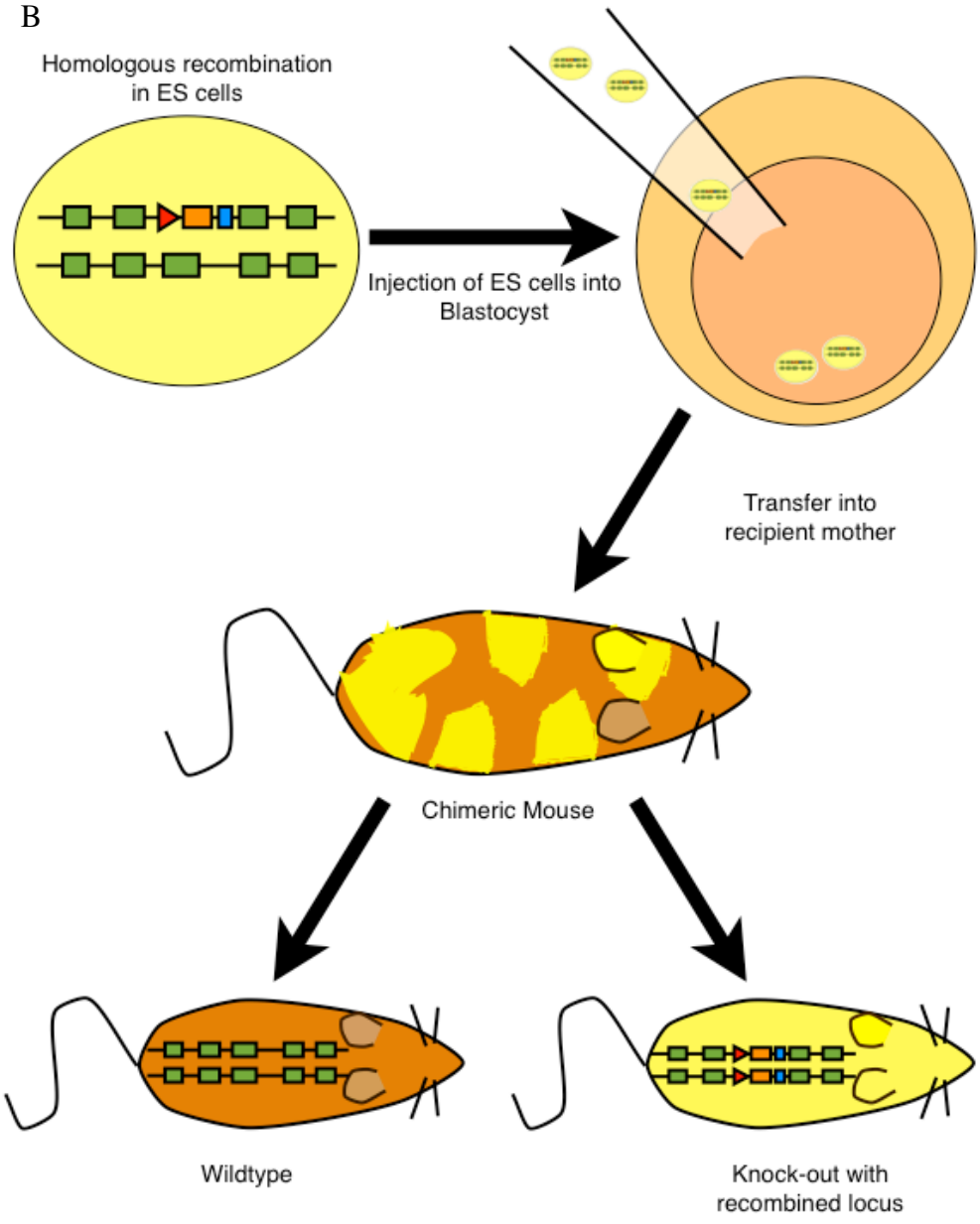
Homologous recombination
in ES cells
Injection of ES cells into
Blastocyst
Transfer into
recipient mother
Chimeric Mouse
Wildtype
Knock-out with
recombined locus

Figure 2-9 Generation of knockout mice using homologous recombination and embryonic stem (ES) cells.

A: A strategy for generating a knockout genotype using homologous recombination is illustrated. The wild-type locus is here shown with five exons (labeled E1 –E5), the gene to be targeted is E3. The targeting construct will recombine with the locus at E2 and E4, thus deleting E3 and introducing a selection marker. Randomly integrated DNA constructs will contain the negative selection marker, but homologously integrated DNA will not: removal of non-homologous DNA outside the flanking region takes place. The negative selection marker can thus be used to select for ES cells with correct homologous recombination. P is a promoter driving expression of the selectable marker, PA Polyadenlation signal.

B: Homologously recombined ES cells are injected into a blastocyst, which in turn is placed into a pseudo-pregnant recipient mother. The injected ES cells are pluripotent, and will contribute to all tissues in the resultant chimeric progeny (including in the germline). Thus breeding from these chimeric mice results in hemizygous knockout mice, which themselves can be inbred to give homozygotes and littermate wild-type controls. Adapted from (Bockamp et al., 2002)

2.4.2 Murine electrical phenotyping

Current understanding of cardiac electrophysiology, particularly cardiac impulse propagation and arrhythmogenisis, has been significantly advanced by the study of transgenic mice. These have added to existing techniques such as cellular imaging, patch clamping and molecular biology to give a broad basic approach to the study of cardiac electrophysiology. Furthermore, transgenic mice offer the opportunity to complement the study of clinical disease with the in-depth and "clean" studies possible in a specific transgenic construct. Single cell experimentation does not reproduce the true tissue and organ level physiology that exist in vivo; there is complex tissue heterogeneity, with multiple cell types and extracellular matrix that contributes to marked regional differences in physiological properties. These are impossible to measure on isolated cells.

Even more pertinent is the observation that arrhythmia, indeed cardiac function *in* vivo, is not a phenomenon of individual isolated cells, but refers to a tissue-level behaviour. This does not to diminish the enormous, fundamental and increasing contribution that

molecular and cell biology has, and is, making to the understanding of cardiac arrhythmia, but does highlight that an understanding of isolated cell behaviour alone is insufficient for a full understanding of cardiac electrophysiology and arrhythmogenesis. The transgenic mouse, with its advantages as a physiological tool, is thus well suited to the study of arrhythmia, particularly on a tissue level.

To this end, several technologies have been developed for murine phenotyping including cardiac monophasic action potential mapping (*ex vivo)*, cardiac optical dye mapping (*ex vivo)*, invasive (*in-vivo*) electrophysiology and ambulatory ECG telemetry and monitoring (*in-vivo*).

Monophasic action potential mapping in the transgenic mouse has revealed important transchamber heterogeneity in activation and repolarisation in models of Brugada syndrome. However, it is limited to point measurements at a single site, and does not reveal the spread of excitation or repolarisation wavefronts. Optical mapping has been developed to allow electrical wavefront mapping in the intact cardiac preparation (Efimov et al., 1994). This technique utilizes the physical properties of wavelength dependent light/excitable tissue interactions to directly observe activation and depolarization activity across the surface of the heart with excellent spatial-temporal resolution. Using this method, mechanisms of arrhythmia induction and maintenance have been directly demonstrated, by allowing direct visualization of complex-re-entry around lines of conduction block (Girouard and Rosenbaum, 1996; Witkowski et al., 1998).

Optical mapping has unquestionably advanced our understanding of cardiac electrophysiology. However, it is not without its limitations. First, accurate registration of tissue with optical sensing requires the heart preparation, usually Langendorff-

perfused (Langendorff, 1895), to be held absolutely still during recordings. Cardiac motion must therefore cease, and this is achieved with pharmacological excitation-contraction uncoupling agents. Such uncoupling agents have their own primary effect on cardiac electrophysiology, and results must be interpreted with a degree of caution (Brack et al., 2013). Second, optical mapping currently provides only a 2D planar view of the myocardial tissue. In practice, this has restricted the overwhelming majority of studies to the epicardial surface. This becomes a major drawback considering the proposed role of tissue-level heterogeneity (e.g. between epicardial and endocardial cell layers) in clinical arrhythmogenisis. Some studies have overcome this by employing ventricular wedge preparations (Antzelevitch et al., 1998; Antzelevitch, 2001; Antzelevitch, 2008; Myles et al., 2010; Myles et al., 2011), and have sought to actively examine tissue-level heterogeneities across the myocardial wall. Third, the 3D nature of the whole heart preparation makes the true course of a wavefront impossible to determine from 2D information alone. Wavefronts and excitation paths may re-enter via pathways concealed deep in the tissue, and thus the true nature of tissue reentry and excitation remains hidden from a surface map (Akar et al., 2002; Bai et al., 2011).

Recent developments in cell culture, particularly in embryonic stem cell technology, have allowed the study of cardiomyocyte syncytia *in vitro* (Zhang et al., 2009). Confluent stem-cell cell cultures that are reprogrammed to form cardiomyocyte have been successfully used to study re-entry. Very recent work has illustrated that these techniques may be applied to stem cells isolated from adult human skin or blood in individuals with cardiac disease (Davis et al., 2012; Itzhaki et al., 2011; Lee et al., 2012; Ma et al., 2013).

Yet drawbacks from this technology remain (Blazeski et al., 2012). First, the resulting cell layers, though exhibiting many features of mature cardiomyocytes, have developed

in an artificial medium. The supporting extracellular matrix, fibrous tissue, blood vessels and structure found in intact tissue is not, and has never been, present. Important developmental interactions may thus be easily missed. Second, the technology is still in infancy, and to achieve success at cell fate reprogramming requires intensive resource and is by no means assured. Third, the access to tissues from well-characterised patients can limit the pursuit of a specific scientific hypothesis, though doubtless this technology will inform us further regarding disease mechanisms of our patients. Forth, despite being classed as cardiomyocytes, cultured cardiac cells cannot be classified regionally. Indeed, currently we cannot reliably distinguish whether a cultured cardiomyocyte is an atrial, ventricular or sinus nodal cell. Anecdotally most cultured cardiomyocytes exhibit properties of all cardiac cell types to greater or lesser degrees. In cardiac arrhythmic disease, where tissue heterogeneity is centre stage, the homogeneity of cell culture preparations is a major limitation.

Myocardial tissue slice preparations have been proposed as a method by which the limitations of cell layer or whole heart electrophysiology studies may be overcome (Pillekamp et al., 2005; Camelliti et al., 2011; Bussek et al., 2012). In brief, very thin (150-400μm) slices of myocardial tissue are shaved from a block of living tissue using a vibrating microtome (vibratome). The electrophysiology of these slices is thus confined to a 2-dimensional plane, and this can be measured with electrode microarrays and extremely high-fidelity electronic amplifiers. This technique has become established as a way of measuring neuronal activity and connections in rodents. Barriers to the use of this technique in the murine cardiac preparation include the extreme fragility of the murine cardiac tissue, its high sensitivity to oxygen stress and the difficulties of achieving reliable stimulation of cardiac slices. Several groups have managed to achieve reliable recordings and stimulation from neonatal murine cardiac slice preparations

(Halbach et al., 2007; Pillekamp et al., 2005); success has also been claimed for larger rodents, including guinea pigs and rats (Bussek et al., 2012), and human ventricular tissue (Brandenburger et al., 2012). However, little published data on adult murine preparations exists. A technique described in the mid-2000s by Halbach appears not to have been reliably reproduced (Halbach et al., 2006). Even here, tissue was taken from mice at 5 weeks, rather than truly adult tissue implied by the paper title.

The attraction of an adult murine tissue slice preparation as a model for investigation of cardiac electrophysiology remains, particularly in light of the mature and unparalleled transgenic technology available. Specifically, a defined tissue-level model of cardiac electrophysiology would enable me to begin to dissect the specific biological mechanisms underlying our human observations. It was intended to establish a reliable tissue slice model of murine ventricular electrophysiology.

2.4.2.1 Objectives

This methods chapter aims to:

1. Describe the animal breeding strategies used and the PCR based genotyping approach used to identify mouse cohorts.
2. Describe the (successful) tissue slice preparation approach.
3. Describe the utilization and setup of the cardiac slice microarray recording procedure and its applicability to the study of tissue-level electrophysiology in mice with a G-protein transgenic deletion

2.4.3 Animal breeding and genotyping

2.4.3.1 General Conditions

Mice were maintained at a UCL animal core facility under stringent UK home office guidelines relating to animal welfare (PPL-6732). All mice were kept in individually ventilated, pathogen-free, temperature controlled cages (21-23ºC) with 12-hour day/night light cycles. Animals had free access to standard rodent chow and water. Mice were studied between 12 and 24 weeks of age under standardized conditions.

2.4.3.2 Transgenic global deletion of individual $G\alpha_{i2}$ isoforms and breeding

All physiological studies were performed following an initial mouse breeding programme designed to generate specific deletion of individual inhibitory G-proteins. Experimental mice from an Sv129 genetic background had selective global deletion of $G\alpha_{i2}$, abbreviated $G\alpha_{i2}$ (-/-). Professor Birnbaumer initially provided the breeding pairs of mice, which were used in the 4th generation. These mice were initially generated using homologous recombination techniques in mouse ES cells. The gene targeting strategies have been previously published, and confirmation of selective G-protein deletions at the protein level has been confirmed by Western Blot analysis in various tissues including the heart (Rudolph et al., 1996; Jiang et al., 1997).

The gene targeting approach used was as follows. A gene map schematic of $G\alpha_{i2}$ incorporating intron-exon boundaries is shown. Exon 3 within the $G\alpha_{i2}$ locus was disrupted *in vitro* at a unique *Ncol* restriction site and a neomycin resistance cassette inserted. This interruption results in a truncated protein with no biological function. The mutation was subsequently incorporated into ES cells by homologous recombination. Mutated ES cells containing one copy of the mutated $G\alpha_{i2}$ gene as well as one wildtype

copy ($G\alpha_{i2}$ +/-) were then positively selected for in antibiotic enriched media. Positive clones were injected into blastocysts and placed in pseudo-pregnant mice to generate "chimeric" animals. Chimeric founder mice incorporating the $G\alpha_{i2}$(+/-) mutation at a germ cell level were then inbred on an Sv129 background. By intercross of $G\alpha_{i2}$ heterozygotes (+/-), Mendelian genetics predict the progeny would be either (+/+) littermate controls, (+/-) $G\alpha_{i2}$ heterozygotes or (-/-) $G\alpha_{i2}$ deleted.

2.4.3.3 Mouse Genotyping

Mice were ear marked for identity purposes at 3 weeks of age. Ear clippings (~2mm diameter) were used for genomic DNA isolation. Polymerase Chain reaction (PCR) based genotyping was performed on isolated DNA to confirm the genotype of individual mice. I performed all stages of the mouse genotyping.

2.4.3.4 DNA extraction of ear clips

Ear punch samples were placed in Epindorf tubes. 150μL of tail lysis buffer (3.5ml 2M Tris-HCL pH 8.8, 1.66ml 1M $(NH_4)_2SO_4$, 1.34ml 0.5M $MgCl_2$, 0.5ml Triton X-100, 92.2ml H_2O, 1ml β-mercaptoethanol) was added and the samples heated to 100ºC for 10 minutes. This aimed to denature mouse proteins. Samples were cooled and 5μL of proteinase K (20mg/ml) was added at 55ºC for 12 hours to cause non-specific protein digestion. Samples were reheated to 100ºC for a further 10 minutes and spun at 13000rpm in a tabletop centrifuge. 1μl of supernatant containing mouse genomic DNA was used per genotyping PCR.

2.4.3.5 $G\alpha_{i2}$ genotyping

The following primers were used for $G\alpha_{i2}$ genotyping:

i2F8 5'-GATCA TCCGA GATGG CTACT CAGAA G-3'

i2F14 5’- CAGGA TCATC CATGA AGATG GCTAC- 3’

i2R7 5’-CCCCT CTCACTCTTGATTTCCTACTGACAC-3’

NeoR2 5’- GCACT CAAAC CGAGG ACTTA CAGAA C-3’

PCR conditions are summarized below

PCR reaction mixture:

- Thermopolymerase buffer 5μL
- dNTP’s (25mM) 1μL
- Mg^{2+} (50mM) 1.2μL
- Molecular H_2O 37.5μL
- i2F8 (100μM) 2.5μL + i2R7 (100μM) 2.5μL (Wild Type allele) *OR*
- i2F14 (100μM) 2.5μL + NeoR2 (100μM) 2.5μL (Mutant allele)
- Taq polymerase (5U/μL) (0.35μL)
- Genomic DNA 1μL

PCR Profile

- 94ºC for 5min
- 94ºC for 1min
- 62ºC for 1min
- 72ºC for 2min

x30

- 72ºC for 10min
- Samples stored at 10ºC until analysis

Two PCRs were run per sample. One used the wild type primers (i2F8 and i2R7), resulting in the presence or absence of an 805bp fragment corresponding to wild-type $G\alpha_{i2}$. A second PCR was performed with the primer set specific for the mutant allele, i2F14 and NeoR2. This allowed determination of presence or absence of a 509bp PCR fragment from the mutant gene. PCR fragments were separated using agarose gel electrophoresis.

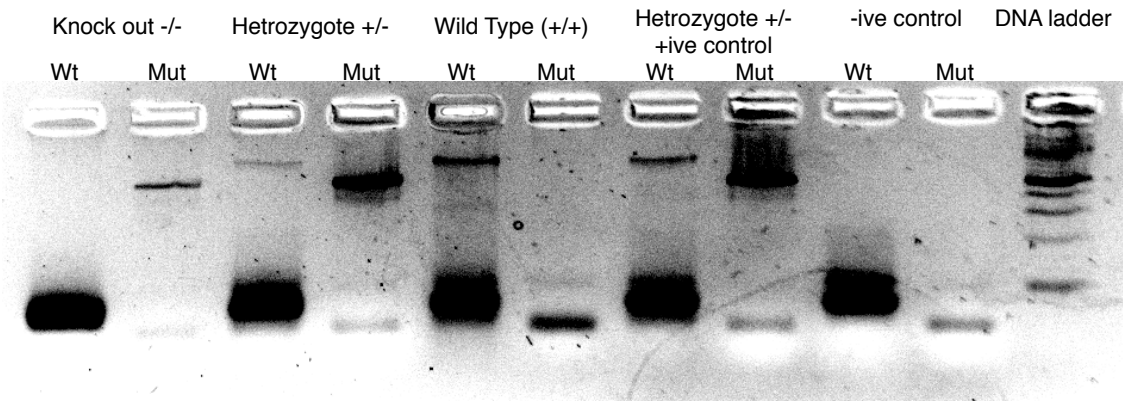

Figure 2-10 Example of Gel Electrophoresis

A typical gel electrophoresis is shown. Data from four animals are shown: a homozygote knock out, with a mutant 509bp band visible, a heterozygote (both 805bp and 509bp bands visible), a wild-type littermate (only 805bp band). A heterozygote control, and a DNA-free negative control are also shown. A 100bp ladder is visible on the right. Wt – wild-type PCR fragment, Mut – mutant PCR fragment.

2.4.4 Murine cardiac slicing and electrophysiology studies

2.4.4.1 Initial attempts and hypotheses

The development of a novel cardiac tissue slice model for studying cardiac electrophysiology presented several challenges. Studies were commenced by using the published work of Halbach et al (Halbach et al., 2006) and by studying Langendorff techniques with Gareth Matthews and Prof. Chris Huang in Cambridge University. Previous tissue slice work had used a low-calcium, Tyrode's-based (HEPES buffered) solution for initial tissue isolation. 2,3-butanedione monoxime (BDM) is frequently been used in cell isolation to reduce myocardial work, acting as a myosin inhibitor.

Cold-cardioplegia had been applied to inhibit contraction. Halbach and colleagues had also employed Blebbistatin to inhibit cardiac contraction and prevent apoptosis.

Initial attempts at reproducing Halbach's methods were unsuccessful. Apparently living tissue slices were occasionally obtained. However, these exhibited uncoordinated spontaneous contractions which ceased rapidly. This was taken to signify tissue death. No reliable electrical signals were recorded from these tissues.

An approach to fully inhibit cardiac contraction and to reliably prevent cell death during slicing was pursued. A zero-calcium, high-potassium, cold perfusate of the whole heart was employed. Blebbistatin is a specific inhibtor of Myosin II ATPase, and as such inhibits apoptosis and reduces muscle energy demands. This compound was added to the perfusate solution aiming to further inhibit apoptosis and reduce cardiac metabolism. It was hoped that this would permit successful tissue slicing, with tissue slices able to readapt to physiological solutions. The low temperature and high potassium would inhibit cardiac electrical activity by reducing metabolic rate and reducing transmembrane potentials. Removing calcium from the solution would reduce contractile function and inhibit programmed cell death.

Hearts were formally perfused with the cardioplegic perfusate via a Langendorff system, this allowed blood washout and full perfusion through the tissue. Solutions were based on Kreb's solution; this has the advantage of robust physiological buffering.

The final, successful, technique is described below.

2.4.4.2 Cardiac slicing

Mice were euthanized with cervical dislocation. The thorax was immediately dissected and the heart exposed. Cardioplegia was instigated by applying 10mls of ice-cold,

oxygenated Ca^{2+}-free Kreb's solution (119mM NaCl, 4mM KCl, 1mM $MgCl_2$, 1.2 mM KH_2PO_4, 25mM $NaHCO_3$, 10mM glucose, 2mM Na Pyruvate, pH 7.4) directly onto the epicardial surface. The heart and great vessels were removed within 20 seconds and placed into a dissection dish containing ice-cold Ca^{2+}-free Kreb's, and a 23 gauge cannula was inserted into the aorta under microscopy. The aorta was secured to the cannula with a clip, cold retrograde perfusion was commenced initially with oxygenated, ice-cold, Ca^{2+} free Kreb's at 16.5mls/min. The time taken from cervical dislocation to establishment of cold Langendorff perfusion was less than 3 minutes.

Following perfusion for 2 minutes, perfusate was changed to ice-cold oxygenated calcium-free Krebs with high K^+ (20mM KCL) and Blebbistatin (Cambridge Bioscience, 20μM) for 3 minutes. Hearts were removed from the Langendorff perfusion rig and placed again into a dissection dish containing cold perfusate. Ventricular tissue was dissected from atrial under light microscopy, and the dissected ventricles were embedded in low-melt agarose (4% low-melting point agarose in Ca^{2+}-free Kreb's), and then rapidly chilled on ice. The agarose block was orientated and fixed to a magnetic stage using cyanoacrylate glue and placed into the cutting chamber of the vibratome. This chamber was kept at 4ºC using external ice, and the cutting chamber was filled with cold, modified Kreb's solution (0.6mM Ca^{2+}, K^+ 10mM).

Tissue sections were performed from apex to base at interval thickness 200μm. The vibrating PTFE-coated steel blade (Wilkinson Sword, Bucks, UK) was advanced at <200μm/sec. x-axis vibration was 2mm at 80Hz. z-axis deviation was calibrated prior to every use to be <1μm.

Cut sections were immediately placed into room temperature, oxygenated low-Ca^{2+} Krebs (4mM KCl, 0.6mM Ca^{2+}) with 10μM Blebbistatin. After 25 minutes, samples

were transferred to oxygenated standard oxygenated Krebs (4mM KCl, 1.1mM Ca^{2+}) and kept at room temperature until electrophysiological studies were performed.

2.4.4.3 Cardiac slice EP studies

The multi-electrode array is a recently developed technology that allows solid-state electrical recording from 59 individual electrodes within a dedicated fluid-filled recording chamber. This allows mapping of electrical wavefronts over a slice of electrically active tissue, e.g. brain, cultured cell layer or, in our case, heart myocardium. Stimulation can be performed either through the recording electrodes themselves or via an external stimulator. The system consists of removable microarray-plates that can be loaded into a recording headstage with integrated amplifier. This communicates with an external breakout and stimulator system. The microarray is held at a constant temperature by a regulated heating block incorporated into the headstage, a magnetically fixed perfusion system also incorporates a temperature-controlled fluid warmer. The entire system is computer controlled from an external PC microcomputer. To allow visualisation of tissue during experiments, the headstage was mounted on a Nikon N5 inverted microscope with 20x objective.

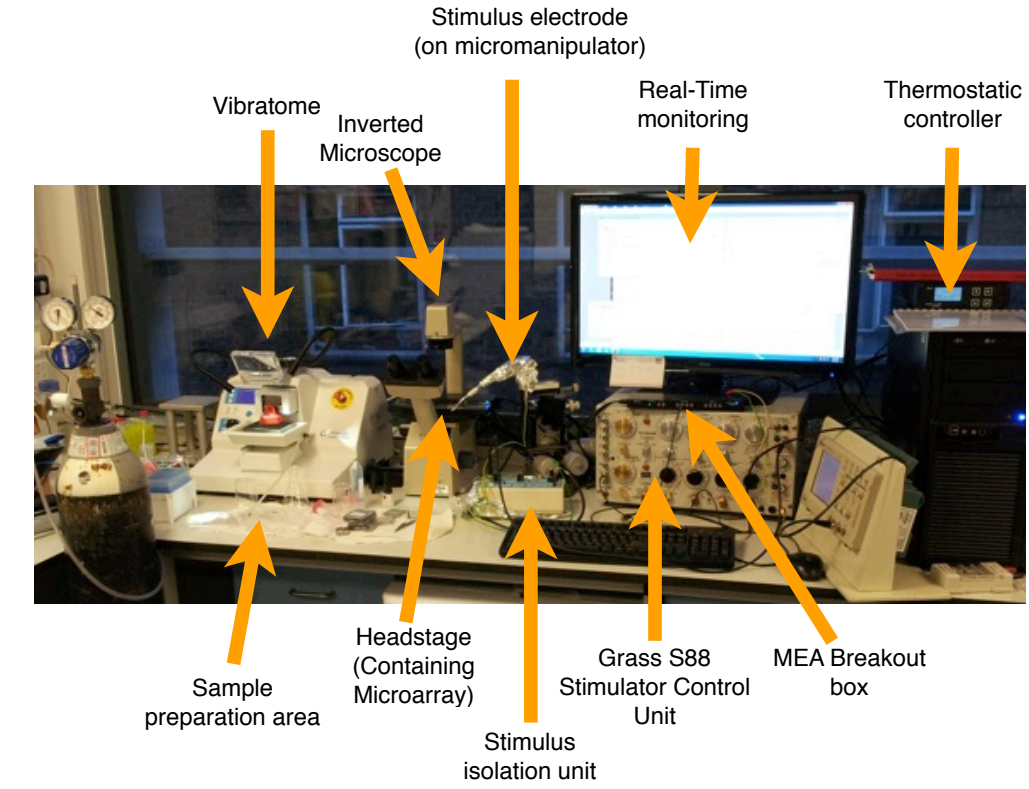

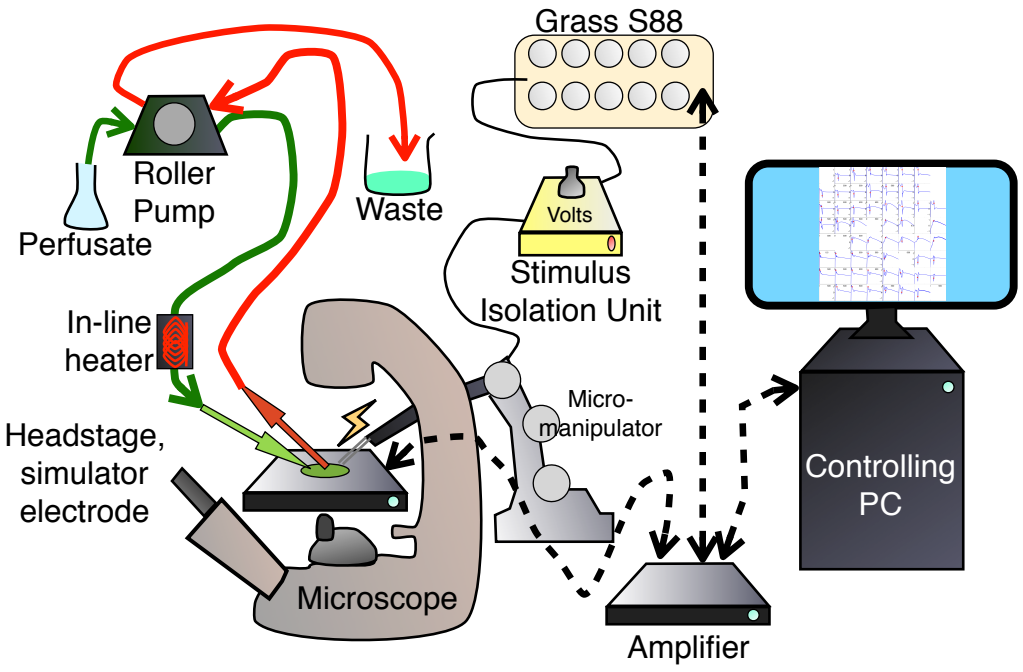

Figure 2-11 Experimental setup for tissue slice measurements (Actual and Schematic)

Photograph shows actual equipment where murine thin cardiac slices were generated and studied. Schematic is shown below. Broken lines represent digital control lines. A roller pump provides a continuous flow to the multi-electrode array within the headstage.

Despite being state-of-the-art for neural tissue and cell-culture measurements, several limitations of this system in cardiac electrophysiological testing were apparent. Pharmacological studies require a smooth transfer of perfusate solutions; this is very hard to achieve using manual pipetting without disturbing the tissue slice on the array. Similarly, any changes in contact with the fluid-filled recording chamber create artefact and electrical interference in the recording system that did not always resolve completely. A constant perfusion system, incorporating a thermostatic fluid warmer, was built. This allowed simultaneous infusion and removal of perfusate from the recording chamber, enabling constant perfusion with fresh solutions. Drugs can be added to the infusion with reliable wash-in and washout, whilst avoiding affecting the temperature, oxygenation or disrupting the tissue.

A further major challenge was to electrically stimulate tissue slices reliably. Although it was possible to stimulate tissue through the array recording electrodes, these are very small (60μM diameter) and thus the current load possible was similarly small. Ensuring reliable contact with tissue was difficult, and electrical stimulation through the array was not robust. Indeed, on many occasions when stimulation was possible, within a few minutes thresholds had risen above voltages possible to deliver directly via the array system. The iridium-titanium alloy electrodes have a lower resistance and capacitance than standard gold electrodes, yet gold electrodes were available at larger spacings and diameters (100μM). However, electrolysis was often visible at gold simulation electrodes at the voltages required for electrical capture of slices (as evidenced by microscopic gas-bubble formation on the electrodes).

Therefore, an external stimulation electrode was built (by myself) to allow stimulation via an external stimulus isolation unit. A bipolar simulation electrode was built from two short lengths of 500μm-diameter silver wires. These were fixed in epoxy resin and

soldered to shielded cabling. The wires were fixed and stabilised to a plastic housing using epoxy resin, and then acid-cleaned (using 100% acetic acid) and moulded into shape. The housing was itself shielded with aluminium foil, electrically grounded and mounted onto a micromanipulator. This allowed placement of the stimulation electrode anywhere on a tissue slice. Gentle force could be applied to ensure reliable tissue contact.

Simulation was via a stimulus isolation unit (DS-2A, Warner Instruments, MA, USA), itself driven from a Grass S88 Stimulator (Natus Neurology, RI, USA). Initially, outputs were driven via PC control, but pulse timings were found to be unreliable (with an error of the digital-out signal of ±100ms). The S88 unit was used for signal/stimulus control.

2.4.4.4 Tissue slice recording protocol

Sections were placed in the recording chamber and carefully positioned manually so that left ventricular tissue overlay the measurement electrodes. A 1cm diameter metal ring with an overlying nylon mesh (Harp-slice grid, Multielectrode systems) was used to hold the tissue flat in place on the electrode grid and ensured adequate tissue electrode contact. The recording chamber was mounted in the headstage and perfusion commenced at 2mls/min. Tissue was allowed to equilibrate for 1 minute before electrode placement. The bipolar stimulating electrode was carefully lowered to just contact the tissue slice on the left ventricular tissue, but not move the slice on the array. Stimulation was started at 5Hz with a monophasic 1ms pulse, and real-time recording of electrical activity commenced. The stimulus voltage increased until electrical capture was apparent. Usually a tiny manual increase in the pressure of the stimulus electrode on the tissue preparation was necessary to ensure reliable threshold parameters to be

obtained. The stimulus voltage was reduced until electrical capture was lost, the lowest voltage stimulus that could reliably capture was taken as the stimulus threshold. Cardiac signals were recorded at 10kHz. A simulation protocol was performed with steady state pacing at 200ms, stimulation during recording was performed at twice threshold.

Around 30 seconds of pacing activity were recorded for each state for each slice. Perfusate solution containing drugs was washed in over 30 seconds at 20mls/min. Slices were then stimulated at 5Hz for 2 minutes before threshold was determined and recording commenced.

2.4.4.5 Electrogram analysis

The large quantity of data acquired from each tissue slice experiment necessitated further development of electrogram analysis tools building on my experience with human recordings. Electrograms were exported to ASCII format, from which they could be imported into Matlab, specifically via ECGsplitter. Around 20-30 seconds of continuous, high quality signals were selected and exported to a .mat file. I extensively modified code originally written for human electrogram processing to analyse murine signals. As the data analysed was predominantly from steady state pacing, signals were divided into 3-beat sections. Pacing artefacts were identified automatically and used for identification of stimuli. Manual windowing allowed activation time, defined as the most negative downstroke of the electrogram, to be performed. Inconsistent electrograms and those that did not have a clear activation time were excluded.

56 signals were obtained from every activation of each slice. Over a 30 second segment, stimulating at 5Hz, around 9000 signals required analysis. Even with an automated system, this was arduous work to define each activation time from each and every signal. Signal averaging of all signals from a segment was therefore used, and the activation

time was calculated on the averaged signal for each electrode.

Classical measurement of conduction velocity relies on knowledge of the path of activation, in 2D planar surface this can be complex to determine. Another approach is to use the overall activation gradients as measured across the entire tissue. To do this, the overall gradient in activation time was assumed to be able to give a precise time/distance measurement, the inverse of this equates to velocity. A topographical function, gridfit.m, was used to fit a 2D least-squares regression surface to activation time data across the entire electrode array grid (D'Errico, 2010). The activation gradients can be measured at each point of the fitted surface, and the mean of these gradients was taken as the overall mean activation gradient. The inverse of this figure gives a measure of conduction velocity.

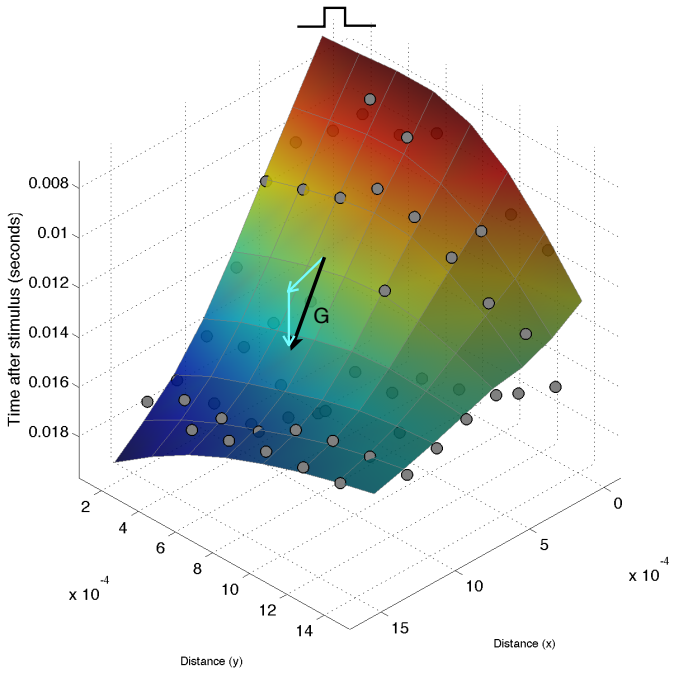

Figure 2-12 Calculation of conduction velocity from regression surface

A typical regression surface used for calculation of conduction velocity is shown. The *x* and *y* axes represent 2D positions. The height of the grey filled circles gives the activation time measured at that location. This *z* axis is inverted (i.e. early activation = high, late activation = low). A regression surface is fitted to these co-ordinates and activation times, which here is colour-scaled to represent activation time (red = early activation, blue = late activation). At any point on this surface, the slope (G,) can be calculated in a Cartesian fashion ($G = \sqrt{(G_x^2 + G_y^2)}$), where G_x is the gradient in the *x* plane and G_y is the gradient in the *y* plane).the inverse of this value (i.e. 1/G) is the conduction velocity at that point. Data presented uses the mean of values from across the entire slice.

Activation time was taken as the time of local activation as measured from the stimulus artefact. Dispersion of activation was defined as the time difference between earliest and the latest activation measured on the array.

2.4.4.6 Future work

MEA high-density mapping on cardiac slice tissue will allow the tissue electrophysiology of the murine slices to be determined. The role of $G\alpha_{i2}$, and how intracellular signalling can contribute to the development of arrhythmia will be observed using restitution protocols and pharmacological intervention, including sympathomimetic (isoprenaline) and cholinergic agents (carbachol).

2.5 Statistical analyses

All statistical computing was performed in R software (R v 2.1.14, R Foundation for Statistical Computing, Vienna, Austria (Team R, 2010)). Continuous parametric data are presented as mean±SD or, in the case of non-parametric data, median [interquartile range], unless otherwise specified. Comparisons in which a single measurement was taken for each subject, e.g. VERP, dispersion of repolarisation time, AG, r^2, MID were made using student's t-test with correction for multiple comparisons. Continuous parametric data derived from electrogram data were modelled using mixed-effects linear regression and statistical significance was inferred from the model (Pinheiro et al., 2009). In brief, models with and without co-variates under examination were compared using ANOVA, a probablitiy of models with and without the covariate being different from one another can be assigned, and the statistical importance of that co-variate inferred. Visual estimates of 95% confidence intervals of the mean for continuous data were constructed using local linear regression (loess function). Quantile regression with bootstrapping was used to compare non-parametric continuous data (Koenker, 2009). 100 bootstrap replications were used. Mixed-effects logistical regression was used to construct predictive models aiming to differentiate RVOTE and ARVC patients based on electrogram data (Imai et al., 2009). Recursive partitioning (a.k.a. classification and regression trees, CART) is a decision-learning technique that enables optimal splits in a group formed on different observations to occur (Therneau et al., 2010). Once a split is made, the same process in run on the child groups until no further gains can be made (hence recursive). This enables discovery of optimum decision strategies and cut-offs rapidly, the outputs are easily understandable and testable. This technique was applied to surface ECG data to determine optimum cut-offs that may enable diagnosis of ARVC from a mixed group of patients. A p value of <0.05 was regarded as statistically

significant.

2.5.1 Power Calculations

ARVC study: Power calculations were performed based on combined definite and probable ARVC against normal patients based on assumed conduction delay data from patients with Brugada syndrome (Lambiase et al, 2009). Assuming a true difference in means between hysteresis in ARVC from controls of 10ms, with a standard deviation of 12ms, 19 patients in each group would have an 80% power to detect a difference between groups with an alpha of 0.95. We were mindful that study numbers would be limited by patient availability and recruitment.

Mental Stress studies: Assuming a ARI of 240±SD of measurements 8ms, 12 subjects will have a 90% power to detect 8ms change and 80% power to detect 7ms true change (Paired data).

Murine study: This was an exploratory study generating pilot data; therefore power calculations were not formally developed. Previous studies had shown marked differences in ERP parameters using 6 animals in each group (e.g. Zuberi et al. 2010) and this was used as a basis to plan experiments.

Chapter 3 RESULTS: One-dimensional cable theory, combined mapping and modelling study

3.1 Introduction

Functional block and wavebreak are necessary events in triggering and sustaining the development of chaotic human arrhythmias, particularly VF, the rhythm underlying the majority of sudden cardiac death (Chow et al., 2004). Large quantities of theoretical data exist, seeking to explain how interactions between activation and repolarisation may explain development of functional block in the absence of overt pre-existing heterogeneity of conduction. Notably, one-dimensional fibre models have been used to explain "at-a-distance" functional block, i.e. how an activating wavefront may impinge upon a prior wave of activation (Otani, 2007; Gilmour et al., 2007). These frameworks incorporate activation potential duration (APD) restitution, describing the shortening of the action potential with decreasing of the diastolic interval following the previous beat, and conduction velocity restitution, the slowing of cell-cell conduction with shortening of diastolic interval. Such a model recently underwent a qualitative validation by Gelzer et al (Gelzer et al., 2008), where it was used to predict whether combinations of up to 5 extrastimuli could initiate VF in a canine model.

A major criticism of this approach has been the question of relevance of models derived from single fibres to the behaviour of the entire in-vivo human heart, and thus whether such models could be relevant to clinical practice. Although one-dimensional models offer simplicity and allow a clear understanding of the passage of a wavefront along a defined pathway, cardiac tissue tends to act as an electrophysiological syncytium in three dimensions. However, single-fibre models can potentially obviate the need for knowledge of the precise conduction pathway through 3D tissue, an advantage when considering that pathways of activation remain impossible to define accurately *in-vivo*. If an assumption of constancy of activation path is made, then a 1-D model should be

useful in predicting boundary conditions for functional block along that path. Few practical solutions to the integration of directly recorded electrophysiology into computer simulations have been proposed. A robust method for building such 1-D models from patient-derived data presents an avenue whereby simulation may be used for clinical benefit e.g. risk stratification, diagnosis or quantitative assessment of electrophysiology substrate behaviour (e.g. advanced electrophysiological phenotyping).

Action potential restitution has been extensively described, theoretically, experimentally and clinically. But few studies have approached APD restitution in the context of in-vivo repolarisation time, and the cumulative effects of conduction delay and APD restitution on the whole human heart has not been approached. Descriptions of the effects of APD and conduction velocity restitution interactions on repolarisation times remain superficial, yet a firm grasp of such interactions is necessary for comprehensive understanding of arrhythmogenisis.

Data acquired from human electrophysiological studies was integrated into one-dimensional models, and this approach validated by testing whether responses to sequential premature stimuli could be predicted in a quantitatively accurate manner. This serves as a validation of the clinical relevance of activation-repolarisation interactions. This chapter then describes how such a technique can be used to predict functional block, and suggest a methodology by which the boundary conditions for at-a-distance block can be derived. Finally, the experimental paradigm allowed examination and prediction of the behaviour of cardiac activation and repolarisation at sites close to a stimulus. This addresses issues raised from previous studies into modulation of dispersion of repolarisation in humans.

3.2 Results

3.2.1 Patient Demographics

11 patients were enrolled in the study, aged 29±10 years, 7 female. All patients had structurally normal hearts on echocardiography, and underwent EP studies for symptoms consistent with paroxysmal supraventricular tachycardia. Final diagnoses were atrioventricular re-entrant tachycardia (5 patients), paroxysmal atrial fibrillation (1). No arrhythmia was induced in 5 patients. Six of these patients underwent S_3 studies and were included in the S_3 validation.

3.2.2 Activation time, ARI restitution and Repolarisation Curves

The dynamics of how activation time, ARI, repolarisation time (RT) and diastolic interval (DI) varied with the coupling interval of the first extrastimulus were examined. This is illustrated in Figure 3-1. Note that these are represented against coupling interval to enable unbiased comparison between measures, rather than against diastolic interval (as is standard convention with ARI/APD restitution curves).

As coupling interval decreases from steady state, ARI restitution is observed, and both ARI and repolarisation time shorten. But as coupling intervals shortened further towards ERP, the effects of conduction velocity restitution became apparent (as illustrated by increasing activation times). This prevents further decrease in local diastolic intervals, and hence ARI restitution is restricted. The local repolarisation time effectively represents the cumulative effect of ARI and conduction velocity restitution; together these produced a distinctive repolarisation time curve illustrated in Figure 3-1.

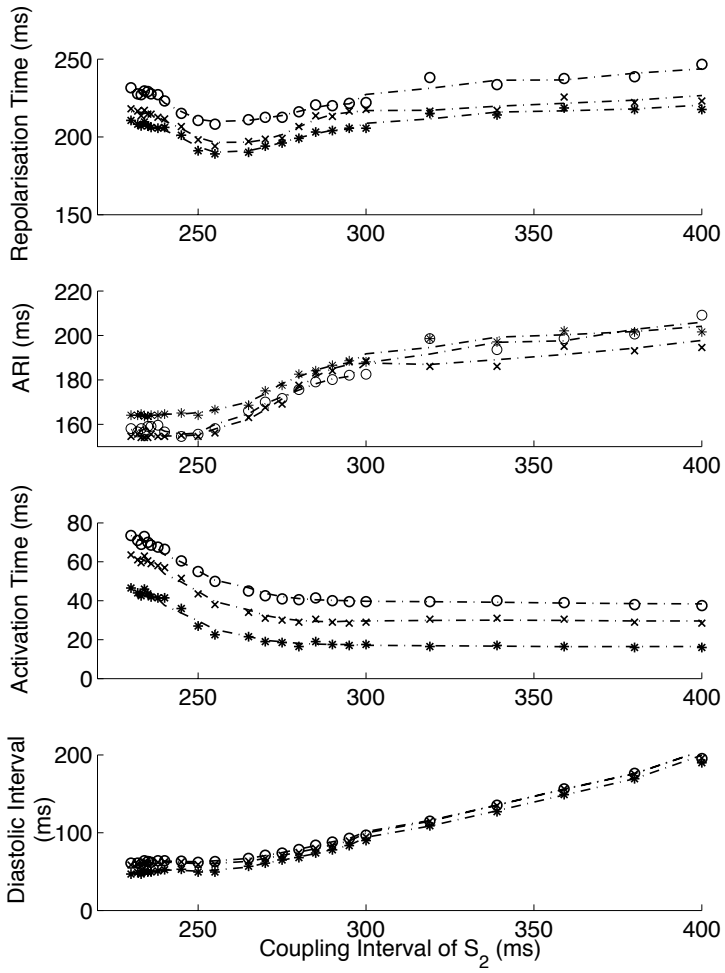

Figure 3-1 Interactions of Activation, ARI and DI leading to repolarisation dynamics

The responses of diastolic interval (DI), activation time and ARI to shortening coupling interval are shown, with the overall repolarisation time dynamic shown in the top panel.

As paced intervals decrease, diastolic intervals decrease initially in a linear fashion (bottom panel). The reduction in DI is associated with a non-linear reduction in ARI (restitution). As coupling intervals become very short, activation time increases due to the effect of conduction velocity restitution acting between the stimulus site and the recording electrode.

Activation time increases prevent further reduction of local diastolic interval (bottom panel), which is seen to level off. ARI restitution is blunted at these short coupling intervals. Repolarisation time thus increases because of increasing activation times.

Representative patient data from RV (Star– early activating site, cross- mid activating site, circle- late activating site, dotted lines represent smoothed dynamics).

3.2.3 Model fitting to S_2 data

One-dimensional models were fitted to clinically acquired S2 data in all 11 patients using the recursive method described in section 2.2.2. ARI restitution curves were accurately described by a simple exponential model (Coefficient of determination, r^2 =0.966 [95% Confidence Interval 0.963 – 0.968], p<0.0001). Activation time curves were similarly accurately reproduced following our derivations of conduction velocity restitution, (r^2 = 0.993 [0.992 – 0.993], p<0.0001).

3.2.4 Activation times following sequential premature stimuli

To show that prediction of activation times following sequential extrastimuli was a reasonable standard by which to assess the accuracy of our model, we compared the activation dynamics following S_2 and S_3 stimuli. At similar coupling intervals, AT following a premature S_3 was significantly shorter than after an S_2 (AT normalized to steady state: 1.1 following S_3 (95% confidence interval 1.1 – 1.2) vs. 1.6 following S_2 (1.5 – 1.7), p <0.0001). ERP of S_3 was shorter than ERP of S_2 (<186±8 vs. 222±25ms, p<0.0001). More activation delay existed after an S_3 pre-ERP than after an S_2 (39±28 vs. 33±16ms, p =0.0003). Activation dynamics were thus significantly different following S_2 and S_3 stimuli, with the ERP of an S_2 considerably shorter than that following the steady state beats.

3.2.5 Validation of 1D models

We tested whether the one-dimensional model, incorporating both ARI and CV restitution, could explain and predict the observed variation in activation dynamics following S_2 and S_3 stimuli. This serves as a quantitative validation of the 1D model incorporating CV and ARI restitution. Validation was performed using data from 6

patients who underwent S_3 protocol. The coefficient of determination (predicted values vs. measured), R^2, was 0.902 [95% Confidence Interval: 0.890 – 0.911] ($p<0.0001$, Figure 3-2). The high predictive accuracy possible with this method serves as a quantitative validation of this one-dimensional model of cardiac activation in human hearts.

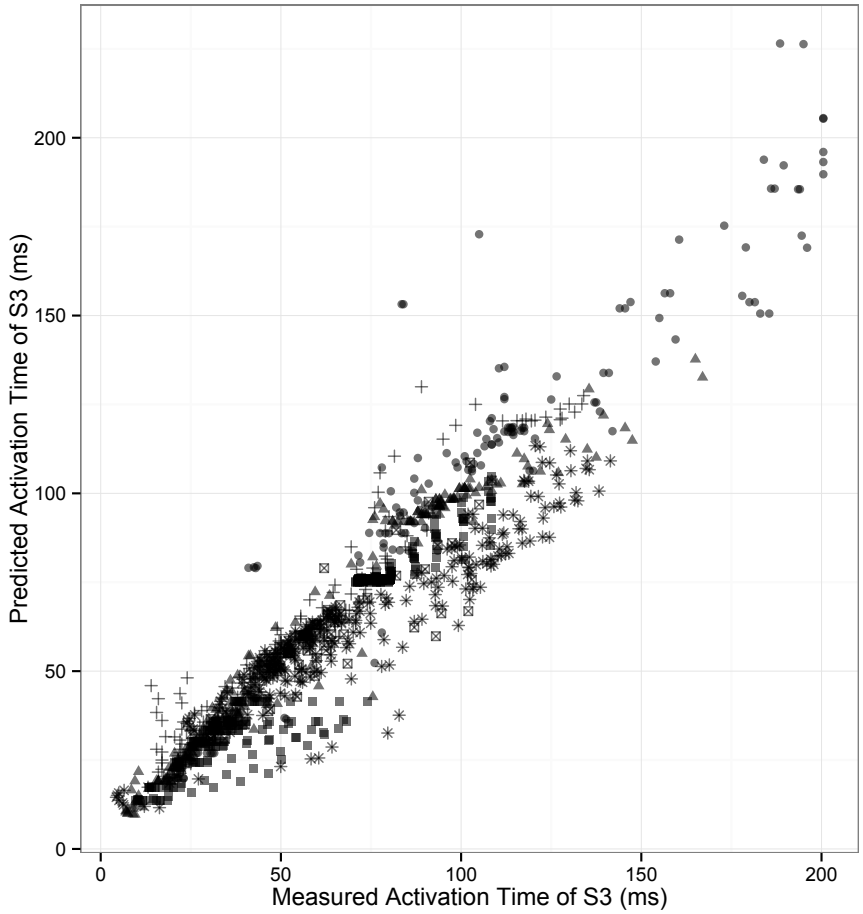

Figure 3-2 Correlation of observed and predicted activation times following a second extrastimulus

The correlation of modeled S_3 activation time with measured S_3 activation is shown. Each patient is represented by individual symbols. $r^2 = 0.90$.

3.2.6 Simulating modulation of dispersion of repolarisation

Simulations based on patient data enable examination of electrophysiology which otherwise remains impenetrable through traditional experimental methods. We examined how dispersion of repolarisation varied with shortening of S_2 coupling

interval. True dispersion of repolarisation, the difference from the earliest repolarisation to the latest repolarisation, has both a spatial and temporal component. It is very hard to measure repolarisation time accurately very close to the stimulus site due to stimulus artefact. But the most significant repolarisation gradients will be close to the stimulus site following a close-coupled S_2; the area immediately at the stimulus site is exposed to very little delay prior to activation, whereas further sites only a very short distance away experience significant activation delay. A patient-based simulation allows appreciation of these gradients (Figure 3-3). In the example shown the dispersion of repolarisation increased from 41ms to 70ms between mid to late activating sites, yet increased fourfold from 25 to 100ms between earlier activating sites. Thus the induction of repolarisation gradients by premature stimuli occurs very close to the stimulus site.

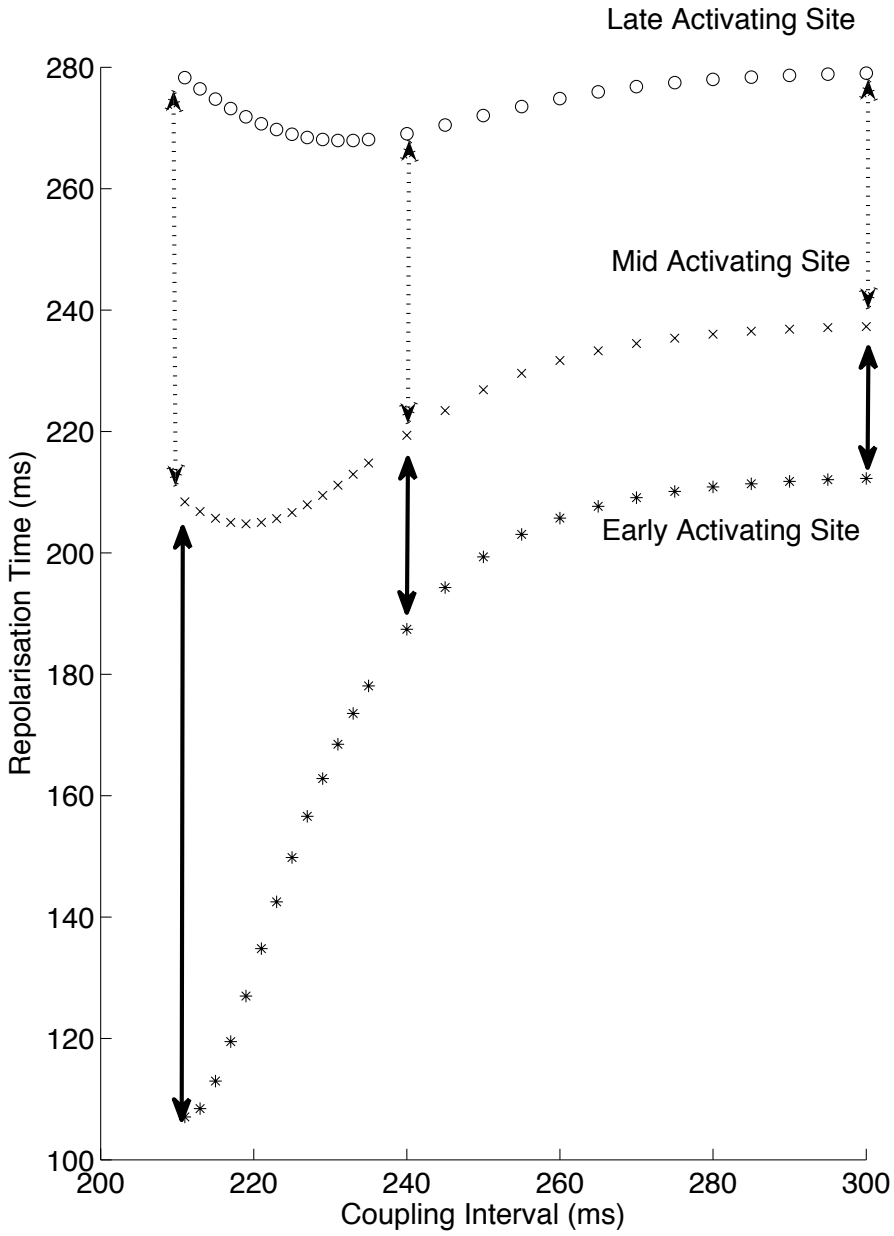

Figure 3-3 Increase in dispersion of repolarisation with decreasing coupling intervals

Repolarisation times from 3 sites are shown against coupling intervals. The early activating site can be considered equivalent to the stimulus site, and is not measured clinically due to artifact. This early site is exposed to only minimal activation time increase at short coupling intervals, thus the repolarisation time is approximately equal to the ARI at this site. The mid and late activating sites do exhibit an increase in dispersion of repolarisation (broken arrows), but this is minor in comparison to the increase from the early to mid site (solid arrows). Thus, there is a marked spatial increase in the repolarisation gradient near the stimulus site following premature extrastimuli.

3.2.7 Validation of repolarisation time predictions against ionic cellular simulations

Repolarisation times of S_3 responses are difficult to measure experimentally, the induced conduction delay with close coupled beats leads to repolarisation of early-activating sites occuring at a similar time to distant site activation. This makes interpretation of the small repolarisation currents almost impossible to reliably distinguish from the unipolar electrogram. Therefore, we validated whether our S_3 repolarisation predictions would be valid by comparing them to the dynamics of simulations of repolarisation produced using the Ten-Tusscher cardiac cell model. For S_3 responses, there was close agreement between repolarisation times determined from our model and repolarisation times acquired using the ionic model (Figure 3-4, coefficient of determination, $r^2 = 0.997$ [95% Confidence Interval 0.993 – 0.999], $p<0.0001$). This supports the validity of our model in comparison to full ionic cellular models undergoing sequential premature extrastimuli.

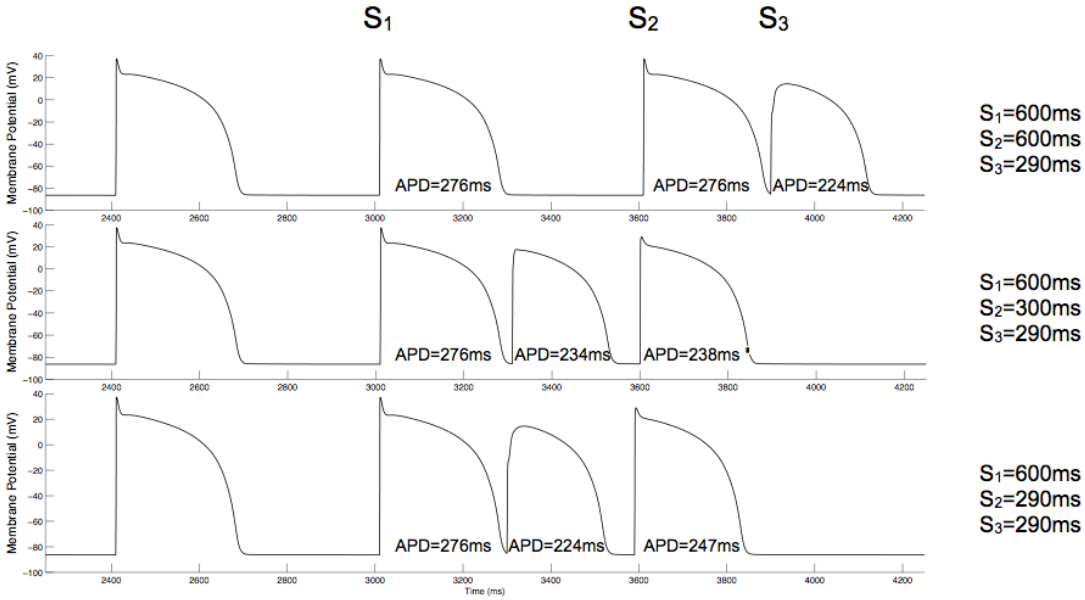

Figure 3-4 Examples of ventricular action potentials from ten Tusscher model, used for validation of S_3 APD restitution

Examples of action potentials used for validation of S_3 APD prediction. APD = Action potential duration.

3.3 Discussion

Using a combination of physiological measurement and simulation, this study demonstrates that the complex dynamic interactions between activation and repolarisation induced by sequential extrastimuli can approximated in terms of ARI (APD) and CV restitution. This serves as a strong validation of a personalized computational approach incorporating biologically acquired variables and it serves as an extension and validation in humans of previous animal work (Gilmour et al., 2007). Our technique provides a platform by which individual patient data may be incorporated into computerized simulations and serves as an example of a method by which the gap between fundamental cardiac simulation and clinical science can be bridged.

This study is the first to quantitatively validate a one-dimensional model of cardiac conduction in man. Such patient-based models provide a method by which physiologically acquired data may be interrogated in a computerized simulation. We have shown that endocardial physiology can be adequately modelled by simple mathematical descriptors of CV and ARI restitution curves, and confirm the relevance of one-dimensional conduction models incorporating both these features to human cardiac electrophysiology. Our validation of a straightforward one-dimension model can allow further in-depth examination of human physiology in a manner that would not be possible experimentally, for both ethical and practical reasons.

The presented modelling is founded on the work of Otani, Gilmour and Fox (Otani, 2007; Fox et al., 2003; Gilmour et al., 2007; Gelzer et al., 2008; Gelzer et al., 2010). Seminal work by this group, along with the single fibre models of Cherry & Fenton (Cherry and Fenton, 2004; Cherry and Fenton, 2007), provided initial validation of the use of one-dimensional conduction simulation in biological systems. The ability of

such a model to predict whether large variations of long-short CIs would induce VF in normal and cardiomyopathic canines was a powerful demonstration of the physiological relevance of such simulations (Gelzer et al., 2008; Gelzer et al., 2010).

We have enhanced these models by fully deriving CV restitution; allowing better approximation to the actual behaviour of the activation wavefront and observation of the heterogeneity introduced by sequential extrastimuli. This adds to our earlier description of the modulated dispersion of repolarisation in humans (Hanson et al., 2009), and addresses questions rising from this work (Poelzing and Rosenbaum, 2009). CV restitution is often assumed to operate over the entire conduction path in a similar manner, obscuring the importance of the spatial differences in CV restitution. Our validation also sought a high fidelity correlation of activation times rather than a binary outcome. The large datasets acquired from the multiple recording electrodes used in each patient (rather than only one in the canine studies) enabled an accurate validation of this concept in humans.

The degree of latency has been described as being important in determining the initiation of VT or VF due to programmed electrical stimulation in earlier clinical studies (Avitall et al., 1992), yet the mechanism of this has been unclear. Our explanation of CV restitution, and of a mechanism by which cumulative interactions can set up conduction heterogeneities is consistent with these previous descriptions.

Knowledge of these timing dynamics may help determine susceptibility to arrhythmia in channelopathies (Nam et al., 2010; Lambiase et al., 2009) or a suspected cardiomyopathy. The demonstration that patient-specific modelling can predict initiation sites of clinical arrhythmia underlines the importance of ARI and CV interactions in human arrhythmogenisis.

Of interest is the variation between our predicted/modeled dynamics and those observed. Although we achieved a very good agreement, it was not perfect. Indeed the error between prediced and observed behaviour appeared to differ to some degree between individuals. This may be explained to a degree by the sequential nature of the data collection. The complex nature of the biological phenomenon that we are trying to observe is more likely to be important in producing the error. Several things could affect this, autonomic change being one of them. Furthermore, ion channel dynamics and cell activation dynamics will only be approximated by exponential mathematical functions: even when we show such apparently excellent agreement between these descriptions and the measured results. As such, this apparent limitation serves to highlight the importance of obtaining biological data experimentally; rather than only relying on simulation to predict experimental responses.

3.3.1 Study Limitations

We used clinically acquired data to observe and explain the complex interactions seen following sequential extrastimuli. These are considered central to the initiation of cardiac arrhythmia. We did not expect to, nor did we induce arrhythmia in any patient undergoing prospective evaluation, and the contribution of these mechanisms in clinical arrhythmogenisis was not fully examined. Prospective patient data was acquired from contact electrodes; simultaneous mapping from the entire endo- and epicardial surface is unfeasible in conscious patients. However, as a result of lack of 3D geometry, conduction path distances were derived from timing data and knowledge of electrode spacings. The demonstration that these techniques can effectively predict wavebreak and arrhythmia initiation requires confirmation in prospective studies.

By design, our modelling and simulation was relatively simple and was limited to a

one-dimensional system. This did not allow examination of wavebreak, arrhythmia development or re-entry, & observations are limited to assumptions of homogenous properties. The APD and CV restitution models used in this paper are in the form of exponential equations, this assumed behaviour is based on the tendency of experimental data and on equations used in previous studies. Biological behaviour would be expected to deviate from these simple exponential models, which in turn will result in discrepancies between simulation and clinical measurement. The use of derivations allowing direct fitting of ionic models to clinical results, perhaps by using an iterative approach, will improve the fidelity of such patient-derived simulations.

The success of our model at predicting local activation times following an S_3 stimulus makes it tempting to assume that it will retain predictive accuracy for S_4, S_5 and so on. This is unlikely. Though the principles demonstrated remain valid, our model did not include myocardial memory effects, post-repolarisation refractoriness or anisotropy. These may have increasing importance with longer extrastimuli sequences, and ARI restitution dynamics may change significantly as a consequence of these (Shimizu et al., 2000; Kobayashi et al., 1992). Despite a very high agreement in predicting S_3 ARI restitution obtained from a complex ionic model, even these ionic models may still not fully reproduce these less studied phenomena. However, our model's simplicity made it accessible to the incorporation of clinical data, and the robust prediction and demonstration of S_3 wavefront dynamics (which do not require knowledge of S_3 ARI restitution) remains impressive.

3.3.2 Future studies

This study provides important information to assist electrophysiological characterisation of myocardial diseases and phenotypes. Some of the techniques we describe may be

applicable to clinical practice e.g. determining an individual patient heart's boundary conditions for functional block as a method for arrhythmic risk stratification. All data was acquired in patients with normal hearts under baseline conditions. Further studies should examine the modulation of changes in conduction/repolarisation interactions under conditions of autonomic stress or drug interactions. More complicated models, such as those based on ionic cellular models could be applied to the data, possibly using our method as an intermediary step to allow parameter fitting. This could produce more detailed and realistic simulations, extending the described parameters into 3 dimensions. Furthermore, new technologies such as non-invasive body surface mapping may allow acquisition of whole heart activation and repolarisation dynamic data.

Specific future uses of the described method may have an early application in patients at risk of inherited ventricular arrhythmias, particularly Brugada syndrome or arrhythmogenic right ventricular cardiomyopathy (ARVC). Both of these conditions have well described changes in invasive electrophysiology, yet risk stratification is incomplete. Patient specific models could give valuable diagnostic information & help quantify the risk of arrhythmia in such patients. Pharmaceutical testing may also benefit from such analysis, as a method to determine arrhythmogenicity of subtle changes in electrophysiological responses after drug challenge. Furthermore, a bullish use of this method would be as an adjunct in early clinical assessments of new anti-arrhythmia agents, to lend support to an investigational compound's antiarrhythmic properties, or otherwise.

We have further studied a series of patients with restitution curves performed before and after Ajmaline challenge to induce sodium channel blockade. This data remains to be analysed, 12 lead ECG changes in sinus rhythm will also be related to underlying

electrographic and electrophysiological parameters.

3.4 Conclusions

Conduction and repolarisation interactions in humans can be described in terms of restitution of CV and APD. Simulations based on clinically acquired data can be used to successfully predict complex activation patterns following sequential extrastimuli. Such modelling techniques may be useful as a method of incorporation of clinical data into predictive models

Chapter 4 RESULTS: Acute mental stress significantly alters activation and repolarisation dynamics towards a pro-arrhythmic state

4.1 Introduction

The ability of conscious mental activity to influence the risk of cardiac arrhythmia has been well recognized, and is illustrated by numerous striking observations illustrated previously (1.5 above). Controlled data have showed ICD shocks to be temporally associated with periods of mental stress (Lampert et al., 2009; Abisse et al., 2011). In a series of elegant studies, mental stress induced by standard psychometric tests increased T-wave alternans and arrhythmia threshold in series of ischemic heart disease patients with implantable cardioverter defibrillators (Lampert et al., 2007; Lampert et al., 2009). Furthermore, previous works have also documented increased arrhythmogenicity in animal models during mental stress (Krantz et al., 2001). These studies have confirmed a clear link between conscious activity and the risk of arrhythmia, but there are few data documenting the direct effects of such activity on cardiac ventricular electrophysiology.

Taggart et al. demonstrated the shortening of the activation repolarisation index (ARI), a well-validated surrogate of action potential duration (APD) in human ventricles in response to isoprenaline (Taggart et al., 2003). A steepening of the ARI restitution was also observed, which may imply an increased susceptibility to arrhythmia. Human work into these effects has been very limited, though. It has been hypothesized that mental stress can contribute to arrhythmia by increasing heterogeneities of repolarisation and activation (or conduction velocity) throughout the heart. These effects may thus amplify pre-existing heterogeneity, for example due to ischemic heart disease or cardiomyopathy, and thus predispose to conduction block, conduction wavebreak and arrhythmogenisis. But currently no evidence exists for pro-arrhythmic changes in any directly measured cardiac electrophysiological parameter in conscious humans during mental stress.

We hypothesized that mental stress would induce pro-arrhythmic changes in cardiac electrophysiology by increasing heterogeneity of conduction and repolarisation in the heart. We tested this by performing electrophysiological studies on patients with apparently normal ventricles during rest and during a controlled mental stress.

4.2 Chapter Aims

This chapter aims to demonstrate alterations in activation and repolarisation dynamics induced in a physiological manner i.e. with induced mental stress.

The specific hypotheses to be addressed are:

- Modulation of activation and repolarisation dynamics occurs as a result of changes in constitutive autonomic tone.
- Such changes in activation and repolarisation dynamics may predispose to arrhythmia.

4.3 Results (Mental Stress)

4.3.1 Patient population

16 patients were enrolled (12 female, 4 male, median age 34 [range 22-64]). Four patients did not undergo full restitution stimulation protocols and results are presented from 12 patients (9 female, 3 male) who completed at least one mental stress protocol satisfactorily.

Final diagnoses were:

Atrioventricular nodal re-entrant tachycardia (7 patients)

Atrioventricular re-entrant tachycardia (3 patients)

No inducible arrhythmia (2 patients, i.e. Normal EP study)

4.3.2 Efficacy of mental arithmetic on induction of mental stress

All twelve patients reported low stress during the relaxation protocol (2.4±0.7, 1= no stress at all, 10 = most stressed possible) and raised stress during mental arithmetic (7.1±0.7, $p < 0.01$). Objective measures of stress induction included an increase in the sino-atrial rate and an increase in blood pressure (Figure 4-1).

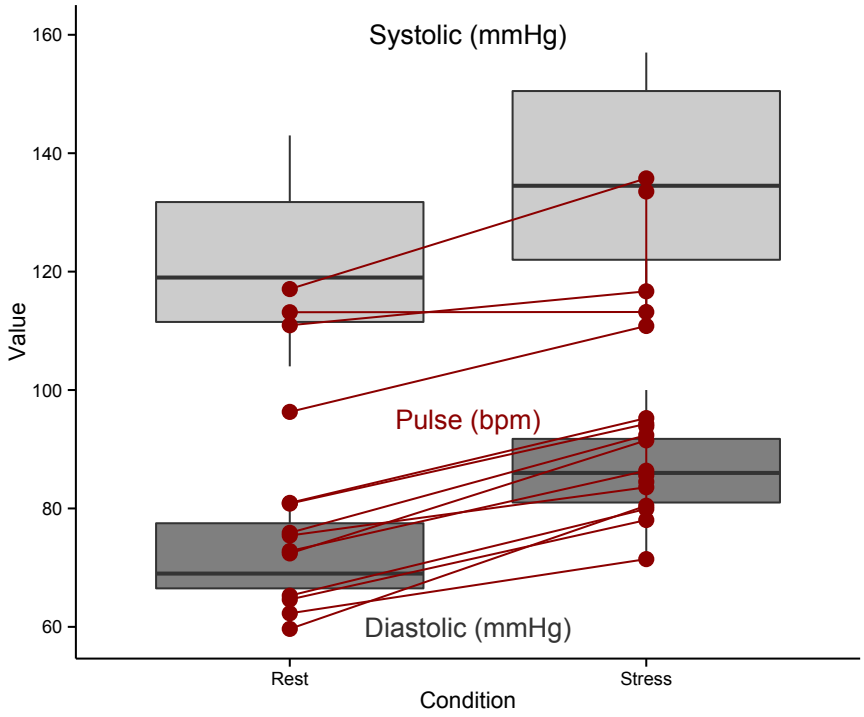

Figure 4-1 Induction of mental stress: non-invasive indicators

Blood pressure and pulse rate (as inverse of RR interval) were measured between episodes of ventricular stimulation. Diastolic & systolic pressures and pulse rate rose with induction of mental stress. Data from maximal stress is shown. Red dots represent paired patient measurements of heart rate. Box plots represent blood pressure measurements.

Serum catecholamine measurements were attempted, but two attempts at assays (performed in the clinical biochemistry laboratory at The Royal London hospital) were unsuccessful. The primary (A) sample test failed due to a technical error in the mass spectroscopy process. A secondary (B) sample was subsequently attempted, but noradrenaline and adrenaline levels were below test sensitivity levels in the majority of samples.

4.3.3 Mental stress reduces steady state conduction times

Measurements were collected across all catheters. Activation times, measured as the time from pacing artefact to local activation, were reduced in the RV 6±5% ($p < 0.01$) and by 2±7% and 2±5% in the LV and epicardium respectively (p= n.s.). Multi-level regression models were employed to investigate whether the apparent reductions in

activation time were due to increase in conduction velocity or reduced latency at the pacing site. Reductions in activation time with mental stress did not interact with the measured steady-state activation time (a surrogate measure of distance from stimulus site, Pearson's coefficient $r^2 = 0.002$ [95%Confidence Interval -0.02, 0.02, p>0.9]). This implies the reduction in activation times occurred close to the pacing site, rather than along the entire conduction course.

4.3.4 Steady State ARI is reduced during mental stress

In steady state, ARI's were longer in the LV endocardium than in the epicardium (LV: 237±32, Epicardium: 204±30ms, p<0.001) or RV endocardium (206±28ms, p <0.001). A weak correlation between ARI and activation time was observed in the epicardium and RV endocardium (coefficient of correlation $r^{2:}$ Epicardium: -0.06 [95% Confidence Interval -0.09, -0.04], p<0.001; RV: -0.14 [95% Confidence Interval -0.22, -0.06], p<0.01), but not in the LV (0.04 [95%Confidence Interval -0.03, 0.12], p= n.s.).

ARI was reduced during mental stress across all sites (p<0.001), with a greater reduction in the LV endocardium than in the Epicardium or RV (LV: -8.1 [95% Confidence Interval -10.2, -6.0] ms; Epicardium: -5.0 [-5.8, -4.2] ms, p<0.001; RV: -4.2 [-6.3, -2.1] ms reduction in ARI, p<0.001, Figure 4-2 inset). The combined reduction in activation time and in ARI leads to shorter absolute repolarisation times (i.e. the time from stimulus to local repolarisation of tissue at the measurement site), (Reduction in repolarisation time, LV: -10.4 [-16.2, -4.6] ms; Epicardium: -6.8 [-9.0, -4.4] ms; RV: -5.6 [-11, 0.14]; p<0.001 for comparisons with baseline). The greater reduction in repolarisation time seen within the LV reached statistical significance compared to the Epicardium or RV (p= 0.03).

No difference in overall ARI dispersion was observed during mental stress (Rest: 70

[95% Confidence Interval 58-81] ms, Stress: 74 [57-91] ms, p= 0.31). However, mental stress reduced the absolute dispersion of repolarisation during steady state by 14ms [95%Confidence Interval 6,22ms], from a median dispersion of repolarisation at rest of 140ms (p<0.001).

4.3.5 Dynamic changes in AT and ARI during mental stress

Mental stress reduced the effective refractory period (ERP) from 228±23 to 221±21ms (p<0.001), consistent with the reductions observed in ARI.

As coupling intervals of S2 stimuli were reduced towards ERP, a marked increase in activation time occurred in both rest and stress. Despite dynamics being similar, the reduction in activation time observed with stress in steady state was maintained following close coupled premature extrastimuli (mean reduction in activation time at coupling intervals <50ms above ERP = 7.9 [95%Confidence Interval 7.1, 8.7] ms, p<0.001). The degree of reduction in activation time was weakly inversely correlated with the distance from stimulus site, as given by the activation time in steady state (slope = -0.15 [95% Confidence Interval -0.20, -0.11], p<0.001, pseudo-r^2 = 0.15).

4.3.6 Restitution of ARI

The reduction in ARI during mental stress was maintained throughout the restitution curve, as were the regional variations in ARI across the ventricle (Figure 4-2 & example data, Figure 4-3). Marked inter-chamber variability was observed in restitution slopes, with the epicardium exhibiting the shallowest restitution slope (slope [95% Confidence Interval] = 0.55 [0.46, 0.64]), and steeper restitution in the LV endocardium (1.0 [0.81, 1.3], p<0.001) and RV (0.78 [0.56,1.00], p<0.001) all comparisons. Maximal restitution curve slopes (S_{max}) were not significantly greater during stress in the LV endocardium

or RV, but a slight increase in slope was observed in the epicardium (∂S_{max} = +0.07 [95% Confidence Interval: 0.05, 0.10, p<0.01]).

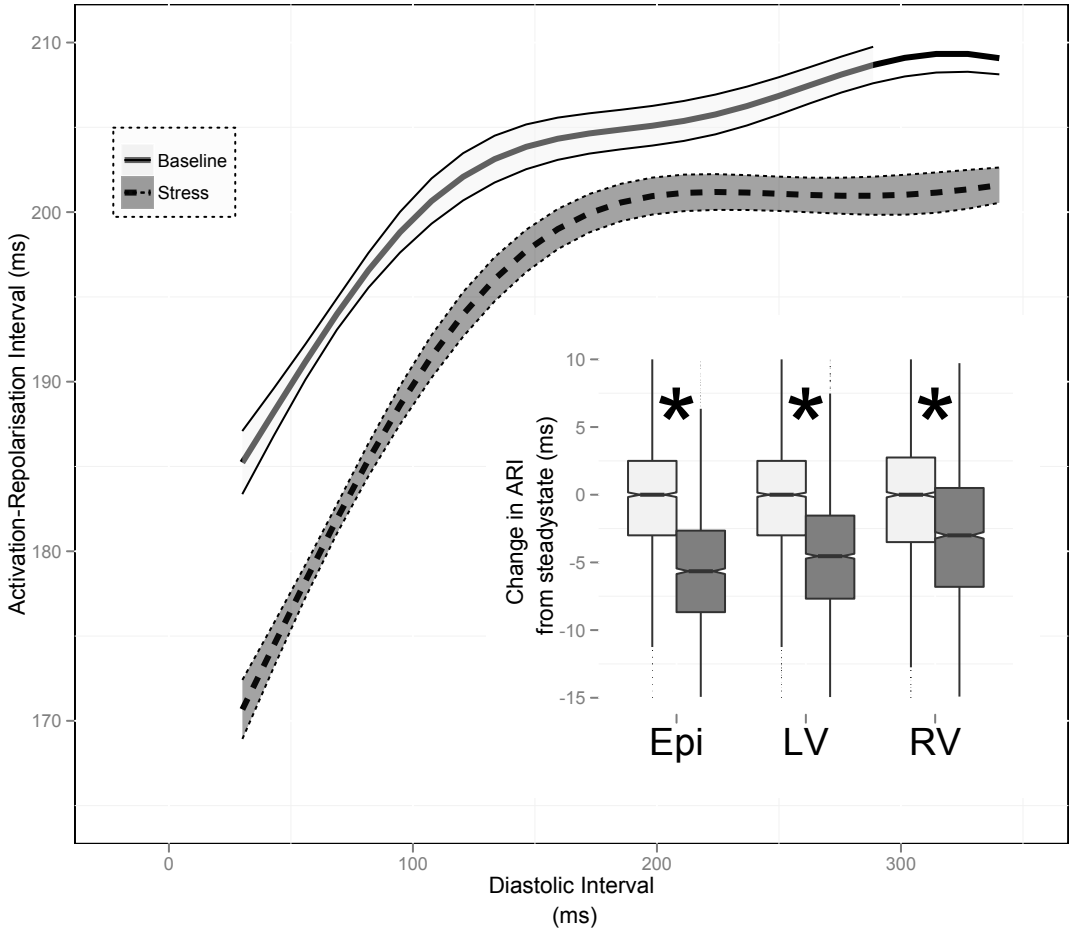

Figure 4-2 ARI and ARI restitution with mental stress

The restitution response of ARI to decreasing diastolic intervals (DIs) is shown (left ventricle data). Combined data is shown using loess regression with shaded band indicating 95% confidence intervals. There is a significant reduction in ARI across all diastolic intervals (p<0.05, by mixed-effects regression). The maximal slope of restitution (Smax) did not appear steeper during mental stress than during baseline conditions. Inset: Changes in ARI from steady state values are shown. All data is normalised to the mean steady state value for each individual electrode site, thereby preserving measurement error. A decrease in ARI in steady state pacing occurred across all sites (asterisk indicates p<0.05).

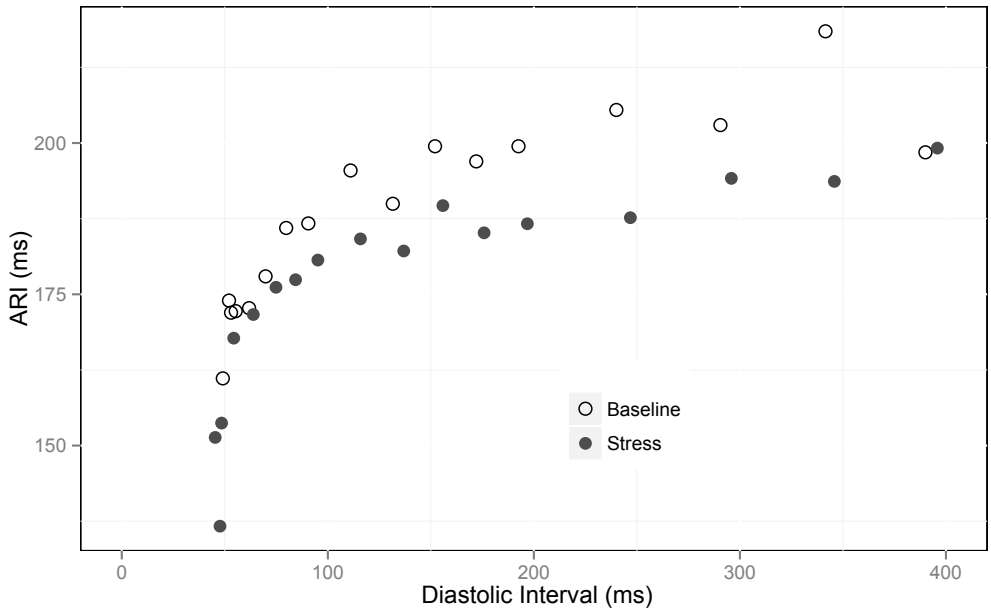

Figure 4-3 Example ARI Restitution Data from Right Ventricle

The restitution response of ARI to decreasing diastolic intervals (DIs) is shown (right ventricle data).

Increases in activation time at short coupling intervals and ARI restitution have a cumulative effect on times of absolute repolarisation across the myocardium. This leads to a distinctive J-shape response in absolute repolarisation time to a reducing coupling interval (as previously observed, e.g. Figure 3-3). The heterogeneity in ARI restitution across the myocardium, coupled with those resulting from mental stress lead to changes in repolarisation gradients across the myocardium (Figure 4-5). These can be expressed in terms of dynamic modulation of dispersion of repolarisation.

4.3.7 Mental stress significantly shortens repolarisation time across all coupling intervals

Decreases in activation time (due to increases in conduction velocity) and shortening of ARI have a cumulative effect on times of repolarisation across the myocardium. The effects of mental stress thus result in a marked decrease in repolarisation time across the myocardium (Steady State: RV 222ms (Rest) vs. 217ms (Stress), LV 310ms (Rest) vs. 305ms (Stress), Epicardium 302ms (Rest) vs. 294ms (Stress). $P<0.001$ all comparisons,

Figure 4-4). As the coupling interval was shortened, relative changes in comparison to steady state persisted, with epicardial changes becoming more marked. The shortening of ARI is the major contributor to this reduction in repolarisation time, and the patterns of repolarisation time shortening reflected those of ARI.

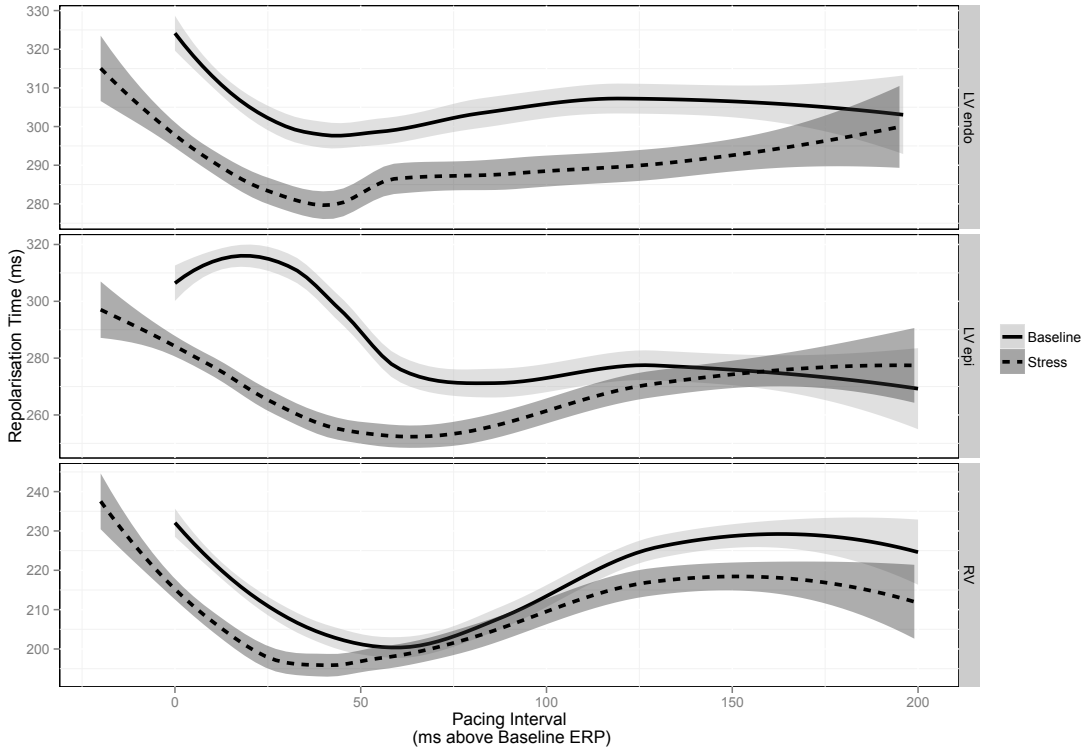

Figure 4-4 Repolarisation dynamics during restitution.

This graph shows decreases in the mean±95% confidence interval repolarisation time in the RV endocardium (RV), LV endocardium (LV) and in the LV epicardium (LV epi). Lines represent LOESS regression. Confidence intervals are represented by shaded areas. To allow comparisons of dynamics from all patients across multiple sites, values are normalised to steady state values in each relevant chamber. Pacing interval is normalised to ERP during active relaxation. Repolarisation time is lower during mental stress throughout all chambers, with variations in dynamics of repolarisation across each chamber.

4.3.8 Alterations in the dispersion of repolarisation

Changes in dispersion of repolarisation in response to stress and to reductions in

coupling intervals were examined. During steady state pacing, no significant change in dispersion of repolarisation was observed across all measured sites, or across the LV/Epicardium, as measured by either the total dispersion (i.e. time difference between earliest and latest repolarisation site) or the standard deviation of repolarisation times (an alternative measure of the dispersion of repolarisation times). However, a sharp increase in dispersion of repolarisation was observed during stress at coupling intervals approaching ERP, this was not apparent at baseline relaxation (Figure 4-5). Dispersion of repolarisation at coupling intervals pre-ERP increased to 126±11% of steady state (±SEM, $p = 0.09$) during stress, but did not increase during relaxation (87±6%). The increase in standard deviation of repolarisation times did reach statistical significance however (122±7% during stress vs. 87±6%, $p = 0.03$).

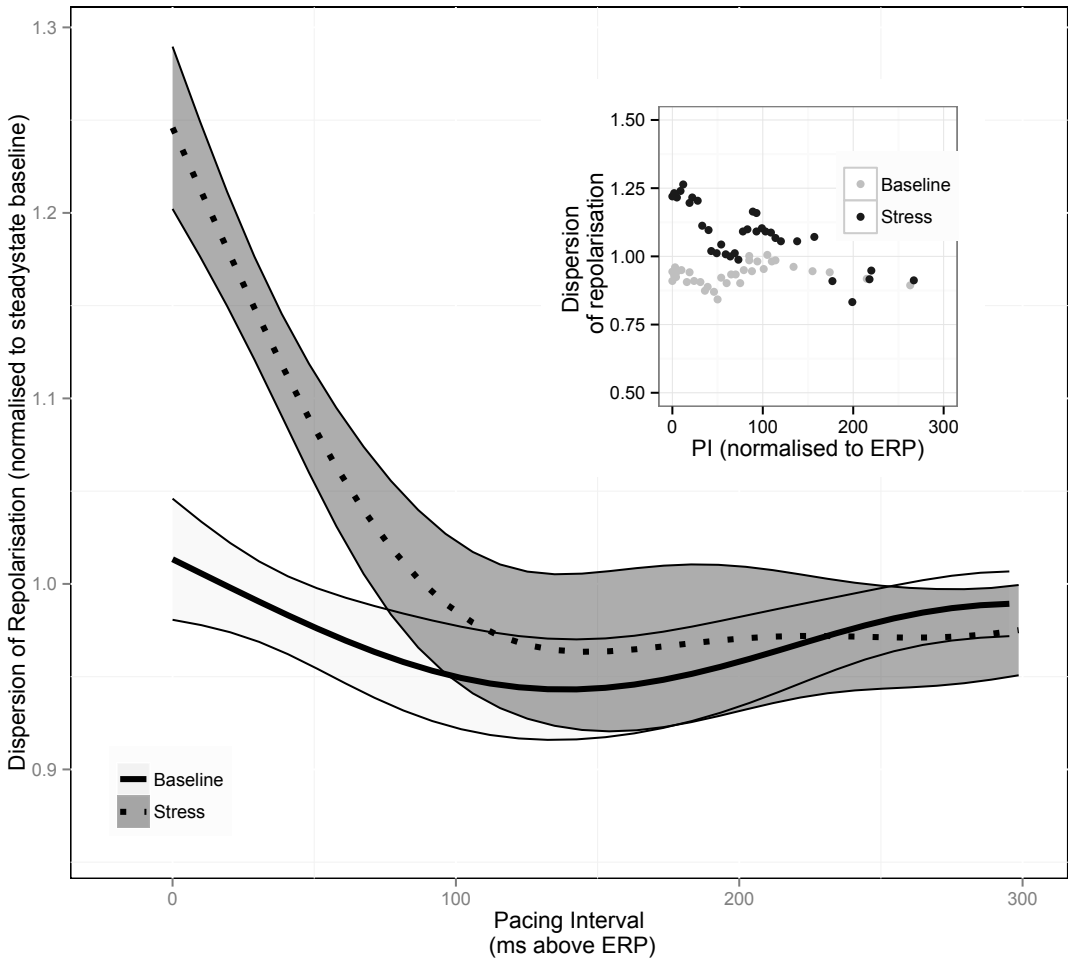

Figure 4-5 Dispersion of Repolarisation

The dynamics of dispersion of repolarisation are shown, normalised to mean dispersion during steady state pacing in baseline conditions. Pacing interval is normalised to ms above ERP. There is a marked increase in the dispersion of repolarisation during stress as pacing intervals approach ERP during stress which is not present at rest. Representative example patient data is shown in the inset.

4.3.9 Arrhythmias associated with mental stress

One patient developed ventricular arrhythmia during mental stress (anger recall stage) following a single short-coupled S_2. The triggering PVC has a near identical morphology to the paced beats suggesting it was arising close to the pacing site, however the onset of the local electrogram of this beat was later than the onset of the surface depolarisation, which would argue against catheter tip pressure as a triggering factor. Arrhythmia did not occur during the relaxation phase at any coupling interval.

No other sustained arrhythmia was observed. No arrhythmia was induced at similar coupling intervals at rest.

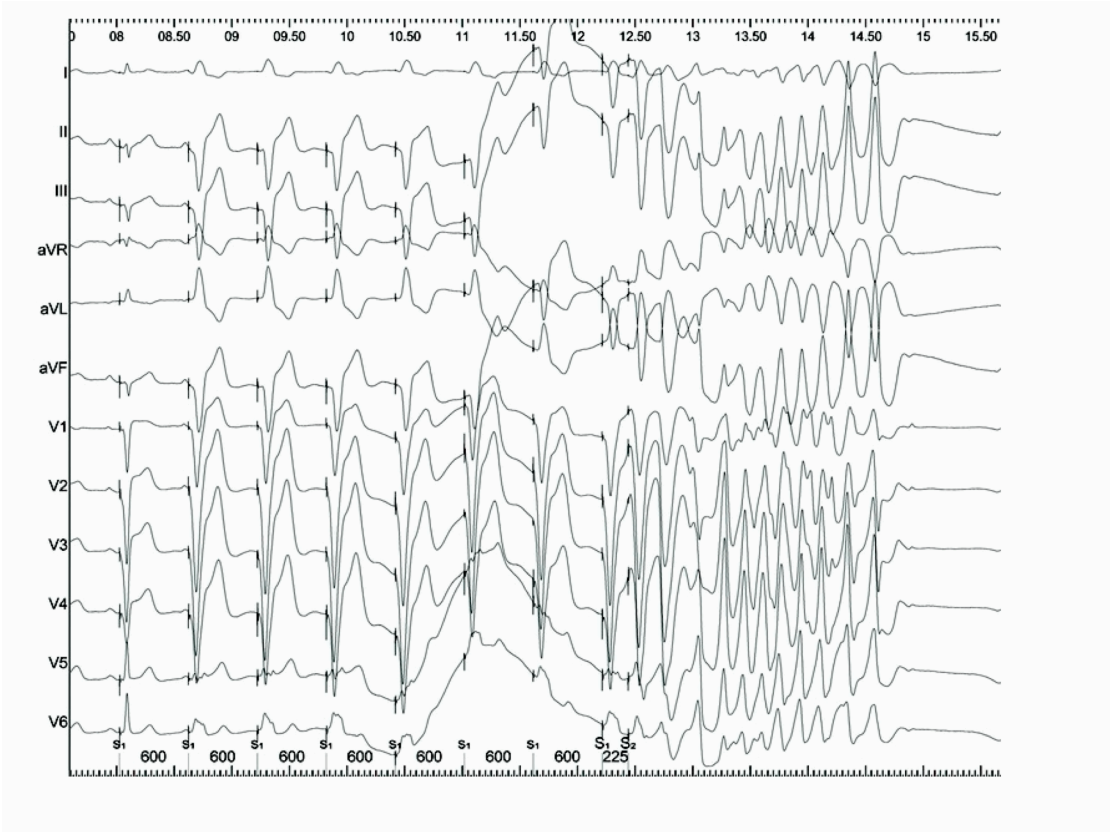

Figure 4-6 Arrhythmia induced during mental stress protocol

An anger recall protocol was being performed, the patient recounting recent disagreements with a work supervisor. Ventricular catheters were placed from the right groin; a small movement of the left leg immediately prior to the S_2 delivery was responsible for the electrical baseline variation.

4.4 Discussion

4.4.1 Principal Findings

In this chapter, alterations in activation and repolarisation in response to induction of mental stress have been demonstrated. Specifically, key findings are:

- Activation times are shortened in response to mental stress, implying increases in tissue excitability or conduction velocity.
- A reduction in ARI occurs in response to mental stress.

This reduction in ARI has a spatial component. It is not uniform across all chambers and predominantly shortens within the LV.

- Repolarisation gradients are dramatically increased following close-coupled extrastimuli during mental stress, but not during rest.
- The steepness of ARI restitution did not change during mental stress.

4.4.2 Discussion of findings

These findings show that alteration of mental state in humans is sufficient to induce changes in tissue level cardiac electrophysiology, and specifically shortening of the cardiac action potential occurs during mental stress, but that the degree of this shortening depends on the location within the heart. A small but statistically significant reduction in activation time indicates that conduction velocity is increased and/or tissue excitability is increased in response to mental stress. Furthermore, these changes have a cumulative effect.

An important and novel finding is that dispersion of repolarisation was markedly increased at short coupling intervals during stress, yet this increase was not seen at

baseline conditions. ERP was reduced during stress, so that the shortest coupling interval possible was shorter during stress than at rest. The short coupling intervals allow access to the right side of the steep conduction velocity restitution curve, thus there is more delay in activation times in stress than in rest. Together with heterogeneity in ARI changes across the heart, this acts to increase the dispersion of repolarisation at short coupling intervals. The decrease in ERP during stress indicates that tissue refractoriness is decreased under stress conditions. This may also impact upon excitability.

This mechanism of increased dispersion of repolarisation secondary to the activation and repolarisation changes induced by autonomic effects provides a plausible explanation for the arrhythmogenic consequences of mental stress. An increased spatial dispersion of repolarisation has previously been shown to be arrhythmogenic in animal and computer models (Antzelevitch, 2008; Gilmour et al, 2007). Pre-existing heterogeneities in repolarisation and conduction (e.g. in the peri-scar region around an old infarct) would be likely to be amplified by autonomic change, and repolarisation gradients thus increased. This mechanism may also play a role in the timing of arrhythmias in inherited arrhythmic syndromes; many of which have well-described autonomic features of arrhythmia predisposition e.g. Increased sympathetic stimulation in LQT type 1 (Akar et al, 2001). The effects of mental stress described here could be sufficient to allow a spontaneous ventricular ectopic beat to initiate wavebreak, re-entry and clinical arrhythmia at a time of very heightened sympathetic drive, whilst appearing benign in resting conditions. This is nicely illustrated here where a single VE with a coupling interval of 225ms triggered VF but the same paced coupling interval with beats triggered from the same site during rest conditions was not arrhythmogenic.

We did not observe a marked increase in the maximal slope of ARI restitution during

mental stress. This is in contrast to the work of Taggart et al, who noted a significant increase in restitution slope during isoprenaline administration in humans (Taggart et al., 2003). Notably, a similar experimental paradigm to this earlier work was used, including the use of ARI as a surrogate for action potential duration and similar baseline pacing intervals. Thus this appears to be a genuine finding, which may be accounted for by the induction of a more subtle increase in intrinsic sympathetic activity through mental stress versus the use of incremental isoprenaline and adrenaline infusions. In these circumstances β-receptor activation is likely to be super-physiological. The physiological induction of sympathetic activity was in the context of preserved parasympathetic activity, thus this work illustrates intrinsic dynamics of repolarisation whilst autonomic regulation is preserved.

Further work on this dataset will concentrate on determining changes in dispersions of activation and repolarisation, in transmural and apical-basal axes as well as across the entire heart. Sinus rhythm ECGs will be compared during rest and mental stress, aiming to relate underlying electrophysiological parameters to the surface ECG changes.

4.4.3 Strengths and Limitations

This study is the first to directly assess human cardiac electrophysiology during mental stress induction. Subjects acted as their own controls, and the use of computer-aided analytic tools allowed large quantities of data to be processed and analysed. Relatively subtle phenomena could thus be confidently observed. Several limitations of this work exist.

Though subjects had structurally normal hearts, these studies were performed on patients just prior to treatment for supraventricular tachycardia. Despite a clinical understanding that these patients have “normal hearts”, it may be that they have an

altered electrophysiological autonomic response. It would be very difficult to ethically perform a similar study on subjects who were not undergoing a medically indicated cardiac catheterisation procedure.

The invasive procedure used to measure cardiac electrophysiology is liable to cause anxiety in itself, however anxiolytic agents would of course be liable to affect the results of the study and make stress induction difficult or impossible. Though the active relaxation protocol was chosen specifically to address this, it is likely a background anxiety remained.

The serum catecholamine assay failure was disappointing. However, the observed increase in sinus rate and increase in blood pressure, as well as the subjectively reported increase in stress during mental stress versus active relaxation allows us to be confident that a level of autonomic response to our psychometric stimulation protocols occurred.

We did not expect to arrhythmia to occur as a result of our protocol during the study, though the observation of an episode of (non-sustained) polymorphic ventricular tachycardia in one patient during the stress protocol lends credence to the assertion that mental stress can be pro-arrhythmic, but can only be viewed as being circumstantial evidence in this case as its reproducibility could not be assessed.

Chapter 5 RESULTS: Arrhythmogenic Right Ventricular Cardiomyopathy manifests as abnormal activation – repolarisation prior to overt disease

5.1 Introduction

Arrhythmogenic right ventricular cardiomyopathy (ARVC) is a primary heart muscle disorder characterised by a high incidence of ventricular arrhythmias. Early in the disease's course, before the classic histological features of right ventricular myocyte loss & fibrofatty replacement become manifest, there is a sub-clinical "concealed phase" (Cox et al., 2011; Thiene et al., 1988b). This presents a major diagnostic and clinical management challenge because arrhythmias and sudden death may arise in the absence of significant clinical and pathological changes. The recent identification of specific desmosomal protein mutations in up to 40% of ARVC patients provides an opportunity to study the pathophysiology of ARVC (Delmar and McKenna, 2010), specifically whether delayed conduction and a pro-arrhythmic substrate occur in the absence of significant fibrosis.

Abnormal desmosomal proteins are known to be associated with reductions in Cx43 (Cx43) expression at the gap junction, this may adversely affect cardiomyocyte electrical coupling. However, there appears to be considerable conduction reserve in ventricular myocardium such that Cx43 reductions of up to 95% reduce transverse conduction velocity (CV) by only 15% and longitudinal conduction by 58% (van Rijen et al., 2004). This has prompted a search for other factors implicated in maintaining conduction reserve, loss of which may exert deleterious pro-arrhythmic effects. It has been posited that desmosomal proteins also directly interact with ion channels at the intercalated disc (Sato et al., 2009; Delmar and McKenna, 2010). Plakophilin-2 (PKP2) and the sodium (Na) channel, Nav1.5, not only interact but reduced PKP2 expression leads to reduced Na^+ current peak density and altered channel kinetics as well as significant reductions in CV in cultured rat neonatal cardiomyocytes suggesting that ion

channel function is disrupted in some forms of ARVC. Recently, our group demonstrated a murine model with conditional genetic deletion of one allele of desmoplakin (DSP) in the adult heart (DSP +/-) shows reduced conduction velocities and increased arrhythmias compared to wild-type (Gomes et al., 2012). This murine model was employed because it results in a clinical phenotype more equivalent to the clinical disease as opposed to transgenic mutant desmoplakin overexpression model which results in a more severe phenotype than that usually seen in patients. Both young (2 month old) and older mice (6 month old) were studied to investigate whether electrophysiological changes occur before overt structural anomalies.

We added to this earlier study by Dr John Gomes, UCL, by comparing the cardiac electrophysiology of patients with known desmosomal mutations (DSP group) but without overt structural disease. We hypothesised that conduction and repolarisation abnormalities may be present despite apparent early disease.

These early manifestations of ARVC pose a significant diagnostic challenge, especially in differentiating benign outflow tract ventricular ectopy from ARVC. This holds significant prognostic implications as sudden death may occur in the concealed phase before structural changes appear (Cox et al., 2011; Thiene et al., 1988b). Although 12 lead ECG anomalies may precede structural changes, these can be transient or non-specific (Quarta et al., 2010). This problem of recognising early ARVC is reflected in recent changes to the consensus diagnostic criteria, which highlight the increasing importance of familial disease and genetic marker (Marcus et al., 2010). Early recognition of disease has potentially important management implications; including avoidance of exercise training, ICD prophylaxis and targeted family screening.

Studies have demonstrated that patients with ARVC exhibit slow conduction within the

right ventricle and low endocardial bipolar voltages, indicative of endocardial scar (Tandri et al., 2009; Corrado et al., 2008). However, these studies all investigated patients with established clinical disease and structural abnormalities & do not represent the more typical diagnostic dilemma of identifying the concealed phase.

We extended our studies on the dynamic conduction and repolarisation differences between desmoplakin mutation carriers and control (Gomes et al., 2012), to compare the dynamic electrophysiological changes in early ARVC versus patients with outflow tract ectopy (RVOTE). In this study we specifically investigated a population including patients who qualify as "definite ARVC" in the modified Task Force Criteria because of a definite family history/mutation carrier status. We thus identified patients with early, concealed non-structural disease.

We hypothesised that patients with early ARVC would exhibit slowing of conduction & repolarisation changes compared to RVOTE patients under conditions of electrical stress, even prior to detectable structural disease being present on conventional imaging. Further, we hypothesized these myocardial electrophysiological changes would manifest on the surface ECG to facilitate the development of a straightforward diagnostic test.

5.2 Comparison of DSP+ patients to controls

5.2.1 Patient demographics and structural abnormalities

The demographics and clinical features of the DSP study subjects are shown in Table 2; mean age was 44(±15) years. These patients had been identified in families with desmoplakin mutations and a diagnosis of ARVC based upon the most recent Task Force criteria (see Table 8-1).

Subject No	Age (M/F)	Mutation	RV Abnormality	T wave inversion	Small QRS	S wave SAECG	NSVT	SVT	PVCs >500/24h	Inducible VT at EP study	FHx	ICD	Criteria Maj/Min
1	43 F	E274f X288	-	-	+	-	-	+	+	+	-	-	+	1/1
2	50 F	S507F	-	-	+	-	-	+	-	+	-	Major	+	1/1
3	61 F	T586fsx594	-	+	-	-	-	-	-	-	-	Minor	+	1/0
4	28 F	T586fsx594	-	-	-	-	-	+	-	-	-	Major	+	1/1
5	72 F	S507F	LVEF 35%	-	-	+	+	-	-	+	-	Major	+	1/2
6	53 F	T586fsx594	-	+	-	-	+	-	-	-	-	-	+	2/1
7	37 M	E274fsX288	-	-	-	-	+	+	-	-	-	+	-	1/2
8	22 M	S922fsX928	-	-	-	-	+	+	-	-	+	-	+	1/2
9	40 F	N408K and R941X	-	-	-	+	+	+	-	-	-	Major	-	1/2
10	33 M	T586fsx594	-	-	-	-	-	+	-	+	-	Major	-	1/1

Table 5-1 Patients studied with Desmoplakin mutations

The patients had well preserved left ventricular function except one subject (no 5) who had an ejection fraction of 35%. No other patients had significant RV or LV wall motion abnormalities meeting Task Force Criteria for ARVC. The 12 control subjects with SVT and structurally normal hearts had an equivalent mean age of 44 (±21) years and sex distribution (3M:9F). (SAECG: signal averaged ECG, SVT: sustained VT, PVC: premature ventricular contraction, VT: ventricular tachycardia, EP study: electrophysiological study, FHx: family history, ICD: implantable cardioverter defibrillator)

5.2.2 DSP+ patients have slowed depolarization of the RV

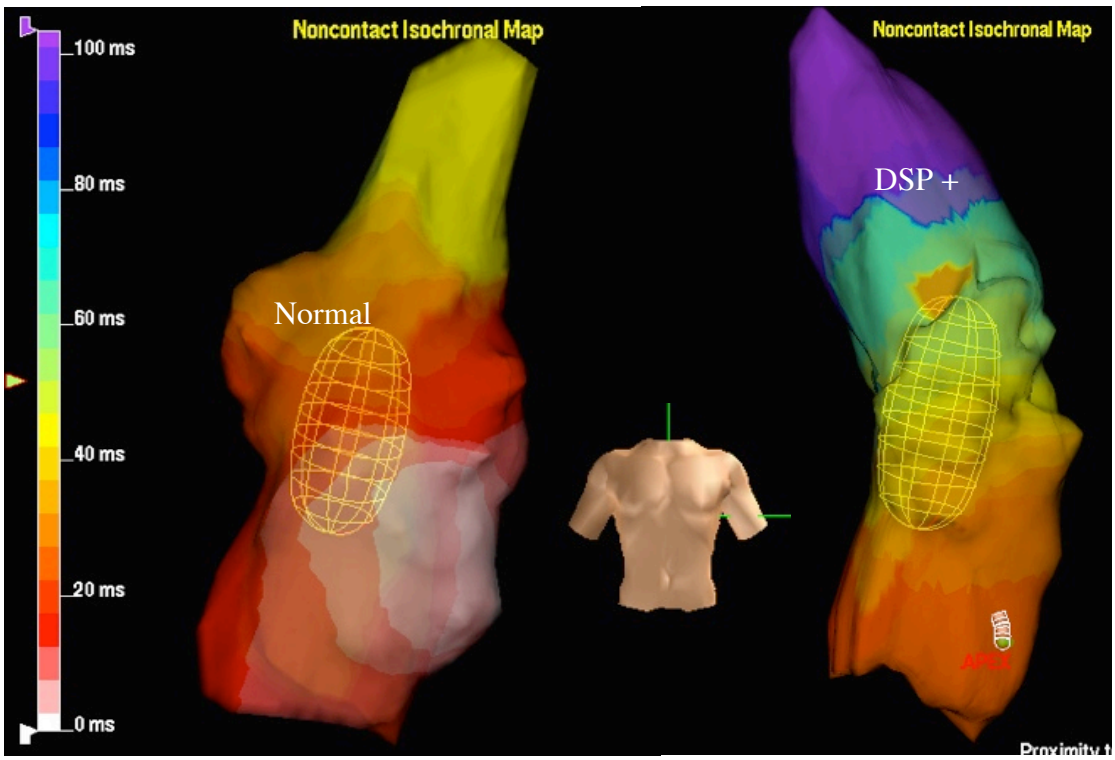

Figure 5-1 Isochronal maps during RV apical pacing

Normal heart is illustrated on left, Desmoplakin on right.

Figure 5-1 illustrates the isochronal maps recorded during RV apical pacing at 400ms obtained from a control and DSP mutation carrier (DSP+) respectively. There are clear differences in depolarization time in the RV between the 2 patients. Overall activation of the RV took almost 2 times longer to propagate across the chamber compared to the control in this example. The isochrones are homogeneously separated in most of the DSP+ RV. However, in the group data mean endocardial activation time in patients with DSP disease was not significantly different from controls either in sinus rhythm (41±8 vs. 40±5 ms in controls) or with steady state RV apical pacing at 400ms cycle length (42±13 vs. 42±8ms). Conduction velocities were assessed, the mean slowest conduction velocity was reduced in the desmoplakin mutation carriers (Figure 5-2), and r2, a measure of heterogeneity of conduction was also reduced compared to normal

controls.

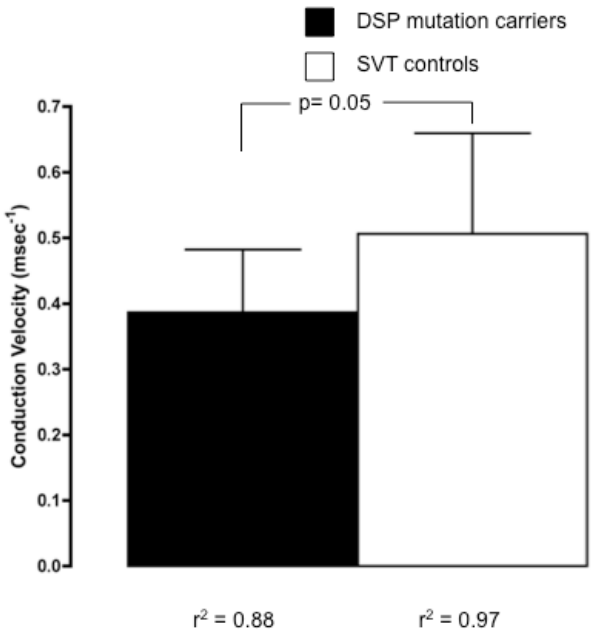

Figure 5-2 DSP mutation carriers have decreased conduction velocities

DSP carriers have a significantly reduced conduction velocity in sinus rhythm compared to normal controls. R^2, a measure of homogeneity of conduction, was reduced in desmoplakin patients compared to controls. (Courtesy Dr E. Ciaccio)

5.2.3 DSP+ patients have increased conduction delay induced by premature stimuli

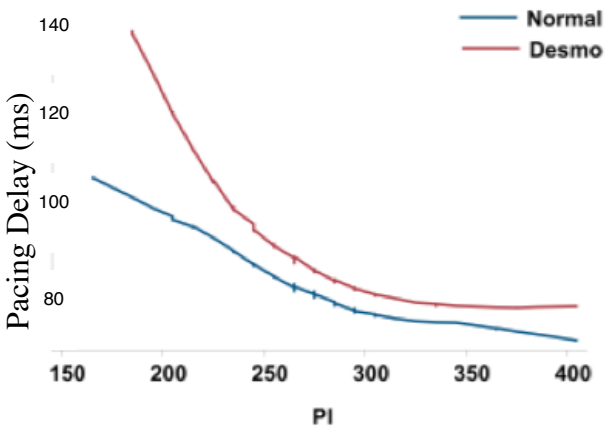

Figure 5-3 Induced conduction delay in DSP+ patients is increased compared to normal patients

The figure shows regression curves created with multilevel non-linear regression using SPSS 11. This demonstrates how the time from stimulation to local tissue activation varies with coupling interval of S1S2 stimulus (PI - pacing interval). The blue line shown the increase in control patients, the red in patients carrying a mutation in DSP. As

S1S2 stimulus interval decreases, an increase in activation delay is seen. This increase is greater in DSP+ patients than in normal controls. The curves are significantly different ($p<0.05$ by multilevel non-linear regression).

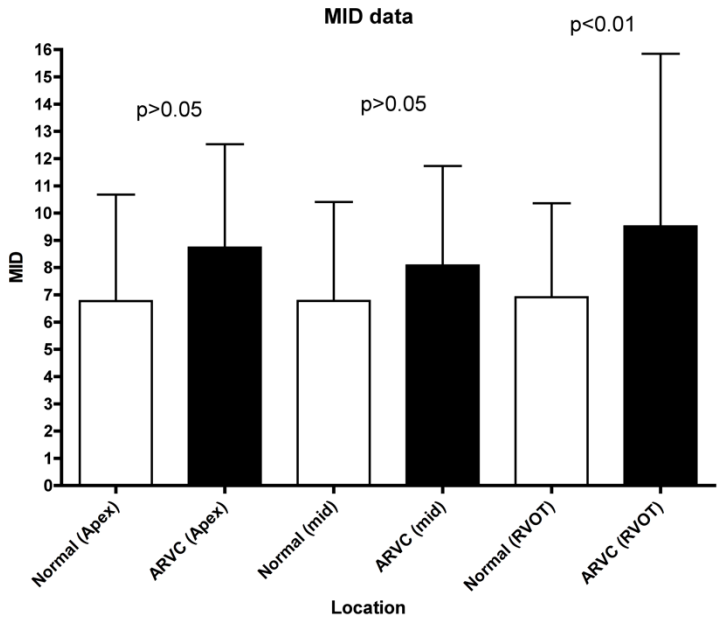

Figure 5-4 Mean increase in delay is increased in DSP+ hearts

Overall DSP+ patients' hearts had significantly more prolonged AT restitution curve profiles versus controls at coupling intervals <250mss ($P<0.001$) (Figure 5-3)). These delays were also significantly different in each of the 3 RV regions-RVOT, body and apex between the DSP mutation carriers and controls ($P<0.001$ per region). Furthermore, statistically significant regional conduction delays (increased mean increase in delay, MID) occurred in the RVOT measuring 38% greater than controls (Figure 5-4).

5.2.4 DSP hearts have more fractionation than controls

Electrograms were analysed using our fractionation algorithm. DSP+ hearts had a significantly greater degree of fractionation versus controls and this fractionation was most marked in the RVOT (Figure 5-5). Figure 5-6 demonstrates this regionality of fractionation in subject 8, with examples of EGM morphology in RVOT & apical sites.

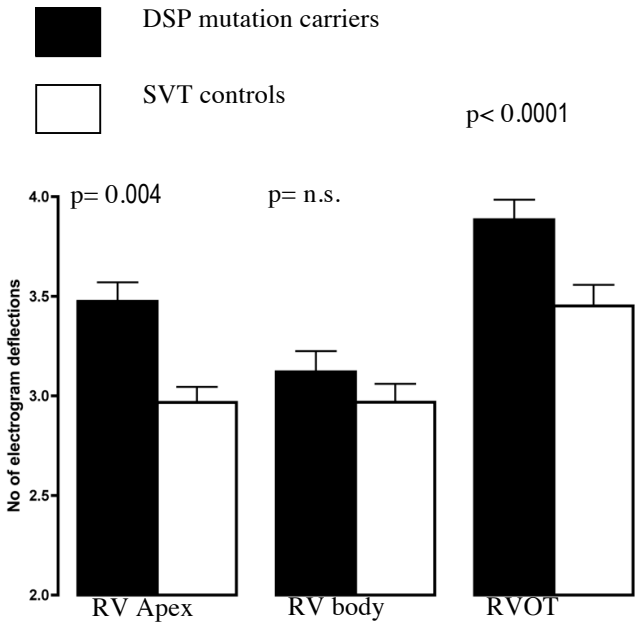

Figure 5-5 DSP+ patients have increased fractionation at the RV apex and RV outflow tract

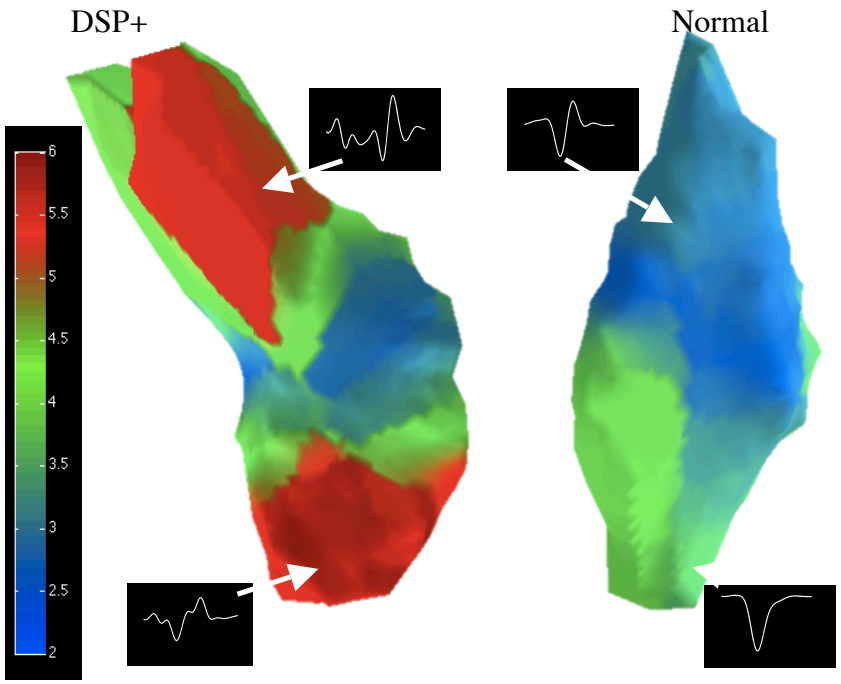

Figure 5-6 Example colourmap of fractionation distribution from two patients

On the left is shown data from a DSP+ patient, on the right a normal control. Example electrograms are illustrated. There is increased fractionation in the DSP+ patient in a patchy distribution.

5.2.5 DSP+ hearts exhibit increased heterogeneity in ARI

The mean ARI of all the segmental restitution curves at 400mec baseline cycle length in the DSP+RV and control RV during RV apical pacing were compared. Analysis of all the curves by model fitting and testing for interaction confirmed significant differences in the ARI at RVOT, RV body versus apex in DSP+ patients at both long and short coupling intervals which did not occur in controls. In control subjects the ARI curves showed a significant ARI prolongation only in the RVOT as compared to the apex over a large range of coupling intervals ($p<0.001$) but the mean RV body ARI curves were similar to the apex. However in the DSP+ patients, the RV body & RVOT both had significantly greater ARI prolongation than the apex ($P<0.001$).

Not only were there differences between regions in the DSP+ group data, differences in the ARI restitution curves could be identified between equivalent RV regions in the patient populations. The ARI curves in control subjects show a profile in which they maximise and then curve downwards with increasing coupling intervals. This profile was similar at the RVOT, body and the apex. In the DSP+ group, the ARI curves had a significantly different profile. The curves at the apex, RV body and RVOT showed a more linear profile in this range of coupling intervals. The ARI values for any given coupling interval were longer in the RV body and RVOT for DSP+ patients versus the same regions in controls ($P<0.001$). This indicates that there is a large interval dependent dispersion of ARI in the DSP+ patients. The maximal slopes of ARI restitution curves were compared between control and DSP+ subjects. The odds of a segment having a maximal restitution slope, S_{max}, of 1 or more in the whole heart was significantly higher in the DSP+ group. The odds of having a segment with a S_{max} >1 was 99% higher (95% Confidence Interval: 13%-351%, $p=0.017$). Although this measure has been associated with an implication of increased likelyhood of disordered

arrhythmogenisis, this association has not been proven in clinical investigations.

5.3 Comparison of ARVC patients with RVOT ectopy patients

Following the successful comparison of patients with desmosomal disease only, this study was expanded to include a wider group of patients with ARVC but no overt structural disease. Comparisons were made to patients with benign right ventricular outflow tract ectopy as well as a group of normal controls.

5.3.1 Patient demographics

22 patients with definite (12 patients) or probable (10 patients) ARVC were studied (mean age 46±11 years) (Marcus et al., 2010). The patients had no major structural features of ARVC with only 2 demonstrating minor modified Task Force imaging criteria. The signal averaged ECG was positive in 13 cases (8 mutation positive) (Syrris et al., 2006b; van der Zwaag et al., 2009; Sen-Chowdhry et al., 2007; Norman et al., 2005; Elliott et al., 2010; den Haan et al., 2009; Gerull et al., 2004). 10 desmoplakin mutation carriers have been described elsewhere, different aspects of their electrophysiological data are presented her (Gomes et al., 2012). Importantly the 12 definite ARVC patients met the criterion because of their mutation carrier/family history status and therefore represent a group of patients with very early disease preceding the development of diagnostic structural abnormalities. Detailed demographic details are given in Table 5-2.

Subject No	Age (M/F)	Mutation	RV Structural Abnormalities	TW inversion V1-V3	Small QRS Complexes	S wave delay	SAECG	NSVT	SVT	PVCs > 500/24hr	Inducible VT at EP study	FHx	ICD	Criteria	
														Maj	Min
Definite ARVC															
1	61 F	T586fsx594	-	+	-	-	-	-	-	-	-	Min	+	2	0
2	28 F	T586fsx594	-	-	-	-	-	+	-	-	-	Maj	+	2	0
3	53 F	T586fsx594	-	+	-	-	+	-	-	-	-	-	+	2	1
4	37 M	E274fsX288	-	-	-	-	+	+	-	-	-	+	-	1	2
5	22 M	S922fsX928	-	-	-	-	+	+	-	-	+	-	+	1	2
6	40 F	N408K and R941X	-	-	-	+	+	+	-	-	-	Maj	-	1	2
7	41 F	PKP2 - 2489+1G>A	-	+	-	-	-	-	-	+		Maj	-	2	1
8	45 M	NIL	Min	+	-	-	-	+	-	+		-	+	1	3
9	42 F	NIL	-	-	-	-	+	+	-	-		Maj	+	1	2
10	57 M	PKP2 S50fsx110	-	-	-	-	+	-	-	+		Maj	-	1	2
11	57 M	NIL	Min	+	-	-	-	+	-	-		-	-	1	2
12	64 M	NIL	-	-	-	-	+	-	-	+		Maj	+	1	2
Probable ARVC															
13	43 F	E274fsX288	-	-	+	-	-	+	+	+	-	-	+	1	1
14	50 F	S507F (19)	-	-	+	-	-	+	-	+	-	Maj	+	1	1
15	33 M	T586fsx594	-	-	-	-	-	+	-	+	-	Maj	-	1	1
16	52 M	DSG2 T335A	-	-	-	-	-	+	-	-		Maj	_	1	1

17	47 F	DSG2 V158G	-	-	-	-	+	-	-			Maj	-	1	1
18	36 M	DSG2 - V392I	-	-	-	-	+	-	-	-		Maj	-	1	1
19	45 F	NIL	-	-	-	-	+					Maj		1	1
20	55 M	NIL	-	-	-	-	+	-	-	-		Maj	-	1	1
21	54 F	Nil	-	+	-	-	-	-	-	+		-	-	1	1
22	57 F	Nil	-	-	-	-	NA	+	-	+		-	-	0	2

Table 5-2 Demographics of Definite and probable ARVC patients.

Abbreviations: Age (M/F): Male/ Female, RV: Right Ventricle, TW: T-wave, SAECG: signal averaged ECG, NSVT: non-sustained ventricular tachycardia, SVT: sustained ventricular tachycardia, PVCs: premature ventricular contractions, VT: ventricular tachycardia, FHx: family history of ARVC in 1st degree relatives, ICD: implantable cardioverter defibrillator, Maj: Major, Min: Minor.

25 consecutive patients with monomorphic ventricular ectopy (9652±8444 beats/24h), structural normal hearts and normal resting ECGs underwent non-contact mapping and EP studies. 14 of these patients had >18m follow-up with no recurrence of ventricular ectopy off antiarrhythmic medication, and no features suggestive of ARVC. These patients were analysed as the RVOTE group (age 45±14 years). Twelve further patients undergoing EP studies ± ablation for SVT with structurally normal hearts acted as Normal controls (age 43±18 years).

5.3.2 Sinus rhythm measurements were similar between groups

No significant differences in RV activation times, ARI or repolarisation time were observed between groups in sinus rhythm (Table 5-3).

Groups	Normal	RVOTE	Definite ARVC	Probable ARVC
	n = 12	n = 14	n = 12	n = 10
Baseline HR	81±17	92±18	85±9	94±11
ERP	212±23	210±13	205±16	214±18
Sinus Activation Time (ms)	71±19	76±25	81±19	80±19
Sinus Repolarisation Time (ms)	302±44	311±49	320±40	317±42*
Sinus ARI (ms)	230±49	235±44	239±38	237±38
Steady State AT (ms)	79±29†	58±24*	75±22†	79±28†
Steady State ARI (ms)	194±25	201±20	203±23	204±19
Steady State RT (ms)	273±46	260±32	278±35	282±39†
Mean AT pre ERP (ms)	104±33	92±29	123±30††	117±35†
Mean ARI pre ERP (ms)	161±26	166±26	170±28	167±26
Mean RT pre ERP (ms)	265±51	258±44	293±50†	284±52
Change in AT pre ERP (ms)	26±16	34±14	48±21***†	38±21*
Change in RT pre ERP (ms)	-7±22	-2±22	15±29*†	1±29
Maximum ARI Restitution Slope (ms)	0.68±0.41	0.83±0.41	0.77±0.4	0.87±0.48
Fractionation at ERP	2.4±0.5	3.4±1.1	3±1*†	3.1±1.1
Fractionation in Steady State	2.5±0.6	3.4±0.9	3.1±1.1*	3.3±1*
Fractionation in Sinus Rhythm	3±1.4	3.44±1.66	2.84±1.31†	2.91±1.1†
Mean Increase In Delay	3.7±10.3	4.1±5.6	6.5±5.6*†	7.4±15.4

Table 5-3 Detailed Surface ECG measurements

Note: Activation and Repolarisation times are given as means±SD for all measurements throughout ventricle. HR: Heart Rate, ERP: effective refractory period, ARI: Activation Recovery Index, AT: Activation Time, RT: Repolarisation Time, Significance codes: * $p<0.05$ vs. Normal, ** $p<0.01$ vs. Normal, ***$p<0.0001$ vs. Normal, † $p<0.05$ vs. RVOTE, †† $p<0.01$ vs. RVOTE

5.3.3 ARVC patients have increased uniformity of conduction in sinus rhythm, but no significant reduction in activation gradient

Differences in slowest measured activation gradient (a measure of slowest endocardial conduction in sinus rhythm) between groups did not reach statistical significance, although activation gradients in ARVC and RVOTE groups were 20% lower than controls) (see supplemental results). r^2, a measure of uniformity of conduction, was higher in both ARVC groups and in normal controls than in the RVOTE patients (definite ARVC: 0.94±0.07, probable ARVC 0.94±0.05, RVOTE 0.85±0.12, Normal: 0.94±0.07, $p<0.05$ vs. RVOTE). There were no differences between either of the ARVC or normal control groups.

5.3.4 Activation and repolarisation increases in ARVC during steady state pacing are subtle

In steady state pacing, RV activation took significantly longer in probable ARVC patients than in RVOTE subjects (98±22ms vs. 77±22ms, $p= 0.01$), this did not reach statistical significance in the definite ARVC group (91±21ms) or normal controls (94±28ms). There was a trend to longer repolarisation times in the ARVC groups when compared to the RVOTE group (definite ARVC: 308±19 $p= 0.07$, probable ARVC: 307±16ms $p= 0.05$, RVOTE: 299±32ms), but no group was significantly different from normal (303±42ms).

5.3.5 Premature stimuli accentuates abnormal conduction slowing in ARVC

VERPs were similar across groups. AT's increased to a greater degree in the definite

ARVC patients (48±21ms) than in other groups (probable ARVC 37±21, RVOTE 34±14, Normal 26±16, $p<0.001$, Figure 3a). The absolute AT pre-VERP was also longer in definite ARVC patients than in RVOTE patients (definite ARVC: 123±30ms, 116±35ms, RVOTE 92±28ms, $p<0.001$, Figure 5-7 Slow conduction induced with premature extrastimuli). There was a trend towards longer absolute ATs in ARVC at VERP when compared to Normal controls (104±33ms, $p= 0.1$).

The activation delay curves were plotted against coupling intervals for each electrode in every patient. Mean increase in delay, a measure of cumulative conduction delay over all coupling intervals, were greater in the ARVC patients (definite ARVC: Median 7.0 [Interquartile range 3.6 – 9.3] vs. 3.1 [0–5.1] ms^2, probable ARVC: 6.3 [3.3 – 9.5]) than in RVOTE patients (4.3 [1.4-7.1] ms^2, $p < 0.01$) or Normal controls (3.4 [0 – 5.2] ms^2, $p<0.001$).

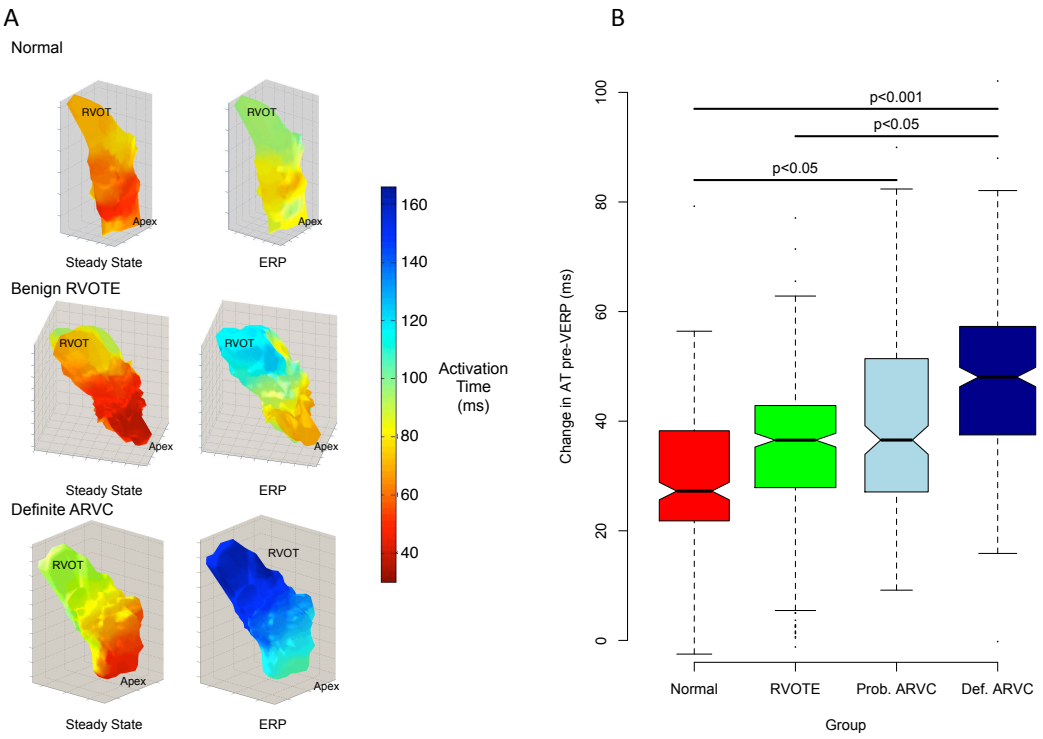

Figure 5-7 Slow conduction induced with premature extrastimuli

A. Example 3D colourmaps showing activation times in steady state and at ERP. The change in activation delay in ARVC patients is greater than in Normal Controls & RVOTE patients. Color scale represents local activation time relative to pacing stimulus. B. Notched box plot of change in activation times from steady state to ERP. Values are normalized to steady state. Notches indicate approx. 95% confidence intervals.

5.3.6 Local Repolarisation Time (RT) is longer in ARVC, and displays different dynamics

Local RT's were plotted against coupling interval (Figure 5-8). Normalising to VERP allowed effective comparison of the AT and RT dynamics at both short and long coupling intervals. The change in RT at VERP compared to steady state was +15±30ms in the definite ARVC group, whereas it was shorter in other groups (probable ARVC +1±19ms, RVOTE -2±23ms p= 0.01, Normal -7±22ms p<0.01).

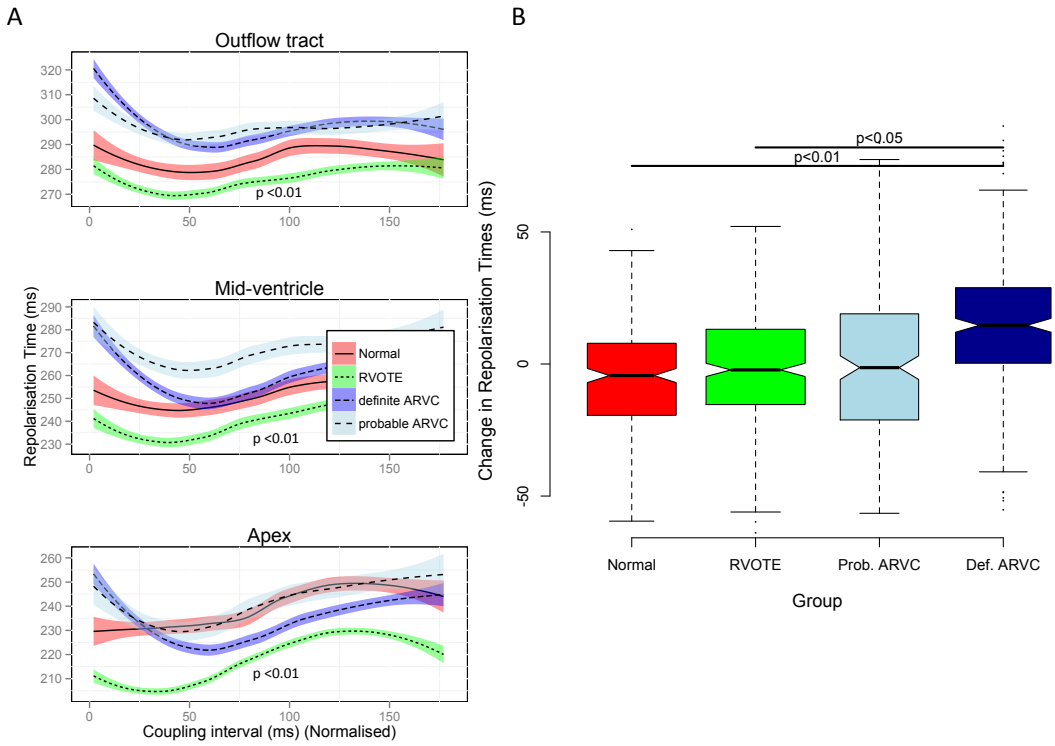

Figure 5-8 Changes in repolarisation time with premature stimuli

Panel A: Repolarisation dynamics are distinct between definite ARVC and RVOTE at almost all coupling intervals and at all locations. There is a marked increase in repolarisation time at short coupling intervals in definite ARVC compared to RVOTE patients and Normal. Transparent color indicates 95% confidence intervals. Coupling intervals are normalised so that 0ms = ERP.

Panel B shows change in repolarisation time at ERP compared to steady state. There is greater increase in repolarisation times in the outflow tract compared to the apex evident across all groups. This increase is significantly greater in the definite ARVC group.

5.3.7 ARI restitution slopes were similar between groups

The maximum slopes of ARI restitution curves, S_{max}, were marginally steeper in the probable ARVC and RVOT groups compared to normal, but there was no statistically significant difference between the definite ARVC group and any other group (definite ARVC: 0.77±0.40, probable ARVC: 0.87±0.48, RVOTE: 0.83±41, Normal: 0.68±0.41; $p<0.05$). Shallower S_{max} were seen in the outflow tract than in the body or apex in all

groups (Outflow tract: 0.71±48, body: 0.83±0.44,apex: 0.84±0.41, p<0.001).

There were no significant differences in the odds ratio of having S_{max}>1 in any segment between patient groups.

5.3.8 RVOT ectopy patients exhibit increased fractionation

In sinus rhythm, more fractionation was observed in RVOTE patients than in definite or probable ARVC or normal controls (Figure 5-9 Global Fractionation). However, during pacing at steady state, RVOTE and both ARVC groups had more fractionation than normal controls. At coupling intervals approaching VERP, the RVOTE group & probable ARVC groups appeared more fractionated than the definite ARVC group (p<0.05), which in turn remained more fractionated than controls (p<0.001).

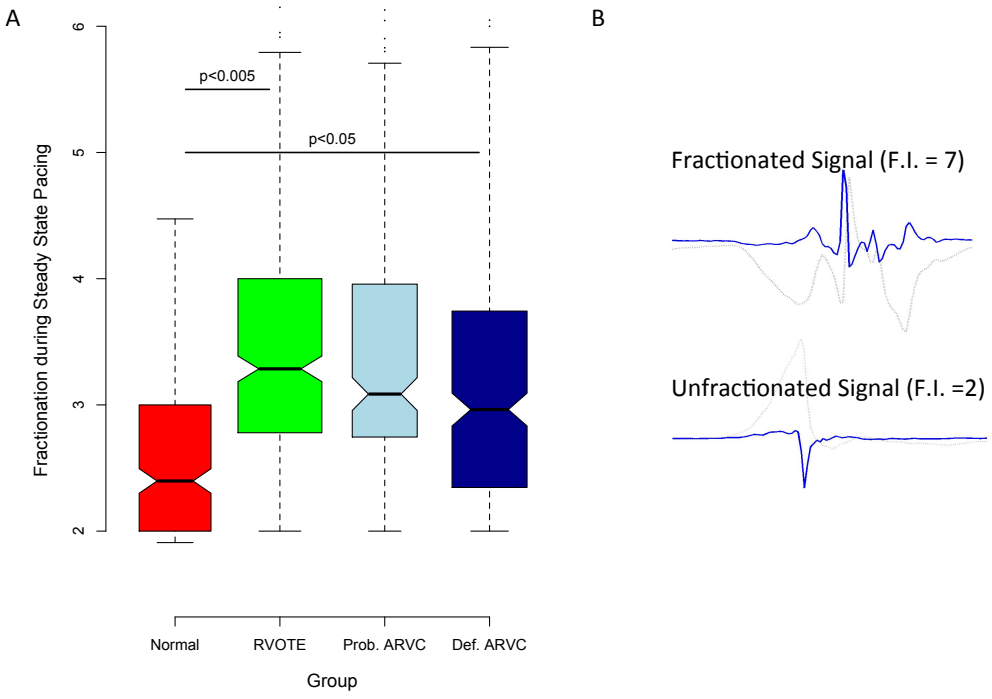

Figure 5-9 Global Fractionation

Panel A shows a notched boxplot of global mean fractionation index. Fractionation is significantly increased in OTE and ARVC patients compared to normal. Panel B shows example electrograms (light grey) and their mathematical differentials, from which fractionation index (FI) was calculated. Panel C shows three example colourmaps of

distribution of fractionation. Higher levels of fractionation are seen in both OTE and ARVC.

5.3.9 Logistic Regression models can help to distinguish ARVC from RVOT ectopy intracardiac measurements

Single intracardiac predictors were generally poor at differentiating definite ARVC from RVOTE, but an increase in the local activation time of >47ms at ERP compared to in steady state pacing gave a sensitivity of 70% and a specificity of 74% in predicting definite ARVC over RVOTE. A mixed-effects logistic regression model was used to combine predictive variables. The best performing model combined (i) degree of AT prolongation in steady state & pre-VERP (ii) repolarisation time in sinus rhythm and (iii) degree of fractionation in sinus rhythm & at short coupling intervals pre-VERP. This model had an area under curve of 0.85 ($p<0.001$) and had peak sensitivity and specificity discriminators of 83% and 72% respectively.

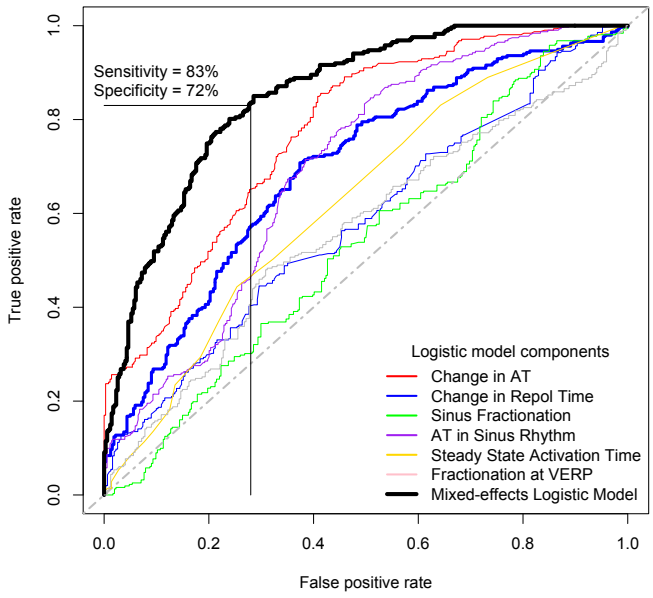

Figure 5-10 Logistic Model of Definite ARVC vs. RVOTE

A comparison of the ability of individual intracardiac measures to distinguish definite ARVC from benign RVOTE. Individual factor receiver-operating characteristic curves are shown in colours. The optimum mixed effects logistic model is demonstrated by the solid black line. Detailed parameters of this model are given below. The grey dot-dash line shows equality.

	Estimate	Std.	z	p
Random				
Location	0.26±0.51			
Fixed Effects				
(Intercept)	3.57	0.78	4.57	<0.0001
Change in AT pre-VERP	-0.03	0.01	-5.83	<0.0001
Fractionation in Sinus	0.37	0.06	6.11	<0.0001
Fractionation at VERP	0.40	0.08	4.76	<0.0001
Repolarisation time (Sinus	-0.01	0.00	-3.12	<0.001
Steady State AT	-0.05	0.00	-10.1	<0.0001

Table 5-4 Coefficients of the logistic regression model for intracardiac predictors of ARVC

5.3.10 The Paced Surface ECG can be used as a surrogate for intracardiac electrophysiology

Although the optimum logistic model constructed from intracardiac signals has a reasonable diagnostic potential, the intracardiac non-contact mapping protocol and analysis is too complex to recommend as a practical clinical test. Therefore, corollaries to features identified by endocardial mapping on the surface ECGs of the study patients were examined.

Absolute surface ECG measurements of activation and repolarisation did not distinguish between RVOTE and ARVC groups at baseline and pre-ERP (Table 5-5), furthermore absolute measurements of surface ECG inscriptions might be very sensitive to the patient-specific placement of the pacing electrode. We thus concentrated our recursive partioning analysis on measurements of hysteresis, lead by our observations of important changes in intracardiac activation/repolarisation. A greater *increase* in activation time at ERP compared to steady-state was observed in the definite ARVC group than in the other groups, measured as an increase in time from pacing artefact to QRS onset (latency), pacing artefact to nadir of S wave and pacing artefact to end of

QRS complex (J-point), (Figure 5-11). The paced QT interval was increased at ERP (c.f. steady state) in definite ARVC patients. No significant change was observed in other groups.

		Definite ARVC (mean ± SD, ms)	Probable ARVC (mean ± SD, ms)	Normal (mean ± SD, ms)	RVOTE (mean ± SD, ms)
Steady State	Latency	34±9	39±11	37±10	42±13
	Stim. To QRS peak	81±19	95±15	85±13	90±11
	Stim. To J-point	142±32	159±9	147±18	149±22
	Stim. To Tpeak	269±24	268±40	269±21	270±24
	Stim. To Tend	347±20	361±17	351±28	342±26
	QRS duration	107±28	120±12	110±15	107±22
	Tpeak to Tend	78±13	94±37*	82±14	72±10
	QT interval	313±19	322±24	314±25	300±29
Pre-ERP	Latency	66±15	66±11	62±14	66±18
	Stim. To QRS peak	128±20	135±16†	115±18	128±22
	Stim. To J-point	191±36	193±15	171±24	180±29
	Stim. To Tpeak	271±25	264±18	264±32	265±26
	Stim. To Tend	383±23	375±28	368±30	359±33
	QRS duration	125±32	126±14	109±14	115±28
	Tpeak to Tend	112±17*	111±23*	104±18	94±19
	QT interval	316±24	309±27	306±27	293±32
Hysteresis (Pre-ERP minus Steady State)	Latency	32±12	27±12	24±9	24±8
	Stim. To QRS peak	47±13††	40±13	30±19	38±15
	Stim. To J-point	50±12*††	33±17	24±24	32±19
	Stim. To Tpeak	1±19	-4±31	-5±25	-5±15
	Stim. To Tend	35±23†	14±21	17±22	17±22
	QRS duration	17±14††	6±11	-1±20	8±18
	Tpeak to Tend	34±19	17±45	22±16	22±17
	QT interval	3±22	-13±20	-7±20	-7±21

Table 5-5 Paced Surface ECG parameters

HR: Heart Rate, ERP: effective refractory period, ARI: Activation Recovery Index, AT: Activation Time, RT: Repolarisation Time, Significance codes: * p<0.05 vs. Normals, ** p<0.01 vs. Normals, ***p<0.0001 vs. Normals, † p<0.05 vs. RVOTE, †† p<0.01 vs. RVOTE

Time from pacing artefact to the end of the T-wave was used as a surrogate marker of complete repolarisation of the ventricles. This interval increased in definite ARVC patients more than in either RVOTE patients or the probable ARVC group (Figure

5-11).

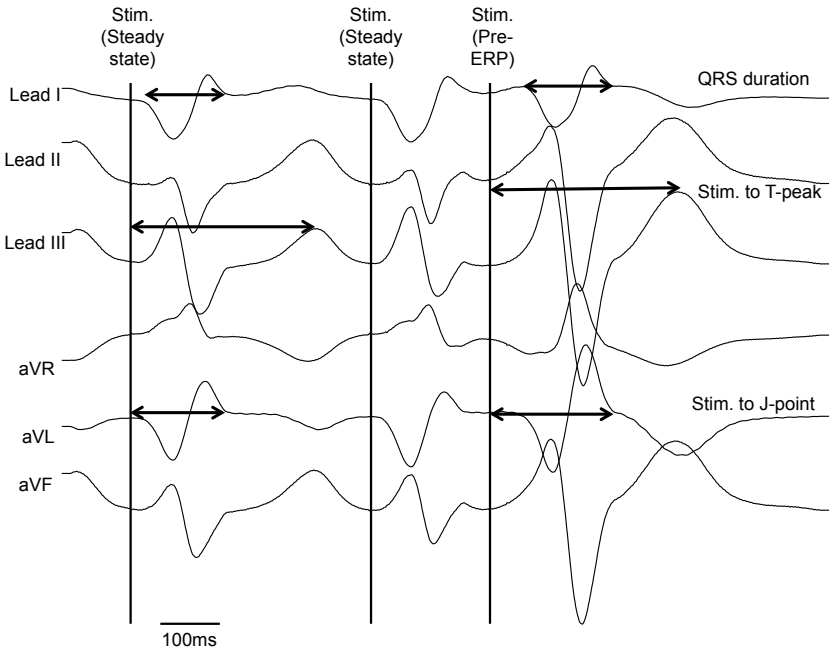

Figure 5-11 Measurements taken from paced surface ECG.

The penultimate and final drive train stimuli, plus a single premature stimulus are shown (vertical lines). The three measurements shown are those used in the recursive partition analysis. The median value over all six limb leads was used.

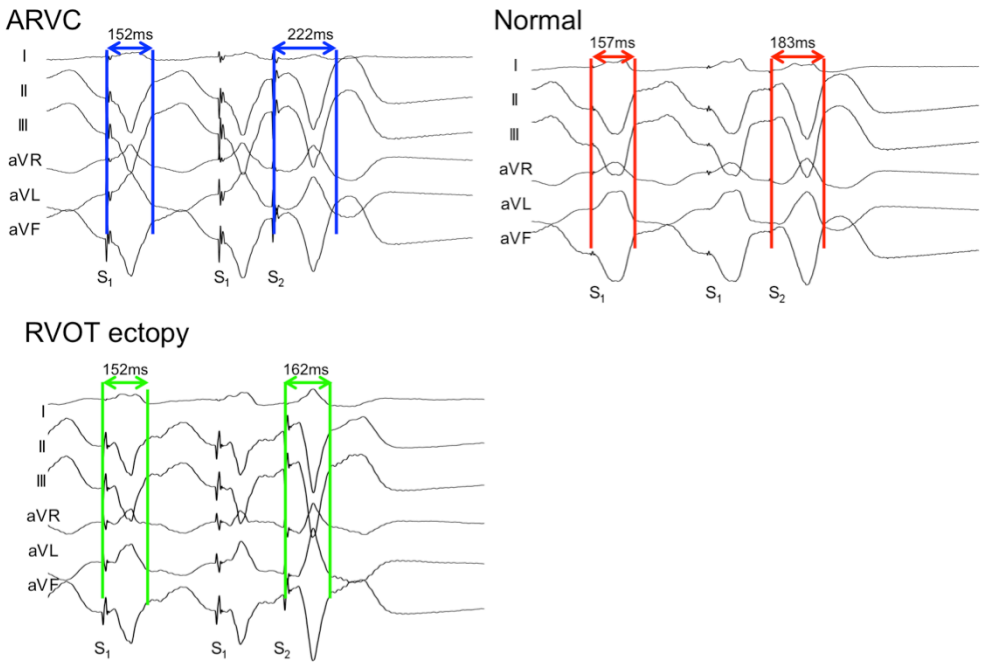

Figure 5-12 Example of Paced Surface ECGs

Representative ECGs from a definite ARVC patient, a patient with RVOT ectopy and a patient with a normal heart are shown. There was a significantly greater increase in the pacing artifact to J-point inflection just prior to ERP in the patients with ARVC than in patients with RVOT ectopy or with normal hearts.

5.3.11 Diagnostic utility of paced ECG changes (CART analysis)

A change in the time from the pacing artefact to the end of the QRS complex of +48ms (pre-ERP minus steady state) gave a sensitivity of 67% and specificity of 88% in the diagnosis of definite ARVC (Figure 5-13). A change in QRS duration of -6ms or lower was insensitive (sensitivity 50%) but specific (specificity 85%) for RVOTE. Further portioning based on a change in the time from stimulus to the peak of the T-wave of greater than - 11ms distinguished possible ARVC and normal groups, with sensitivity and specificity of 71% and 59% respectively.

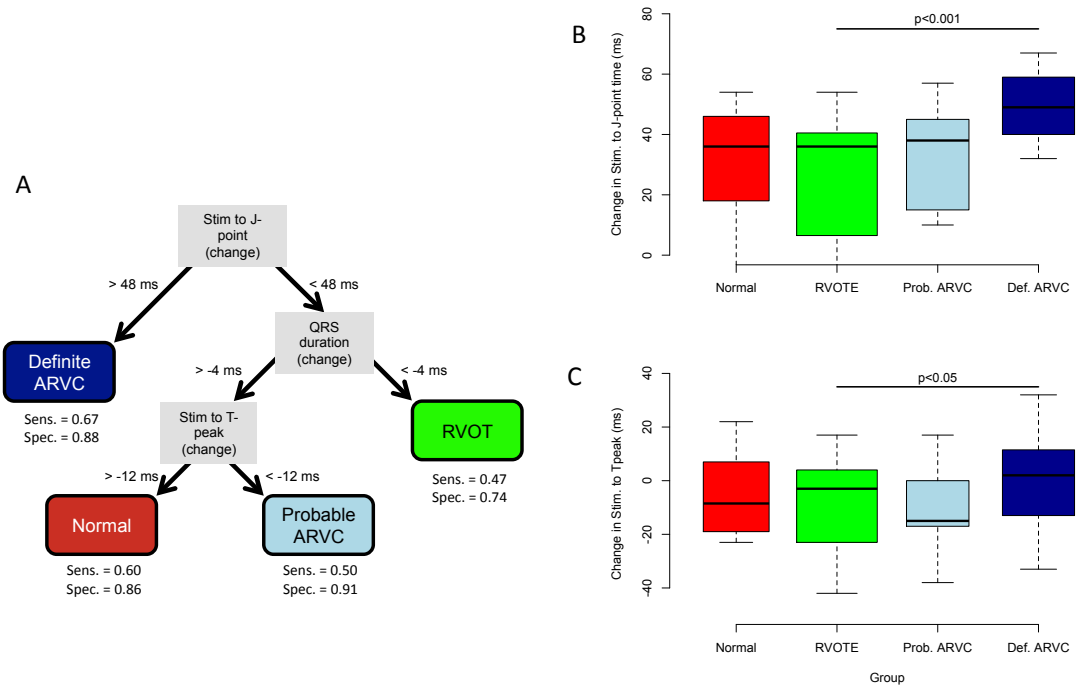

Figure 5-13 Results of CART analysis

Panel A shows the optimum recursive partition tree. An increase in the time from the stimulus to the end of the paced QRS complex (J-point) of >48ms gave a sensitivity of 67% and specificity of 88% for definite ARVC. B and C show raw data for the principal branches. These measurements were able to distinguish any ARVC patient from RVOTE/Normal patients with a sensitivity of 67% and specificity of 84%.

5.3.12 Further work

Data will be re-examined to observe how different genotypes related to phenotypic expression of conduction delay. A larger cohort of genotyped ARVC patients without evidence of structural heart disease on MRI would allow optimisation of the diagnostic algorithm proposed in the CART analysis to increase the paced-ECG algorithm's sensitivity and specificity.

5.4 Discussion

5.4.1 Principal observations

Our major finding has been the identification of conduction abnormalities that exist prior to the development of structural abnormalities in early ARVC. Our initial study in patients known to carry mutations of the desmoplakin gene was extended to a wider group of patients with ARVC and detailed electrophysiology of these patients was compared to that of patients with benign outflow tract ectopy.

The differentiation of ARVC from benign outflow tract ectopy is clinically important to ensure the institution of prognostically significant treatment and lifestyle recommendations. The recent revision of diagnostic criteria for ARVC has placed increased weight on family history and gene status (Marcus et al, 2010). This emphasises the probability of disease development but not necessarily the presence of disease. This is the first study to examine differences in conduction and repolarisation kinetics in an ARVC population that we have identified with earlier disease than customarily reported.

The key findings include: 1) Marked conduction delay in patients with early ARVC when pacing at short coupling intervals, which was not evident in sinus rhythm. 2), Progressively longer local repolarisation times as coupling intervals decrease towards VERP in ARVC patients versus normal controls & RVOT ectopy subjects. 3) Marked differences in fractionation at short coupling intervals pre-VERP throughout the right ventricle between patient groups, with more fractionation in both ARVC and RVOT ectopy patients. 4) Surface ECG corollaries of conduction/repolarisation dynamics provide diagnostic information - an increase in the time from pacing stimulus to full ventricular activation (defined as paced complex J-point) of greater than 48ms gave an

88% specificity and 68% sensitivity of distinguishing definite ARVC from other groups.

Previous studies have demonstrated electrophysiological abnormalities in established ARVC with significant structural disease, including prolonged RV ATs in sinus rhythm and low endocardial bipolar electrogram voltage (Tandri et al., 2009; Corrado et al., 2010). However, this has not been validated for the clinical differentiation of benign RVOT ectopy or VT from early ARVC. At least 40% fibro-fatty replacement is required before detectable attenuation of endocardial voltages occurs and thus disease expression in the early concealed phase will be missed (Corrado et al., 2010; Avella et al., 2010).

Our initial study of desmoplakin mutation carriers demonstrated that these patients have significantly greater mean increases in delay during an S_1-S_2 restitution protocol, particularly in the outflow tract compared to SVT control (Gomes et al., 2012). The question arose as to whether these changes in conduction and repolarisation dynamics could be utilised to differentiate benign outflow tract tachycardia from concealed ARVC. We therefore investigated cases with little or no imaging abnormalities plus patients classed as borderline ARVC using updated consensus criteria. Importantly, it was primarily the family history of ARVC or mutation carrier status that allocated these patients to the "Definite ARVC" group. In the absence of gene testing, 4/12 of the definite ARVC cases would be regarded as borderline. This implies that in a population of combined probable and definite cases the predictive accuracy of this partitioning method may be increased. Indeed, when both groups are combined, the classification tree was able to distinguish any ARVC patient from a combined group of RVOT/Normals with a sensitivity of 67% and specificity of 84%.

The patients with more advanced disease did not demonstrate global RV activation

delays in sinus rhythm, but it was more marked at short coupling intervals during RV pacing. The dynamics of repolarisation were also significantly affected, amplifying effects of conduction delay in ARVC creating significantly more prolonged repolarisation times pre-VERP than steady state versus controls and RVOT ectopy patients.

5.4.2 Endocardial Electrophysiological changes in RVOT ectopy

Two phenomena were observed in the RVOT ectopy patients: consistently shorter RT's versus SVT and ARVC cases and increased fractionation. The shorter RT's may reflect a memory phenomenon induced by the high ventricular ectopic burden promoting shortening in ARI as a result of ion channel current remodelling & cause local myocytes to be more susceptible to activation. The high degree of fractionation in benign RVOT ectopy patients similar to that seen in ARVC deserves comment. Conduction delay and fractionation occurs in ARVC due to early fibrofatty replacement and/or dissociation of preferentially conducting myocardial pathways through worsening gap junction coupling & possibly Na channel downregulation (Gomes et al., 2012; Delmar and McKenna, 2010). However, the conduction delays measured in benign RVOT ectopy patients were indistinguishable from normal hearts, yet significantly more fractionation existed. Cellular and theoretical work has indicated that a single plane of non- or slowly conducting fibroblasts could facilitate ectopic formation through source-sink mismatching & fractionation in one direction of activation, but preserving conduction in another (Xie et al., 2010; de Bakker and Wittkampf, 2010). This hypothesis could be tested using differential pacing in a future study. In the ARVC patients, higher r^2 values indicating uniformity of conduction were observed compared to RVOT ectopy cases. Similarly, we have reported more uniform conduction in Brugada Syndrome vs. control

(Lambiase et al., 2009) suggesting that diseases that promote dissociation of the myocardial layers whether due to structural or ion channel differences reduce the contribution of activation from the Purkinje network breaking through the endocardium to allow more homogeneous & consistent endocardial activation & wavefront propagation.

Taken together, features of conduction delay, increased repolarisation times and mild fractionation at short coupling intervals pre-VERP would support a diagnosis of early ARVC over that of a benign RVOT ectopy, with a logistic model demonstrating a positive predictive value of 80% from the presented data. These differences can also be identified simply using paced-QRS-T-wave parameters.

This study confirms that reduced conduction reserve develops early in ARVC before detectable structural RV changes ensue. This has important implications since sudden cardiac death can occur in patients with minimal histological changes in the sub-clinical phase of ARVC and thus a more sophisticated clinical evaluation using dynamic conduction-repolarisation changes is require (Thiene et al., 1988b). In a recent study, a positive signal averaged ECG correlated with the size of reduced endocardial voltage regions and histological evidence of cardiomyopathic disease but had a low sensitivity; 21% cases studied still had evidence of major RV structural abnormalities on imaging, indicating that static surface ECG markers may be too insensitive in the concealed phase (Santangeli et al., 2010). In a recent study of examining ventricular ectopic morphology in ARVC, the extent of structural disease was not described (Haqqani et al., 2012). This study illustrates that dynamic surface ECG conduction-repolarisation parameters are of diagnostic value.

5.4.3 Relationship to Conduction-Repolarisation interactions

This study has partially confirmed our hypothesis that conduction and repolarisation dynamics are altered in arrhythmogenic disease, namely ARVC. We observed marked dynamic conduction changes in the ARVC group, which were able to differentiate this group from normal subjects or those with benign RVOT ectopy. However, repolarisation changes in early disease appeared secondary to alterations in conduction dynamics. In the earlier study of desmoplakin mutation carriers, we also observed regional differences in ARI in patients with disease. This was not the case in a latter group of patients with early disease.

5.4.4 Study limitations

The human mapping technique evaluates endocardial electrophysiology and thus mid-myocardial and epicardial effects of ARVC could not be assessed. This is important since structural changes manifest epicardially prior to progressing endocardially (Haqqani et al., 2012). Although differences in myocardial electrophysiology between benign RVOT ectopy patients followed for >18 months post ablation and ARVC were identified, a prospective long-term follow-up study this patient cohort would be required to confirm these observations.

5.4.5 Conclusions

Early ARVC exhibits greater conduction delay and dispersion of repolarisation, particularly at short coupling intervals, than either normal hearts or benign RVOT ectopy. Fractionation is mildly increased in early ARVC, but also significantly in benign RVOT ectopy.

The dynamic differences in conduction, repolarisation and fractionation manifest on the surface paced ECG & can help refine the early identification of ARVC patients from

those with benign outflow tract ectopy.

Chapter 6 RESULTS: A Murine Optimised Tissue Slice Model highlights increases in conduction velocity by sympathomimetics

6.1 Introduction

The study of cardiac tissue electrophysiology is limited by the experimental preparations available. Though many biological and *in silico* models exist of cardiac disease (e.g. Janse et al., 1998; Gehrmann and Berul, 2000; Clayton et al., 2011), access to genetically modified tissue, which allows the dissection of mechanistic pathways, has been limited. This is principally due to the difficulties in handling murine cardiac tissue *ex vivo* (Halbach et al., 2006).

However, despite the apparent differences in cellular electrophysiology from larger mammals, the murine heart has been established as an important model of cardiac electrophysiology. The short generation times, large litters and relative ease of performing specific genetic modifications has led to increased interest in the genetically modified mouse as a tool for investigation of arrhythmia mechanisms. This is despite caveats of the murine model, which exhibits shorter action potentials and different repolarising currents compared to humans (Kaese and Verheule, 2012). This has enabled important insights into the pathogenesis of various electrophysiological syndromes, including Brugada syndrome (Papadatos et al., 2002), ARVC (Sato et al., 2009; Lombardi et al., 2011; Gomes et al., 2012) and cholinergic polymorphic ventricular tachycardia (Liu et al., 2006; Cerrone et al., 2005; Watanabe et al., 2009). This work has been performed *in vivo, in vitro* (i.e. as single cell investigations) or in whole heart Langendorff preparations, for which 2D measurements are limited to the epicardial surface (for example Remme et al., 2006).

The differences between the human and murine action potential are summarised below.

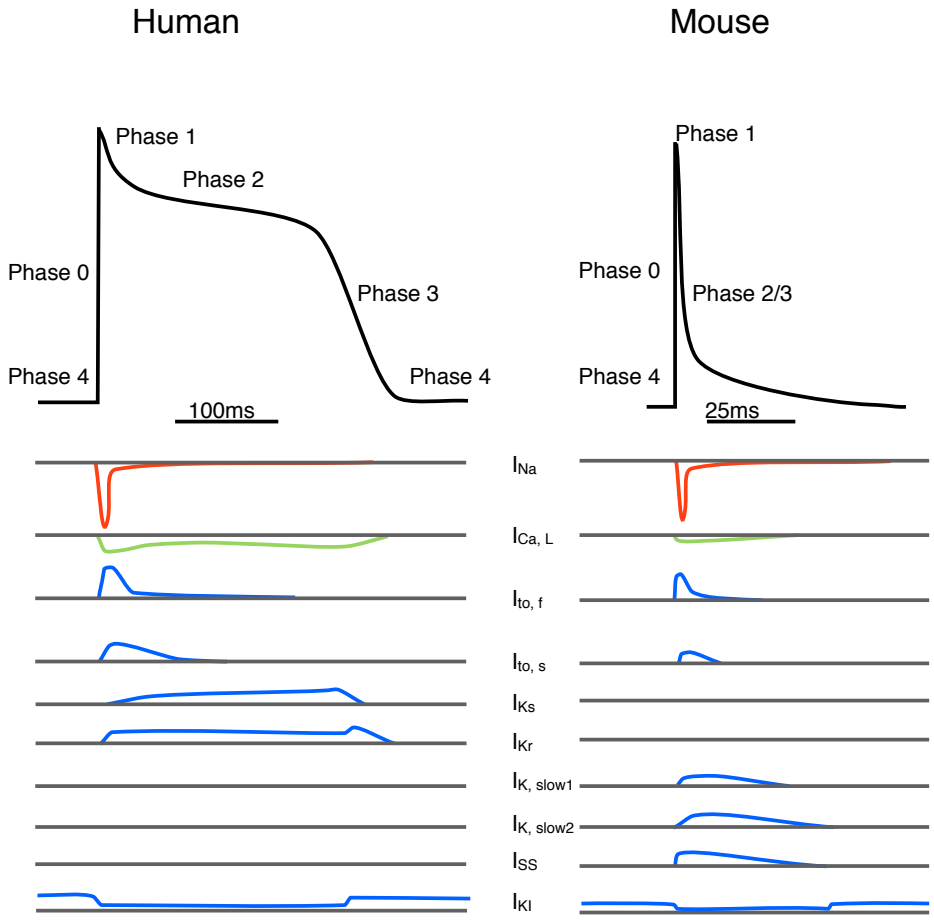

Figure 6-1 Comparisons of Human and Murine action potentials and their contributing ionic currents

Representative human and murine action potentials are shown with the phases labeled (top). Below is a schematic of the contributing currents, with sodium in red, calcium in green and potassium currents in blue. Principal interspecies heterogeneity occurs between the repolarising currents. (Adapted and redrawn from Nerbonne, 2004)

The most important contrasts are in the repolarisation dynamics between the species, the voltage-gated rectifying K^+ current being the most diverse (Pond and Nerbonne, 2001). In the mouse, repolarisation is governed by a different set of potassium currents than in the human, with predominant repolarisation determined by I_{Kslow} activation. The transient outward current (I_{to}) also plays a role. The voltage-gated rectifying currents have a shorter time-course of activation in the mouse than in the human, which accounts for the shorter action potential in the murine heart. The heart rate ranges of the species can account for the marked interspecies differences in Phase 2 and 3 of the action

potential; the resting murine heart rate of around 5 – 10 Hz requires a far more rapid repolarisation than the human (Knollmann et al., 2007). However, the principles of regulation of repolarisation (such as phosphorylation, calcium-dependence and voltage gating) are similar across higher species.

In contrast, the rapid upstroke of the action potential varies very little between the species. This similarity is highlighted by the successful translation of disease models of syndromes of conduction disease; both from human to mouse and vice-versa (Nerbonne, 2004). The sodium channel, desmosomes and connexions are all highly conserved elements of cardiac electrophysiology, adding confidence that patterns and mechanisms elucidated in the mouse might at least be relevant to human physiology and disease.

Despite these advantages, the murine ventricle has proven a difficult source of tissue for investigation of electrophysiological mechanisms. Whereas guinea-pig, rabbit, dog, cat and human hearts (e.g. Bussek et al., 2012; Myles et al., 2011; Allison et al., 2007; Camelliti et al., 2011; Brandenburger et al., 2012) have all been shown to be amenable to tissue level investigation, the mouse heart appears underused. This is likely to the fragility of murine ventricular tissue & whereas the myocytes from large species have been robust to tissue slice techniques, murine hearts have been almost exclusively investigated either *in vivo*, on the Langendorff preparation or in cellular preparations (Sabir et al., 2008). Establishing tissue dissection and recording techniques from the murine heart offers considerable opportunity for novel investigation of cardiac arrhythmia physiology (Pillekamp et al., 2005).

Specifically, I wished to use a murine tissue technique to establish whether conduction velocity and tissue excitability was affected by sympathetic stimulation. Furthermore, access to genetically modified animals enabled investigation into the intracellular

signalling responsible for the effects uncovered in the wild type tissue.

6.1.1 G-protein coupled receptors and their role in arrhythmogenisis

In the human heart, β-adrenoceptors (β-AR) are coupled to heterotrimeric G-proteins (Gilman, 1987). The coupling of a ligand to the receptor causes a conformational change and effects the subsequent dissociation of both the receptor from the G proteins, and a dissociation of the G-protein's constitutive elements into Gα and Gβγ subunits. Both of these subunits have intracellular signalling properties. The predominant β-AR subtype expressed in the normal ventricle, β_1, is coupled to the stimulatory G-protein Gs in the ventricle (Grimm and Brown, 2010). When dissociated from the Gβγ subunit, Gαs acts to stimulate adenyl-cyclase, and thus raises intracellular cAMP. A rise in cytoplasmic concentrations of this second messenger in turn stimulates Protein Kinase A (PK-A) by binding to regulatory PK-A subunits and allowing the release of active catalytic PK-A subunits, through which β-AR stimulation is thought to ultimately have its primary effects. A second β-AR subtype, β_2, is also coupled to the inhibitory alpha-subunit Gαi, which tends to oppose the Gs-mediated actions.

The predominant muscarinic receptor expressed in the (murine) ventricle is the M2 receptor. Likewise consisting of a seven-transmembrane element, this receptor couples to an inhibitory G-protein. Recent work by our group has established that in the ventricle the G-protein $G\alpha_{i2}$ is responsible for principle intracellular effects of muscarinic stimulation (Zuberi et al., 2008; Zuberi et al., 2010). Knockout of this protein results in a cardiac electrical phenotype, with action potential duration lengthening at low heart rates, steepening of the restitution curve and predisposition to ventricular arrhythmia. This can be seen in the light of unopposed sympathetic effects.

Increased accumulation of a repolarisation reserve (due to I_{Kslow} upregulation in the mouse) allows rapid repolarisation at short coupling intervals. But at longer coupling intervals diastolic intervals are too long to allow this accumulation of channels in easily-recruited states. Thus the effects of raised cAMP upon L-type Ca channels dominates, and acts to increase calcium transients, and the action potential extends. At short coupling intervals, the repolarisation reserve will accumulate, the action potential shorten and hence the restitution curve will become steeper (Grimm and Brown, 2010). This combination appears highly arrhythmogenic, as was detailed by the easily induced ventricular arrhythmias and sudden death in these mice.

The effects on sympathetic stimulation on conduction velocity in cardiac muscle have not been fully described. A single investigation into the effects of isoprenaline on canine Purkinje fibres was performed by Packer and colleagues (Cragun et al., 1997). This showed increased conduction velocities with sympathetic stimulation following the administration of flecanide, but this work does not appear to be reproduced. This work can be seen as demonstrating that adrenergic stimulation may overcome conduction slowing induced by a class 1 antiarrhythmic. However, it does not tell us if adrenergic stimulation has constitutive effects on conduction velocities.

Indeed, absolute conduction velocities can be very difficult to measure in the intact heart. A measurement of activation gradients allows the determination of conduction velocity over a field of interest robust to conduction direction or manual measurement of conduction paths. More importantly, it is easy to compare results from different experimental preparations and under different conditions. Even if the conduction path apparently changes due to e.g. induced conduction block, conduction velocities should be comparable to an extent. This technique was used to measure conduction velocities

derived from our experimental preparation.

I aimed to examine whether sympathomimetics did have tissue level effects on conduction velocity, a phenomenon implied by our observation of reduced activation times during mental stress. I also aimed to determine whether this represented an effect purely governed by β-AR signalling, or whether parasympathetic stimulation also has a role.

6.2 Hypothesis

I hypothesised that sympathetic stimulation increases conduction velocity via second-messenger effects at the tissue level, which may be antagonised by parasympathetic stimulation.

To test this hypothesis, a novel murine tissue slice technique was developed. This allowed electrophysiological studies to be performed on very thin (~200μm thick) slices of myocardial tissue using a multi-electrode microarray. Initially, investigations aimed at proving the experimental paradigm valid. Subsequently, the response of tissue conduction to isoprenaline was tested, with attempts to antagonise this response using the parasympathetic agonist Carbachol.

Finally, mice deficient in the inhibitory G protein $G\alpha_{i2}$, which is the G-protein effector linked to the muscarinic M2 receptor. Tissue from these animals was used to further elucidate parasympathetic effects on conduction velocity.

6.3 Results

6.3.1 Validation of cardiac slice analysis

Consistent success at obtaining viable ventricular slices was achieved using the method described in 2.4.4 above, with 13 of 14 attempts yielding viable tissue slices.

A stepwise approach to validation of our signal analysis methodology was taken. Validation was performed in 6 slices obtained from 3 mice. A total of 633 individual excitations following stimulation were examined, with a median of 54 electrode sites examined per slice. Raw signals and averaged signals demonstrated very similar waveforms, with far less noise apparent on the averaged signals (Figure 6-2).

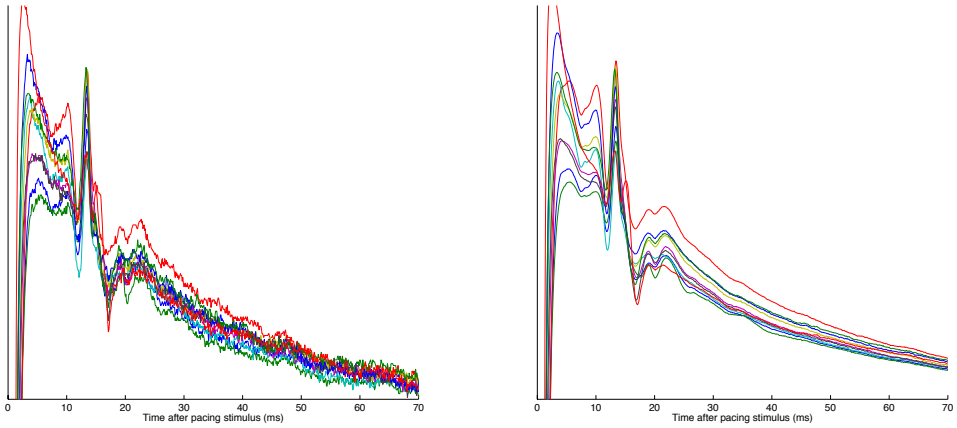

Figure 6-2 Raw and averaged signals

On the left, raw signals obtained from the MEA are shown. 86 signals following paced stimuli were averaged to give the resultant smooth waveform, shown on the right. 10 electrograms from separate electrodes are shown in different colours.

Activation times (ATs) derived from raw signals and those from the averaged-signals were compared. There was an excellent agreement between ATs from averaged signals and the mean of ATs derived from the raw signals ($r^2 = 0.97$). We compared the activation gradient surfaces derived from the signal averaged signals and those derived from raw signals. Panel B shows an example regression surface of activation (Z axis),

with ATs from the averaged signals represented by grey filled circles. Panel C shows the same surface, but now surfaces derived from every constituent raw activation are shown in translucent green. ATs for raw used for each surfaces are shown as green points. There is excellent agreement between regression surfaces from the two methods.

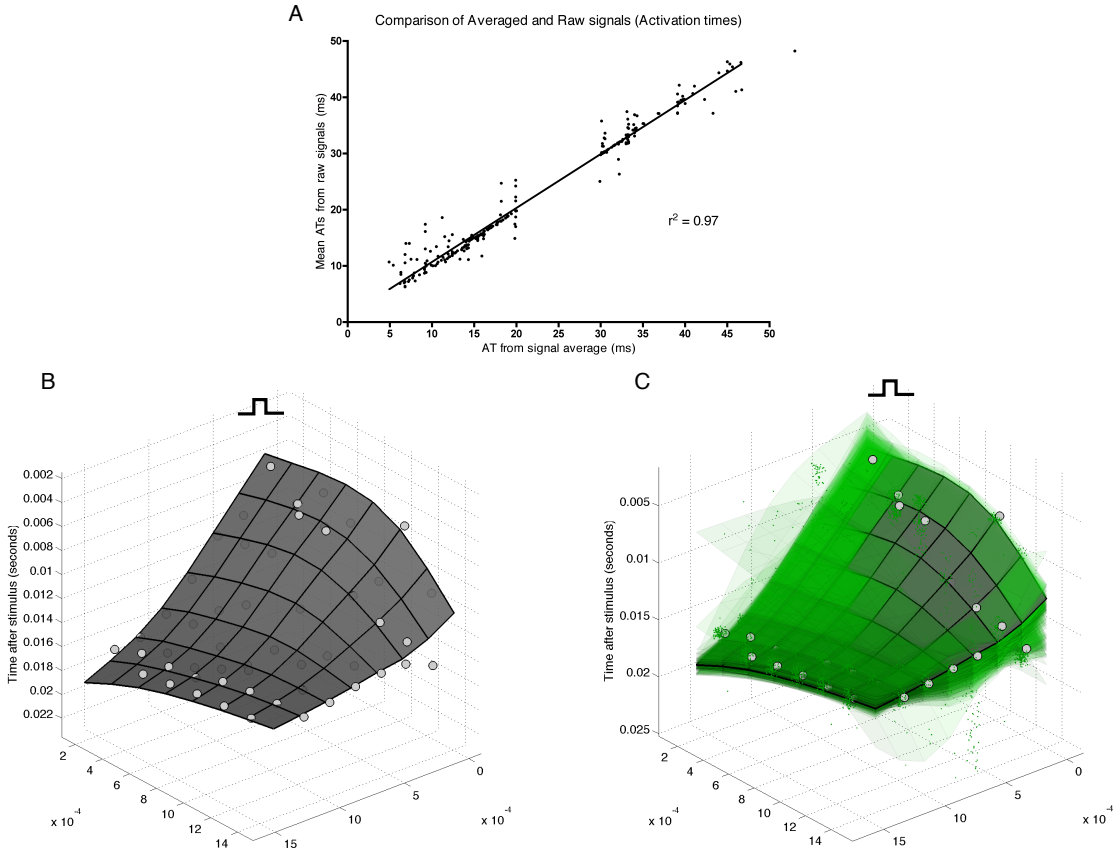

Figure 6-3 Validation of Signal Averaging

A: Comparison of activation times (AT) derived by two methods. The x axis shows ATs from signal averaged ECGs. The y axis shows the mean of ATs from the raw signals constituent in the respective averaged signal. B and C show typical least-squared regression surfaces created using the gridfit function, showing how an activation gradient surface can be fitted over the ATs. B shows a single surface created from signal-averaged data, C shows surfaces created from all the raw data used to make the averaged signals (green, translucent). Raw data points are shown as green points. The grey surface in C (partially hidden by green surfaces) is identical to that in B, this fits entirely within regression surfaces created from raw (non-signal averaged) dara.

To show that the values for conduction velocity obtained by the activation gradient

method were valid, these values were compared with those obtained from a rough distance/time method (d/t method). The difference between the maximum and minimum AT (in ms) was divided by 1.6mm, the length of one dimension of the array. The resultant value gives an estimate of conduction velocity across the tissue. This technique discounts activation paths entirely, and assumes homogenous wavefront activation across the slice and MEA i.e. a direct pathway of activation. This results in a propensity for the conduction velocity to be significantly underestimated. It is also sensitive to erroneous AT measurements. Nonetheless, it is useful as a "face" validation of our gradient derived technique.

There was a significant correlation between conduction velocities obtained by the activation gradient method and those from the d/t method (slope = 1.93 ± 0.25, $r^2 = 0.2889$, $p<0.0001$). This should not be taken as a comparison of the gradient method against a gold standard, but rather a proof of concept and confirmation that realistic conduction velocities were obtained by the gradient method. Occasional higher than expected values were obtatined by the gradient method. It may be that from time to time activation wavefronts may have spread across the tissue preparation in a discontinous manner. This could have lead to several areas of tissue activating simultanously and thereby a higher (or even falsely high) conduction velocity than expected being measured.

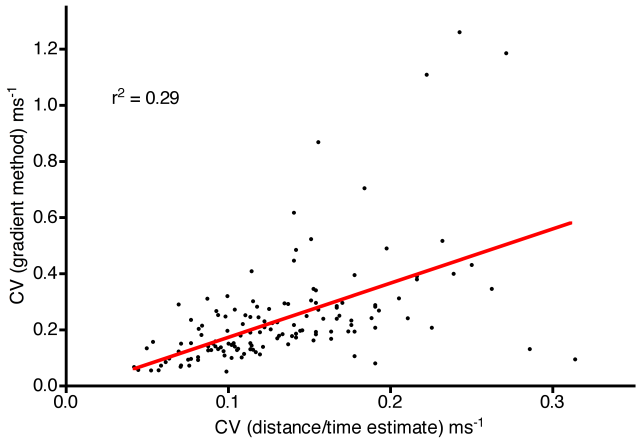

Figure 6-4 Comparison of Conduction velocities obtained by two methods

There was a significant relationship between CV as estimated by an activation gradient method and the approximation achieved by a rough distance/time methodology. Some high values for conduction velocity were occasionally observed with the gradient method.

6.3.2 Isoprenaline decreases pacing thresholds and increases conduction velocities

Initial confirmation of effect of isoprenaline on thresholds and conduction velocities were performed on 11 slices obtained from 3 wild-type mice. Pacing thresholds were defined as previously described. There was a marked drop in the threshold required for consistent capture of ventricular slices in the presence of isoprenaline, from 0.92±0.13V to 0.49±0.07V ($p<0.01$), with a strong trend in dose response ($p= 0.07$ for trend). Similarly, conduction velocities rose markedly in the presence of isoprenaline from a baseline value of 0.15±0.01ms^{-1} to 0.22±0.01ms^{-1}, an increase of nearly 50% ($p<0.0001$).

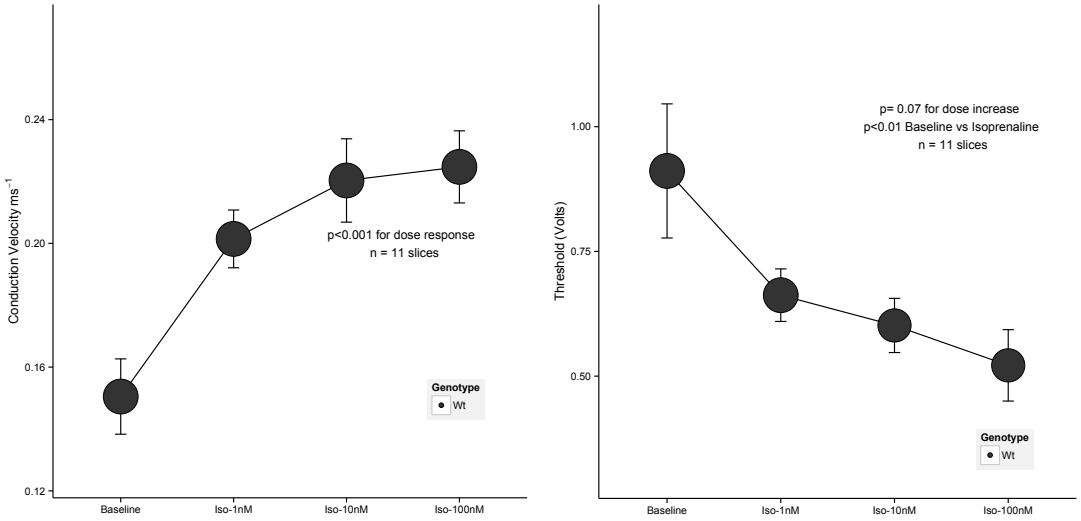

Figure 6-5 Effect of Isoprenaline on Conduction Velocity & Stimulus Threshold

Slices (n = 11) were exposed to isoprenaline in increasing concentrations; the effect on conduction velocity and threshold is shown. Isoprenaline markedly increased conduction velocity, this was accompanied by a decrease in threshold. (Error bars: ±SEM)

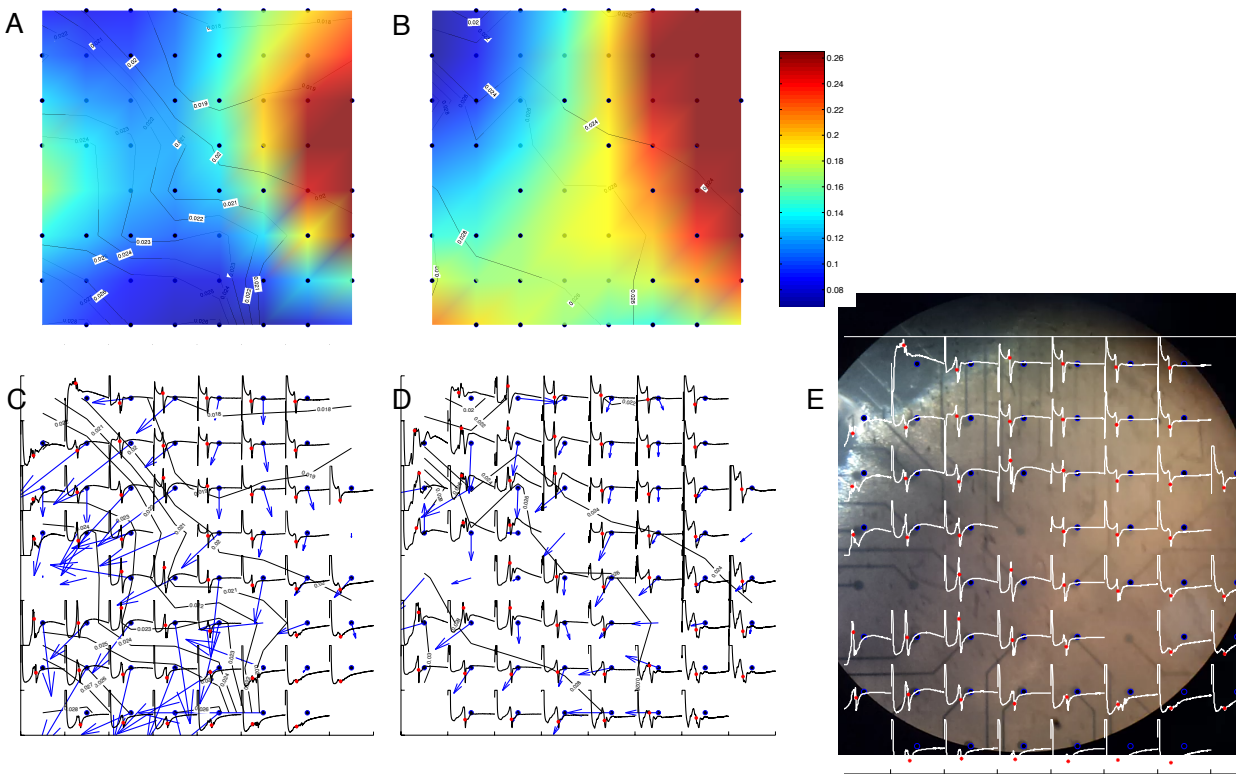

Figure 6-6 Representative Conduction velocities on microarray

A & B: Example colour maps of conduction velocity across the microarray are shown at baseline (A) and in the presence of isoprenaline 100nM (B). Colour scale is in ms^{-1}, and is relevant to both figures, with red indicating high conduction velocity and blue low. The isochronal lines join identical activation times (times in seconds following stimulus), and are constructed without regression smoothing (i.e. from raw data). Stimulation was from the upper right corner (external stimulus). There are higher conduction velocities with isoprenaline.

C & D: Original electrogram data used to construct maps A & B are shown. The blue dot indicates electrode location, the red asterisk indicates the moment of activation on the electrogram. Blue arrows indicate vector of activation gradient, the length of arrow being proportional to the calculated gradient (thus inversely proportional to the conduction velocity).

E: Microscope view of tissue slice (representative) on microarray (20x magnification) with superimposed electrograms. Electrograms with noise or non-interpretable signals are not shown.

6.3.3 Carbachol antagonises the effects of isoprenaline on conduction velocity

The response to isoprenaline and carbachol was tested in 11 slices obtained from 6 wild-type mice. This was compared to 13 slices obtained from 4 $G\alpha_{i2}$-/- mice. Carbachol (10μM) antagonised the effect of isoprenaline (100nM) in the wild-type slices, reducing conduction velocity from 0.26±0.01 ms^{-1} to 0.23±0.01ms^{-1} ($p<0.05$). $G\alpha_{i2}$ deficient slices had a trend to lower baseline conduction velocity than the wild-type slices to which they were compared, but this did not reach statistical significance (Wt: 0.21±0.01 ms^{-1} , KO:0.15±0.01ms^{-1}, p=0.07). There was an increase in conduction velocity in response to isoprenaline in $G\alpha_{i2}$-deficient slices, with a similar proportional increase as the wild-type controls. In contrast to wild-type slices, carbachol did not reduce conduction velocity in the $G\alpha_{i2}$ deficient slices (0.18±0.01 with isoprenaline to 0.19±0.01 with carbachol, p= n.s.).

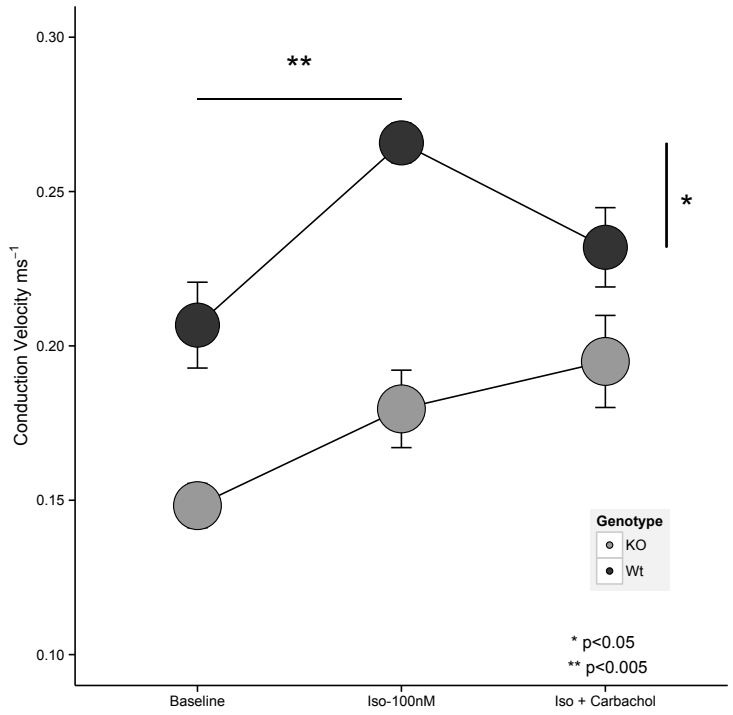

Figure 6-7 Effect of Isoprenaline and Carbachol on $G\alpha_{i2}$ -/- slices

Isoprenaline (100nM) was infused into cardiac tissue slices on the microarray. An increase in conduction velocity is observed in both WT (n = 11) and $G\alpha_{i2}$-/- (n = 13) slices. This is antagonised by carbachol (10μM) in the WT, but not the $G\alpha_{i2}$-/-, slices. (Error bars : ±SEM)

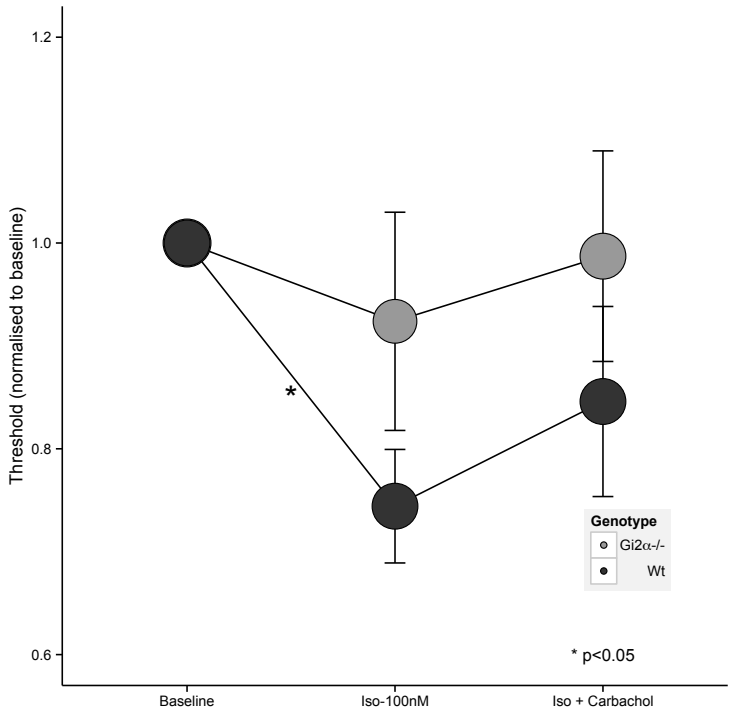

Figure 6-8 Effect of Isoprenaline and Carbachol on Thresholds in wild-type and $G\alpha_{i2}$ -/- slices

Changes in thresholds in response to isoprenaline and carbachol in wild-type and $G\alpha_{i2}$ deficient slices are shown, normalised to baseline values. There was a significant decrease in thresholds with isoprenaline in wild-type slices, but changes due to carbachol did not reach statistical significance. (Error bars: ±SEM)

Thresholds were reduced in $G\alpha_{i2}$ deficient slices in the presence of isoprenaline (0.58±0.12V to 0.44±0.11V), but, in contrast to wild-type controls, this did not reach statistical significance (p= 0.11). The small increase in thresholds observed with carbachol in wild-type slices did not reach statistical significance, nor was a significant increase seen in $G\alpha_{i2}$ deficient slices.

6.3.4 Isoprenaline reduces dispersion of activation

The dispersion of activation (defined as the time difference between the earliest and the latest activation measured) was examined in the presence of isoprenaline and carbachol. Isoprenaline 100nM reduced the dispersion of activation in wild-type slices from 13±1 to 9±1ms (p= 0.07), there was a slight, but non-significant, recovery with carbachol.

No significant changes in dispersion of activation were observed in $G\alpha_{i2}$ deficient slices.

6.4 Discussion

6.4.1 Principal findings

In this study a novel tissue slice and micro-array recording technique for adult murine cardiac tissue was developed. β-AR stimulation has been shown to enhance conduction velocity. Furthermore, muscarinic stimulation acting through the inhibitory G-protein $G\alpha_{i2}$ negatively regulates this effect. This presents a novel potential mechanism of stress-induced arrhythmia by enhancement of conduction through increased sympathetic tone and/or decreased parasympathetic tone. It also confirms that increased conduction velocity is at least partially antagonised by activation of cardiac muscarinic receptors acting via $G\alpha_{i2}$.

6.4.2 Value of results

Conduction velocities in cardiac tissue have been inaccessible to study for several reasons. Firstly, as previously explained in this thesis, the exact pathway of cardiac conduction in the intact myocardium is very hard to determine. By using a quasi-2D tissue whilst retaining tissue structure to a greater extent, a conduction path can be visualised within the tissue. Nonetheless, determining an accurate conduction velocity is complex, and several methodologies were required to ensure that a reproducible value could be determined.

First, signals were averaged from many (between 50 and 100) individual slice stimulations. This dramatically reduced the noise in signals analysed, furthermore signal averaging followed by analysis is a far lighter computational process than repetitive signal analysis followed by averaging determined parameters. Without this process, the amount of data generated would be overwhelming and analysis overly time consuming.

Second, a derivation of the activation gradient in the tissue was used to determine conduction velocity. Activation gradients have been used previously to determine conduction velocity *in vivo* in humans, but were limited by lack of knowledge of exact conduction paths. Only the velocity of the slowest activating area of endocardium could be determined in these methods, which have principally used non-contact mapping data. A 2D linear regression algorithm was used to determine the optimum and true activation gradient over the measured tissue. Originally, this method was used for automated analysis of cartographic data, but it fits our requirements superbly as it minimised chance error and prevents single outlier activation signals from grossly affecting conduction velocity. The mean gradient over the entire tissue slice was used to derive velocity. Using these methods it was possible to determine reliable and consistent measurements of conduction velocity in the tissue slices.

Previous work has documented an increase in conduction velocity in cardiac tissue in the presence of isoprenaline. Packer and coworkers showed that dog Purkinje fibres treated with Flecanide would increase conduction velocities in the presence of isoprenaline (Cragun et al., 1997). However, the effect of parasympathetic agents on conduction velocity has not to our knowledge been previously documented. The presented work shows that conduction velocity increases due to isoprenaline can be antagonised by carbachol, and that this antagonism acts through $G\alpha_{i2}$. The increased excitability of the tissue (i.e. the ease at which cells within the tissue may depolarise causing an action potential) was implied by decreases in pacing threshold. This may be seen as allegorical to increased clinical ectopy during stress or isoprenaline administration, and stands as a potential mechanism for increases in conduction velocity.

The observation of increases in conduction velocities in the presence of sympathomimetic agents deserves comment. Our measured conduction velocities were

low in comparison to published data from whole heart preparations (e.g. Mirnov et al. 2008). Manual checking of these data confirmed that conduction velocities within our preparation were lower than those previously described in intact tissue. This may be due to disruption in cell-cell communication brought about during the slicing process; aniostropy in particular may have been increased in this process due to physical disruption along strands of tissue. This was not directly investigated.

It may be that minor tissue disruption may have made our preparation more sensitive to sympathetically mediated conduction velocity changes than would be observed in intact tissue. Such a situation could arise if minor disruption to desmosomal and connexin intercellular connections were rescued by increased cycling of membrane proteins under sympathetic drive. Increased recruitment of connexin to the cell membrane would lead to reductions in intercellular impedance, an eased passage of current from cell to cell and consequently an increase in conduction velocity. Recent data demonstrates co-trafficking of Connexin 43 with Nav1.5 sodium channels; an increase in membrane sodium channel concentration at the cell membrane would also lower cell-cell impedance by adding to a "sodium channel reserve" (Rhett et al, 2012). Action potential upstroke would be more rapid and higher conduction velocities thus result.

Downstream effects on cellular calcium stores provides a third way for sympathetic stimulation to increase apparent conduction velocities. The downstream effects of adrenergic agonist stimulation include phosphorylation of the Ryanodine receptor (RYR2), the L-type calcium channel and phospholamban, which is responsible for regulation of SERCA activity. This may be via direct phosphorylation via the cAMP/ Protein Kinase A pathway and/or Ca^{2+}/Calmodulin Kinase II, though there is debate over whether the latter of these pathways represents a direct or indirect pathway (Grimm and Brown, 2010). The net consequence, however, is an increase in Ca^{++}

uptake and release from the sarcoplasmic reticulum. Thus the calcium transients involved in the action potential will increase. These increases in Ca^{++} transients will be expected to increase sodium-calcium exchanger activity, raising the membrane potential and thus facilitate depolarisation of the cell. The tissue level consequence of these changes would be expected to be an increase in conduction velocity as end result.

Tissue disruption in our preparation may have increased the senility of our assay to conduction velocity changes. It may be that increases in conductivity due to cell-cell connection upregulation and increases in calcium transients could overcome intracellular barriers in an all-or-nothing manner on a cell-to-cell basis. A strongly non-linear relationship between intercellular conductance and conduction velocity may result (van Rijen et al 2006, Dhillon et al. 2013). A tissue-level result of this would be that an experimental preparation that itself poses constraints on conduction velocity might be more sensitive at revealing changes in this metric.

The presented work provides a novel platform by which tissue level consequences of molecular perturbations can be examined. This study establishes that adult murine tissue slices from genetically modified animals can be examined with this tissue-slice model. There is significant potential to study more than just steady state activation times and excitation, as has been demonstrated. Repolarisation and repolarisation dynamics are potentially amenable for study using this system. Though the T-wave visible on many electrograms is indistinct, techniques to exclude far-field signal and highlight local repolarisation (such as using cross- or star- laplacians (Coronel et al., 2000)) are certainly feasible. A further development would be to couple the direct electrical mapping using the microelectrode array system with optical mapping of voltage, calcium or other fluorescence-labelled dynamic markers of electrical or regulatory activity. In this study, re-entrant arrhythmias were not convincingly demonstrated in

slice preparations. However, this may primarily due to limitations in the stimulation system used. Computer control and automated programming of this will enable more arrhythmogenic stimuli trains to be administered.

6.4.3 Limitations

There are several important limitations to this work.

First, the relevance of murine tissue to clinical human arrhythmia may be questioned. Clearly species variability is important, particularly in the repolarising phase. Nonetheless, important corollaries between activation and activation/repolarisation kinetics and regulation of cardiac behaviour appear to exist across mammalian species. These are particularly notable in activation dynamics. This limitation may be addressed by demonstrating living human cardiac tissue slices using the same *ex vivo* system. This is possible with biopsy samples acquired intraoperatively, and some early work has shown that this is at least possible.

Second, the tissue slice technique may profoundly alter tissue dynamics. Tissue disruption may accentuate anisotropy and reduce/prevent conduction. This may explain the low conduction velocities measured compared to standard reference values (approximately $70cm.s^{-1}$, e.g. van Rijen et al 2006, Dhillon et al. 2013). Nonetheless, contemporary control samples enable comparisons to be drawn.

Third, the tissue preparation ionic behaviour may have been severely disrupted by the exposure to calcium free, high potassium modified Kreb's perfusate during initial suspension of animation. Attempts were made to minimise this by ensuring that tissue slices were exposed to normo-calcaemic, normo-kalaemic solution for at least 30 minutes prior to attempt of measurements. Nonetheless, irreversible disruption of

important cellular processes by this method has not been ruled out.

Fourth, the experimental process did not allow myocyte orientation to be determined. Ventricles were sliced in the short axis, measurements were by necessity mainly acquired from the mid-myocardium. We are unable to determine whether the effects on the epi- or true endocardium would be different from those described. The issue of tissue slice orientation could be addressed by immunohistochemical assessment of myocyte orientation using standard techniques post procedure.

Fifth, the effects of isoprenaline on the morphology of the electrograms acquired from the multi-electrode array were not quantified.

Sixth, the stimulation control used required arduous manual selection of timings. It was impossible to perform reliable restitution curves and determine ERP whilst managing the perfusion system and tissue viability. A computerised controller for the stimulus generator will be required for repetitive S_1S_2 protocols, and for more complex arrhythmogenic protocols.

6.4.4 Further Work

Several further stages are required to complete this investigation. Improved stimulus protocols are required to establish the arrhythmogenicity of the tissue preparation and to examine ERP. Likewise, the contribution of anisotropy to conduction velocity dynamics should be examined. Repolarisation must be examined formally, and it will be important to test apparent tissue conduction velocities using the activation gradient technique against manually plotted distance/time measures.

Furthermore, questions remain regarding longevity of tissue slices, and optimal tissue storage conditions are yet to be determined.

6.5 Conclusions

The murine tissue slice technique yields viable myocardial tissue, which can be examined using the multielectrode array system. Reproducible measurements of conduction velocity and measurements can be obtained from this.

Isoprenaline administration increases conduction velocity and tissue excitability, these effects are antagonised by carbachol. This antagonism is dependent on $G\alpha_{i2}$-mediated signalling.

Chapter 7 Overall Discussion

7.1 Summary of achievements

This thesis has addressed the overarching hypothesis: activation and repolarisation dynamics are subject to modulation by autonomic stress and disease- using several different experimental series and techniques.

First, human studies on normal individuals were used to test the validity of one-dimensional conduction models in the clinical setting. I was able to model the dynamics of activation and repolarisation using simple parameters and assumptions. These successfully predicted activation-repolarisation interactions following serial premature extrastimuli. This provides a framework by which biologically acquired data on conduction velocity and repolarisation dynamics may be incorporated into more complex simulations. The ability of a simple, patient specific model to recapitulate human conduction dynamics is notable, and validates earlier work (such as those by Gelzer et al. (2008)) in the human. Moreover, it establishes that activation and repolarisation dynamics are reproducible in the human and do follow patterns expected from theoretical wave models. This technique does not currently enable observation of wavebreak and determination of the spatial patterns of arrhythmia determination as presented. However, confirmation of these dynamics may be important in future patient-specific simulation model constructions utilising additional extrastimuli from dynamic restitution protocols.

We have demonstrated that activation and repolarisation dynamics were modifiable by conscious mental stress, thus demonstrating *in vivo* direct cardiac electrophysiological effects of purely psychological stimuli. A key observation was the marked increase in dispersion of repolarisation at short coupling intervals during mental stress. This provides a plausible mechanism for the arrhythmogenic effects of acute mental stress.

A small apparent increase in conduction velocity during mental stress was noted. Measurements from different chambers of the heart allowed determination of gradients in repolarisation times in the normal heart. These observations enable us to translate observed cellular mechanisms with the societal-level observations of sudden death in extreme emotional stress. We did not confirm that sudden death in heightened emotional circumstances was due to these interactions, but the dynamics of activation and repolarisation do show significant alterations during mental stress. As such they could facilitate re-entry and wavebreak. Future studies will confirm if these are responsible for increased arrhythmia susceptibility.

In order to further determine if conduction velocity and repolarisation interactions were affected by autonomic tone at the tissue level, a novel murine cardiac slice model was developed. This allowed the testing of the effects of direct tissue beta-receptor and muscarinic receptor stimulation on cardiac conduction. Beta-receptor stimulation increased conduction velocities, and muscarinic activity acting through $G\alpha_{i2}$ antagonised them. This is important as the $G\alpha_{i2}$ -/- mouse has a propensity to ventricular arrhythmia and sudden cardiac death, in the absence of structural abnormality. It has been thus viewed as model of mental-stress induced arrhythmia, though a caveat to this is that actual spontaneous arrhythmias have not been directly observed *in vivo* in this model, merely sudden death of undetermined cause. The observations from both wild type and knockout mice confirm that conduction (as well as previously reported repolarisation (Zuberi et al., 2010)) can be affected by autonomic stimuli. It also confirms that activation and repolarisation are both under significant autonomic control, and that the parasympathetic system has important effects on cardiac conduction dynamics. Stimulation protocols that would be able to reliably determine VERP in the tissue slice preparation or that could induce arrhythmia have not been fully tested at the

time of writing; this work is currently on going. It will be an important further demonstration of the validity of this technique to fully recapitulate observations from *in vivo* and cellular studies in the tissue preparation.

Finally, these concepts have been used to show that activation and repolarisation dynamics can be modulated in human disease, specifically in early arrhythmogenic cardiomyopathy prior to the onset of overt structural changes. Activation dynamics, but not steady state conduction properties, appear to be affected early in this disease. These dynamics can be used to differentiate early ARVC from benign right ventricular outflow tract tachycardia. I suggest that this could be the basis of a clinically useful test to allow differentiation of pre-clinical ARVC from benign outflow tract tachycardia. However, though my data convincingly demonstrate electrophysiological differences, it was not confirmed that the measurement of J-point hysteresis would be clinically useful with the available data. To do this, a significant prospective study would be required, examining patients presenting with outflow tract tachycardia. We did not observe that repolarisation dynamics were independently affected in this disease; rather they appeared to change secondary to activation delays. The interplay between conduction and repolarisation in disease will be best studied in animal models in the first instance, for example by using the murine knockout models of ARVC with tissue-slice technology.

A significant achievement has been methodological. Establishing the thin-slice murine model enables tissue level study of cardiac conduction and (possibly) repolarisation in the knockout mammal. This experimental paradigm will be useful in exploring the complex molecular interactions that contribute to arrhythmia generation and regulation. Signals acquired from this system are very similar to those observed in clinical studies, and thus this paradigm lends itself towards clinical translation. Further methodological

achievements include my extensive use of automation for data management and analysis.

The successful integration of patient-acquired data into a predictive model stands as a conceptual proof of this pathway of investigation. However, an ideal predictive model would operate using defined parameters derived non-invasively. This may be from global ECG data (such as ECG-I technology (Rudy, 2009; Wang et al., 2011)), which could be used to develop patient-specific models of arrhythmogenic risk incorporating myocardial structure, conduction-repolarisation dynamics and changes in autonomic tone. It is conceivable that electrophysiologically relevant genomic data could even be incorporated in defined conditions. The ultimate aim of this would be to create accurate personalised arrhythmia predictive models in specific disease states.

7.2 Further work

Further integration of the different techniques and data described in this thesis would significantly strengthen the assertion that wavebreak could be promoted by the modulation of dynamics in activation and repolarisation observed in the three experimental conditions: mental stress, ARVC and in the $G\alpha_{i2}$ -/-model of arrhythmia. Ongoing work with Lei Xu and Dr Ben Hanson of UCL continues to examine whether the mathematical 1-D models validated in our study can be used to establish changes in the conditions for functional block. Specifically, they are examining whether functional block is more likely to occur during mental stress compared to baseline conditions.

Such techniques can be applied to whole-ventricular data (e.g. acquired using non-contact mapping or new technologies such as ECG-I (Cuculich et al., 2010; Rudy, 2009)) to form whole-chamber or even whole heart simulations. Knowledge of regional heterogeneity in functional block thresholds could conceivably be a useful tool in cardiac risk prediction. It would attempt to measure induced heterogeneity in substrate/trigger interactions, and could be calculated using our 1-D model derivation.

The series of human experiments where mental stress was induced through psychometric protocols was very challenging to perform within the confines of the invasive catheter lab. In order to extend these observations, I would seek to perform non-invasive measurements of cardiac activation and repolarisation. As previously mentioned, several new technologies seek to solve the inverse problem by using cardiac MRI data integrated with very high-density ECG electrode jackets. This may allow appreciation of regional activation and repolarisation changes during testing. Adopting a non-invasive approach would be technically far less challenging and allow more complex and more detailed psychometric protocols to be employed in a serial fashion.

Dr Lambiase and Professor Taggart, at the Heart Hospital, UCL, are seeking to obtain such information from patients with predisposition to stress-induced arrhythmias, particularly Long-QT patients.

Our dataset of electrophysiological measurements in patients with very early stage ARVC is unique, but the use of the non-contact array is cumbersome. The first patients in this data set were studied eight years ago, since then the non-contact array has fallen out-of-favour as a clinical tool as its limitations in mapping dilated cardiac chambers have been highlighted. This thesis has shown that the dynamic conduction changes that may be a hallmark of early ARVC can be identified using the surface ECG alone. This could be further examined in an ARVC population with ICDs, and in patients undergoing catheter ablation for suspected benign outflow tract tachycardia. Thus whether our identified criteria of J-point hysteresis represents a useful clinical diagnostic observation could be critically appraised.

The thin-slice multielectrode array preparations represent a potentially useful new approach to electrophysiological examination. They allow reliable and consistent examination of tissue level electrophysiology in a pseudo-2D structure, retaining tissue architecture and could be extended to patients. Preliminary work has established that human atrial tissue (acquired intraoperatively) can be used on our array system. Other groups have reported successful use of human ventricular tissue with a similar technique (Brandenburger et al., 2012; Bussek et al., 2012; Camelliti et al., 2011). The potential as a translational tool is obvious. Further work needs to be also performed on murine preparations to establish their longevity and structural integrity.

Initially, further work will concentrate on completing electrophysiological assessments of $G\alpha_{i2}$ -/- tissue using the microarray by more complex stimulation protocols. A practical limitation is utilising a manual stimulator (over the several hours of an

experiment) whilst ensuring tissue viability and homeostasis. It is essential to replace a manual stimulator control with a fully automated system. Unfortunately, the digital outputs that would allow us to sync an external stimulus with the multi-electrode array inbuilt stimulator are not real time, i.e. they exhibit an inconsistent latency of around several hundred milliseconds. To address this, I have already instituted an Arduino™-based microcontroller to control stimulator timings. This can be flexibly programmed to any complexity of stimulator protocols thus consistent data to establish ERP and arrhythmia induction should be achievable.

There are several further technical advances that could be achieved using the tissue-slice and multi-electrode array. It would be conceptually straightforward to couple our direct electrical recording with optical mapping. Initially, voltage sensitive dyes would allow determination of repolarisation phases. Further imaging could study calcium flux or metabolic activity in slices during stimulation & arrhythmia.

The tissue-slice system holds several advantages over classical whole heart preparations for examining the systems biology of cardiac conduction and arrhythmia. First, many comparable samples can be acquired from a single animal. This actively contributes to the principle of "three R's" (Reduction, Refinement and Replacement), but also allows pharmacological studies to occur on serial slices rather than having to rely on washout stages. Second, cardiac cellular and tissue function can be studied in isolation, yet with tissue structure intact. Third, mature adult tissue can be used, rather than the immature monolayers of cultured myocytes. Fourth, highly regional tissue samples can be obtained. This makes it possible to compare functional electrophysiology of the right versus left atrium, right versus left myocardium and potentially epi-, mid- and endocardial electrophysiology. I look forward to developing this system to further elucidate the functional regulation of cardiac arrhythmia.

Chapter 8 References

Abisse, S.S., Lampert, R., Burg, M., Soufer, R. & Shusterman, V. (2011) Cardiac repolarization instability during psychological stress in patients with ventricular arrhythmias. *Journal of Electrocardiology*, **44**, 678-683.

Abrams, D.J., Earley, M.J., Sporton, S.C., Kistler, P.M., Gatzoulis, M.A., Mullen, M.J., Till, J.A., Cullen, S., Walker, F., Lowe, M.D., Deanfield, J.E. & Schilling, R.J. (2007) Comparison of noncontact and electroanatomic mapping to identify scar and arrhythmia late after the Fontan procedure. *Circulation*, **115**, 1738-1746.

Akar, F.G., Yan, G.X., Antzelevitch, C. & Rosenbaum, D.S. (2002) Unique topographical distribution of M cells underlies reentrant mechanism of torsade de pointes in the long-QT syndrome. *Circulation*, **105**, 1247-1253.

Al-Khatib, S.M., Hellkamp, A., Curtis, J., Mark, D., Peterson, E., Sanders, G.D., Heidenreich, P.A., Hernandez, A.F., Curtis, L.H. & Hammill, S. (2011) Non-evidence-based ICD implantations in the United States. *JAMA*, **305**, 43-49.

Allessie, M.A., Bonke, F.I. & Schopman, F.J. (1973) Circus movement in rabbit atrial muscle as a mechanism of tachycardia. *Circulation Research*, **33**, 54-62.

Allison, J.S., Qin, H., Dosdall, D.J., Huang, J., Newton, J.C., Allred, J.D., Smith, W.M. & Ideker, R.E. (2007) The transmural activation sequence in porcine and canine left ventricle is markedly different during long-duration ventricular fibrillation. *J Cardiovasc Electrophysiol*, **18**, 1306-1312.

Antzelevitch, C. (2001) Transmural dispersion of repolarization and the T wave. *Cardiovascular Research*, **50**, 426-431.

Antzelevitch, C. (2008) Drug-induced spatial dispersion of repolarization. *Cardiol J*, **15**, 100-121.

Antzelevitch, C., Shimizu, W., Yan, G.X. & Sicouri, S. (1998) Cellular basis for QT dispersion. *Journal of Electrocardiology*, **30 Suppl**, 168-175.

Antzelevitch, C. & Yan, G.X. (2010) J wave syndromes. *Heart Rhythm*, **7**, 549-558.

Asimaki, A., Syrris, P., Wichter, T., Matthias, P., Saffitz, J.E. & McKenna, W.J. (2007) A novel dominant mutation in plakoglobin causes arrhythmogenic right ventricular cardiomyopathy. *American Journal of Human Genetics*, **81**, 964-973.

Avella, A., d'Amati, G., Zachara, E., Musumeci, F. & Tondo, C. (2010) Comparison between electroanatomic and pathologic findings in a patient with arrhythmogenic right ventricular cardiomyopathy/dysplasia treated with orthotopic cardiac transplant. *Heart Rhythm*, **7**, 828-831.

Avitall, B., McKinnie, J., Jazayeri, M., Akhtar, M., Anderson, A.J. & Tchou, P. (1992) Induction of ventricular fibrillation versus monomorphic ventricular tachycardia during programmed stimulation. Role of premature beat conduction delay. *Circulation*, **85**, 1271-1278.

Bai, R., Di Biase, L., Shivkumar, K., Mohanty, P., Tung, R., Santangeli, P., Saenz, L.C., Vacca, M., Verma, A., Khaykin, Y., Mohanty, S., Burkhardt, J.D., Hongo, R., Beheiry, S., Dello Russo, A., Casella, M., Pelargonio, G., Santarelli, P., Sanchez, J., Tondo, C. & Natale, A. (2011) Ablation of ventricular arrhythmias in arrhythmogenic right ventricular dysplasia/cardiomyopathy: arrhythmia-free survival after endo-epicardial substrate based mapping and ablation. *Circ Arrhythm Electrophysiol*, **4**, 478-485.

Bardy, G.H., Lee, K.L., Mark, D.B., Poole, J.E., Packer, D.L., Boineau, R., Domanski, M., Troutman, C., Anderson, J. & Johnson, G. (2005) Amiodarone or an implantable cardioverter–defibrillator for congestive heart failure. *New England Journal of Medicine*, **352**, 225-237.

Basso, C., Bauce, B., Corrado, D. & Thiene, G. (2012) Pathophysiology of arrhythmogenic cardiomyopathy. *Nat Rev Cardiol*, **9**, 223-233.

Beffagna, G., Occhi, G., Nava, A., Vitiello, L., Ditadi, A., Basso, C., Bauce, B., Carraro, G., Thiene, G., Towbin, J.A., Danieli, G.A. & Rampazzo, A. (2005) Regulatory mutations in transforming growth factor-beta3 gene cause arrhythmogenic right ventricular cardiomyopathy type 1. *Cardiovascular Research*, **65**, 366-373.

Bernus, O., Van Eyck, B., Verschelde, H. & Panfilov, A.V. (2002) Transition from ventricular fibrillation to ventricular tachycardia: a simulation study on the role of Ca(2+)-channel blockers in human

ventricular tissue. *Phys Med Biol*, **47**, 4167-4179.

Blazeski, A., Zhu, R., Hunter, D.W., Weinberg, S.H., Zambidis, E.T. & Tung, L. (2012) Cardiomyocytes derived from human induced pluripotent stem cells as models for normal and diseased cardiac electrophysiology and contractility. *Prog Biophys Mol Biol*, **110**, 166-177.

Bloomfield, D.M., Steinman, R.C., Namerow, P.B., Parides, M., Davidenko, J., Kaufman, E.S., Shinn, T., Curtis, A., Fontaine, J., Holmes, D., Russo, A., Tang, C. & Bigger, J.T.J. (2004) Microvolt T-wave alternans distinguishes between patients likely and patients not likely to benefit from implanted cardiac defibrillator therapy: a solution to the Multicenter Automatic Defibrillator Implantation Trial (MADIT) II conundrum. *Circulation*, **110**, 1885-1889.

Bockamp, E., Maringer, M., Spangenberg, C., Fees, S., Fraser, S., Eshkind, L., Oesch, F. & Zabel, B. (2002) Of mice and models: improved animal models for biomedical research. *Physiol Genomics*, **11**, 115-132.

Brack, K.E., Narang, R., Winter, J. & Ng, G.A. (2013) The mechanical uncoupler blebbistatin is associated with significant electrophysiological effects in the isolated rabbit heart. *Exp Physiol*, **98**, 1009-1027.

Brandenburger, M., Wenzel, J., Bogdan, R., Richardt, D., Nguemo, F., Reppel, M., Hescheler, J., Terlau, H. & Dendorfer, A. (2012) Organotypic slice culture from human adult ventricular myocardium. *Cardiovascular Research*, **93**, 50-59.

Brownstein, S.L., Hopson, R.C., Martins, J.B., Aschoff, A.M., Olshansky, B., Constantin, L. & Kienzle, M.G. (1988) Usefulness of isoproterenol in facilitating atrioventricular nodal reentry tachycardia during electrophysiologic testing. *The American journal of cardiology*, **61**, 1037-1041.

Burdon-Sanderson, J. (1880) On the Time-Relations of the Excitatory Process in the Ventricle of the Heart of the Frog. *Journal of Physiology*, **2**, 384-435.

Bussek, A., Schmidt, M., Bauriedl, J., Ravens, U., Wettwer, E. & Lohmann, H. (2012) Cardiac tissue slices with prolonged survival for in vitro drug safety screening. *J Pharmacol Toxicol Methods*, **66**, 145-151.

Burg, M.M., Jain, D., Soufer, R., Kerns, R.D. & Zaret, B.L. (1993) Role of behavioral and psychological

factors in mental stress-induced silent left ventricular dysfunction in coronary artery disease. *Journal of the American College of Cardiology*, **22**, 440-448.

Buxton, A.E., Lee, K.L., Fisher, J.D., Josephson, M.E., Prystowsky, E.N. & Hafley, G. (1999) A randomized study of the prevention of sudden death in patients with coronary artery disease. Multicenter Unsustained Tachycardia Trial Investigators. *New England Journal of Medicine*, **341**, 1882-1890.

C Butcher, M.F., WL Yao, M Lowe, O Segal, R Ben-Simon, E Rowland, A Chow, P Lambiase (2011) Long-term follow up post-elective, outflow tract ventricular tachycardia ectopy ablation. (ECAS 2011 Special Issue). *J Interv Card Electrophysiol*, **Journal of Interventional Cardiac Electrophysiology 30**, 87-198.

Cabo, C., Pertsov, A.M., Baxter, W.T., Davidenko, J.M., Gray, R.A. & Jalife, J. (1994) Wave-front curvature as a cause of slow conduction and block in isolated cardiac muscle. *Circulation Research*, **75**, 1014-1028.

Camelliti, P., Al-Saud, S.A., Smolenski, R.T., Al-Ayoubi, S., Bussek, A., Wettwer, E., Banner, N.R., Bowles, C.T., Yacoub, M.H. & Terracciano, C.M. (2011) Adult human heart slices are a multicellular system suitable for electrophysiological and pharmacological studies. *J Mol Cell Cardiol*, **51**, 390-398.

Cerrone, M., Colombi, B., Santoro, M., di Barletta, M.R., Scelsi, M., Villani, L., Napolitano, C. & Priori, S.G. (2005) Bidirectional ventricular tachycardia and fibrillation elicited in a knock-in mouse model carrier of a mutation in the cardiac ryanodine receptor. *Circulation Research*, **96**, e77-82.

Cherry, E.M. & Fenton, F.H. (2004) Suppression of alternans and conduction blocks despite steep APD restitution: electrotonic, memory, and conduction velocity restitution effects. *Am J Physiol Heart Circ Physiol*, **286**, H2332-41.

Cherry, E.M. & Fenton, F.H. (2007) A tale of two dogs: analyzing two models of canine ventricular electrophysiology. *Am J Physiol Heart Circ Physiol*, **292**, H43-55.

Chow, A.W., Segal, O.R., Davies, D.W. & Peters, N.S. (2004) Mechanism of pacing-induced ventricular fibrillation in the infarcted human heart. *Circulation*, **110**, 1725-1730.

Clayton, R.H., Bernus, O., Cherry, E.M., Dierckx, H., Fenton, F.H., Mirabella, L., Panfilov, A.V., Sachse, F.B., Seemann, G. & Zhang, H. (2011) Models of cardiac tissue electrophysiology: progress, challenges and open questions. *Prog Biophys Mol Biol*, **104**, 22-48.

Clayton, R.H. & Taggart, P. (2005) Regional differences in APD restitution can initiate wavebreak and re-entry in cardiac tissue: a computational study. *Biomed Eng Online*, **4**, 54.

Coronel, R., Wilms-Schopman, F.J., de Groot, J.R., Janse, M.J., van Capelle, F.J. & de Bakker, J.M. (2000) Laplacian electrograms and the interpretation of complex ventricular activation patterns during ventricular fibrillation. *J Cardiovasc Electrophysiol*, **11**, 1119-1128.

Coronel, R., Wilms-Schopman, F.J., Opthof, T. & Janse, M.J. (2009) Dispersion of repolarization and arrhythmogenesis. *Heart Rhythm*, **6**, 537-543.

Corrado, D., Basso, C., Leoni, L., Tokajuk, B., Turrini, P., Bauce, B., Migliore, F., Pavei, A., Tarantini, G., Napodano, M., Ramondo, A., Buja, G., Iliceto, S. & Thiene, G. (2008) Three-dimensional electroanatomical voltage mapping and histologic evaluation of myocardial substrate in right ventricular outflow tract tachycardia. *Journal of the American College of Cardiology*, **51**, 731-739.

Corrado, D., Calkins, H., Link, M.S., Leoni, L., Favale, S., Bevilacqua, M., Basso, C., Ward, D., Boriani, G., Ricci, R., Piccini, J.P., Dalal, D., Santini, M., Buja, G., Iliceto, S., Estes, N.A.r., Wichter, T., McKenna, W.J., Thiene, G. & Marcus, F.I. (2010) Prophylactic implantable defibrillator in patients with arrhythmogenic right ventricular cardiomyopathy/dysplasia and no prior ventricular fibrillation or sustained ventricular tachycardia. *Circulation*, **122**, 1144-1152.

Costantini, O., Hohnloser, S.H., Kirk, M.M., Lerman, B.B., Baker, J.H.n., Sethuraman, B., Dettmer, M.M. & Rosenbaum, D.S. (2009) The ABCD (Alternans Before Cardioverter Defibrillator) Trial: strategies using T-wave alternans to improve efficiency of sudden cardiac death prevention. *Journal of the American College of Cardiology*, **53**, 471-479.

Courtemanche, M., Glass, L. & Keener, J.P. (1993) Instabilities of a propagating pulse in a ring of excitable media. *Physical review letters*, **70**, 2182-2185.

Cox, M.G., van der Zwaag, P.A., van der Werf, C., van der Smagt, J.J., Noorman, M., Bhuiyan, Z.A.,

Wiesfeld, A.C., Volders, P.G., van Langen, I.M., Atsma, D.E., Dooijes, D., van den Wijngaard, A., Houweling, A.C., Jongbloed, J.D., Jordaens, L., Cramer, M.J., Doevendans, P.A., de Bakker, J.M., Wilde, A.A., van Tintelen, J.P. & Hauer, R.N. (2011) Arrhythmogenic right ventricular dysplasia/cardiomyopathy: pathogenic desmosome mutations in index-patients predict outcome of family screening: Dutch arrhythmogenic right ventricular dysplasia/cardiomyopathy genotype-phenotype follow-up study. *Circulation*, **123**, 2690-2700.

Cragun, K.T., Johnson, S.B. & Packer, D.L. (1997) Beta-adrenergic augmentation of flecainide-induced conduction slowing in canine Purkinje fibers. *Circulation*, **96**, 2701-2708.

Cuculich, P.S., Wang, Y., Lindsay, B.D., Faddis, M.N., Schuessler, R.B., Damiano, R.J.J., Li, L. & Rudy, Y. (2010) Noninvasive characterization of epicardial activation in humans with diverse atrial fibrillation patterns. *Circulation*, **122**, 1364-1372.

Cutler, M.J. & Rosenbaum, D.S. (2009) Risk stratification for sudden cardiac death: is there a clinical role for T wave alternans? *Heart Rhythm*, **6**, S56-61.

Damato, A.N., Lau, S.U.N.H., Helfant, R.H., Stein, E., Berkowitz, W.D. & Cohen, S.I. (1969) Study of atrioventricular conduction in man using electrode catheter recordings of His bundle activity. *Circulation*, **39**, 287-296.

Davidenko, J.M., Pertsov, A.V., Salomonsz, R., Baxter, W. & Jalife, J. (1992) Stationary and drifting spiral waves of excitation in isolated cardiac muscle. *Nature*, **355**, 349-351.

Davis, R.P., Casini, S., van den Berg, C.W., Hoekstra, M., Remme, C.A., Dambrot, C., Salvatori, D., Oostwaard, D.W., Wilde, A.A., Bezzina, C.R., Verkerk, A.O., Freund, C. & Mummery, C.L. (2012) Cardiomyocytes derived from pluripotent stem cells recapitulate electrophysiological characteristics of an overlap syndrome of cardiac sodium channel disease. *Circulation*, **125**, 3079-3091.

de Bakker, J.M. & Wittkampf, F.H. (2010) The pathophysiologic basis of fractionated and complex electrograms and the impact of recording techniques on their detection and interpretation. *Circ Arrhythm Electrophysiol*, **3**, 204-213.

Delmar, M. & McKenna, W.J. (2010) The cardiac desmosome and arrhythmogenic cardiomyopathies:

from gene to disease. *Circulation Research*, **107**, 700-714.

den Haan, A.D., Tan, B.Y., Zikusoka, M.N., Llado, L.I., Jain, R., Daly, A., Tichnell, C., James, C., Amat-Alarcon, N., Abraham, T., Russell, S.D., Bluemke, D.A., Calkins, H., Dalal, D. & Judge, D.P. (2009) Comprehensive desmosome mutation analysis in north americans with arrhythmogenic right ventricular dysplasia/cardiomyopathy. *Circ Cardiovasc Genet*, **2**, 428-435.

Desantiago, J., Ai, X., Islam, M., Acuna, G., Ziolo, M.T., Bers, D.M. & Pogwizd, S.M. (2008) Arrhythmogenic effects of beta2-adrenergic stimulation in the failing heart are attributable to enhanced sarcoplasmic reticulum Ca load. *Circulation Research*, **102**, 1389-1397.

Dhillon, P.S., Gray, R., Kojodjojo, P., Jabr, R., Chowdhury, R., Fry, C.H. & Peters, N.S. (2013) Relationship between gap-junctional conductance and conduction velocity in mammalian myocardium. *Circ Arrhythm Electrophysiol*, **6**, 1208-1214.

Duncan, E., Thomas, G., Johns, N., Pfeffer, C., Appanna, G., Shah, N., Hunter, R., Finlay, M., Schilling, R.J. & Sporton, S. (2010) Do Traditional VT Zones Improve Outcome in Primary Prevention ICD Patients? *Pacing Clin Electrophysiol*,

Efimov, I.R., Huang, D.T., Rendt, J.M. & Salama, G. (1994) Optical mapping of repolarization and refractoriness from intact hearts. *Circulation*, **90**, 1469-1480.

Elliott, P., O'Mahony, C., Syrris, P., Evans, A., Rivera Sorensen, C., Sheppard, M.N., Carr-White, G., Pantazis, A. & McKenna, W.J. (2010) Prevalence of desmosomal protein gene mutations in patients with dilated cardiomyopathy. *Circ Cardiovasc Genet*, **3**, 314-322.

Elliott, P. & Spirito, P. (2009) Risk assessment in hypertrophic cadiomyopathy, The author's reply (to Sauaurez 2009). *Heart*,

Ellison, K.E. (2002) Effect of beta-Blocking Therapy on Outcome in the Multicenter UnSustained Tachycardia Trial (MUSTT). *Circulation*, **106**, 2694-2699.

Elzinga, G., Lab, M.J., Noble, M.I., Papadoyannis, D.E., Pidgeon, J., Seed, A. & Wohlfart, B. (1981) The action-potential duration and contractile response of the intact heart related to the preceding interval and the preceding beat in the dog and cat. *Journal of Physiology*, **314**, 481-500.

Epstein, A.E., DiMarco, J.P., Ellenbogen, K.A., Estes, N.A.M., Freedman, R.A., Gettes, L.S., Gillinov, A.M., Gregoratos, G., Hammill, S.C., Hayes, D.L., Hlatky, M.A., Newby, L.K., Page, R.L., Schoenfeld, M.H., Silka, M.J., Stevenson, L.W. & Sweeney, M.O. (2008) ACC/AHA/HRS 2008 Guidelines for Device-Based Therapy of Cardiac Rhythm Abnormalities: Executive Summary: A Report of the American College of Cardiology/American Heart Association Task Force on Practice Guidelines (Writing Committee to Revise the ACC/AHA/NASPE 2002 Guideline Update for Implantation of Cardiac Pacemakers and Antiarrhythmia Devices): Developed in Collaboration With the American Association for Thoracic Surgery and Society of Thoracic Surgeons. *Circulation*, **117**, 2820-2840.

Fenton, F.H., Luther, S., Cherry, E.M., Otani, N.F., Krinsky, V., Pumir, A., Bodenschatz, E. & Gilmour, R.F.J. (2009) Termination of atrial fibrillation using pulsed low-energy far-field stimulation. *Circulation*, **120**, 467-476.

Finlay, M.C., Xu, L., Taggart, P., Hanson, B. & Lambiase, P.D. (2013) Bridging the gap between computation and clinical biology: validation of cable theory in humans. *Front Physiol*, **4**, 213.

Fox, J.J., Riccio, M.L., Drury, P., Werthman, A. & Jr, R.F.G. (2003) Dynamic mechanism for conduction block in heart tissue. *New Journal of Physics*, **5**, 101.1–101.14.

Franz, M.R., Bargheer, K., Rafflenbeul, W., Haverich, A. & Lichtlen, P.R. (1987) Monophasic action potential mapping in human subjects with normal electrocardiograms: direct evidence for the genesis of the T wave. *Circulation*, **75**, 379-386.

Gallicano, G.I., Kouklis, P., Bauer, C., Yin, M., Vasioukhin, V., Degenstein, L. & Fuchs, E. (1998) Desmoplakin is required early in development for assembly of desmosomes and cytoskeletal linkage. *Journal of Cell Biology*, **143**, 2009-2022.

Garfinkel, A., Kim, Y.H., Voroshilovsky, O., Qu, Z., Kil, J.R., Lee, M.H., Karagueuzian, H.S., Weiss, J.N. & Chen, P.S. (2000) Preventing ventricular fibrillation by flattening cardiac restitution. *Proceedings of the National Academy of Sciences of the United States of America*, **97**, 6061-6066.

Gehrmann, J. & Berul, C.I. (2000) Cardiac electrophysiology in genetically engineered mice. *J*

Cardiovasc Electrophysiol, **11**, 354-368.

Gelzer, A.R., Koller, M.L., Otani, N.F., Fox, J.J., Enyeart, M.W., Hooker, G.J., Riccio, M.L., Bartoli, C.R. & Gilmour, R.F.J. (2008) Dynamic mechanism for initiation of ventricular fibrillation in vivo. *Circulation*, **118**, 1123-1129.

Gelzer, A.R.M., Otani, N.F., Koller, M.L., Enyeart, M.W., Moise, N.S. & Gilmour, R.F. (2010) Dynamically-induced spatial dispersion of repolarization and the development of VF in an animal model of sudden death. *Computers in Cardiology, 2009*, 309-312.

Gerull, B., Heuser, A., Wichter, T., Paul, M., Basson, C.T., McDermott, D.A., Lerman, B.B., Markowitz, S.M., Ellinor, P.T. & MacRae, C.A. (2004) Mutations in the desmosomal protein plakophilin-2 are common in arrhythmogenic right ventricular cardiomyopathy. *Nature Genetics*, **36**, 1162-1164.

Gilman, A.G. (1987) G proteins: transducers of receptor-generated signals. *Annual Review of Biochemistry*, **56**, 615-649.

Gilmour, R.F. & Chialvo, D.R. (1999) Electrical restitution, critical mass, and the riddle of fibrillation. *Journal of cardiovascular electrophysiology*, **10**, 1087-1089.

Gilmour, R.F.J., Gelzer, A.R. & Otani, N.F. (2007) Cardiac electrical dynamics: maximizing dynamical heterogeneity. *Journal of Electrocardiology*, **40**, S51-5.

Girouard, S.D. & Rosenbaum, D.S. (1996) Unique Properties of Cardiac Action Potentials Recorded with Voltage-Sensitive Dyes. *Journal of cardiovascular electrophysiology*, **7**, 1024-1038.

Gold, M.R., Ip, J.H., Costantini, O., Poole, J.E., McNulty, S., Mark, D.B., Lee, K.L. & Bardy, G.H. (2008) Role of microvolt T-wave alternans in assessment of arrhythmia vulnerability among patients with heart failure and systolic dysfunction: primary results from the T-wave alternans sudden cardiac death in heart failure trial substudy. *Circulation*, **118**, 2022-2028.

Goldreyer, B.N. & Bigger, J.T. (1971) Site of Reentry in Paroxysmal Supraventricular Tachycardia in Man. *Circulation*, **43**, 15-26.

Gomes, J., Finlay, M., Ahmed, A.K., Ciaccio, E.J., Asimaki, A., Saffitz, J.E., Quarta, G., Nobles, M.,

Syrris, P., Chaubey, S., McKenna, W.J., Tinker, A. & Lambiase, P.D. (2012) Electrophysiological abnormalities precede overt structural changes in arrhythmogenic right ventricular cardiomyopathy due to mutations in desmoplakin-A combined murine and human study. *Eur Heart J*, **33**, 1942-1953.

Grant, A.O. (2009) Cardiac ion channels. *Circ Arrhythm Electrophysiol*, **2**, 185-194.

Gray, K.A., Daugherty, L.C., Gordon, S.M., Seal, R.L., Wright, M.W. & Bruford, E.A. (2013) Genenames.org: the HGNC resources in 2013. *Nucleic Acids Research*, **41**, D545-52.

Grimm, M. & Brown, J.H. (2010) Beta-adrenergic receptor signaling in the heart: role of CaMKII. *J Mol Cell Cardiol*, **48**, 322-330.

Grimm, W., Hoffmann, J., Menz, V., Luck, K. & Maisch, B. (1998) Programmed ventricular stimulation for arrhythmia risk prediction in patients with idiopathic dilated cardiomyopathy and nonsustained ventricular tachycardia. *Journal of the American College of Cardiology*, **32**, 739-745.

Halbach, M., Pfannkuche, K., Pillekamp, F., Ziomka, A., Hannes, T., Reppel, M., Hescheler, J. & Muller-Ehmsen, J. (2007) Electrophysiological maturation and integration of murine fetal cardiomyocytes after transplantation. *Circulation Research*, **101**, 484-492.

Halbach, M., Pillekamp, F., Brockmeier, K., Hescheler, J., Muller-Ehmsen, J. & Reppel, M. (2006) Ventricular slices of adult mouse hearts--a new multicellular in vitro model for electrophysiological studies. *Cell Physiol Biochem*, **18**, 1-8.

Hallaq, H., Yang, Z., Viswanathan, P.C., Fukuda, K., Shen, W., Wang, D.W., Wells, K.S., Zhou, J., Yi, J. & Murray, K.T. (2006) Quantitation of protein kinase A-mediated trafficking of cardiac sodium channels in living cells. *Cardiovascular Research*, **72**, 250-261.

Hanson, B., Sutton, P., Elameri, N., Gray, M., Critchley, H., Gill, J.S. & Taggart, P. (2009) Interaction of activation-repolarization coupling and restitution properties in humans. *Circ Arrhythm Electrophysiol*, **2**, 162-170.

Haqqani, H.M., Tschabrunn, C.M., Betensky, B.P., Lavi, N., Tzou, W.S., Zado, E.S. & Marchlinski, F.E. (2012) Layered Activation of Epicardial Scar in Arrhythmogenic Right Ventricular Dysplasia:

Possible Substrate for Confined Epicardial Circuits. *Circ Arrhythm Electrophysiol*,

Haws, C.W. & Lux, R.L. (1990) Correlation between in vivo transmembrane action potential durations and activation-recovery intervals from electrograms. Effects of interventions that alter repolarization time. *Circulation*, **81**, 281-288.

Hjalmarson, Å., Goldstein, S., Fagerberg, B., Wedel, H., Waagstein, F., Kjekshus, J., Wikstrand, J., El Allaf, D., Vítovec, J. & Aldershvile, J. (2000) Effects of controlled-release metoprolol on total mortality, hospitalizations, and well-being in patients with heart failure. *JAMA: the journal of the American Medical Association*, **283**, 1295-1302.

Huang, J.L., Chiou, C.W., Ting, C.T., Chen, Y.T. & Chen, S.A. (2001) Sudden changes in heart rate variability during the 1999 Taiwan earthquake. *American Journal of Cardiology*, **87**, 245-8, A9.

Imai, K., King, G. & Lau, O. (2009) Zelig: Everyone's statistical software. *R package version*, **3**,

Itzhaki, I., Maizels, L., Huber, I., Zwi-Dantsis, L., Caspi, O., Winterstern, A., Feldman, O., Gepstein, A., Arbel, G., Hammerman, H., Boulos, M. & Gepstein, L. (2011) Modelling the long QT syndrome with induced pluripotent stem cells. *Nature*, **471**, 225-229.

Janse, M.J., Opthof, T. & Kleber, A.G. (1998) Animal models of cardiac arrhythmias. *Cardiovascular Research*, **39**, 165-177.

Jansen, J.A., Noorman, M., Musa, H., Stein, M., de Jong, S., van der Nagel, R., Hund, T.J., Mohler, P.J., Vos, M.A., van Veen, T.A., de Bakker, J.M., Delmar, M. & van Rijen, H.V. (2012) Reduced heterogeneous expression of Cx43 results in decreased Nav1.5 expression and reduced sodium current that accounts for arrhythmia vulnerability in conditional Cx43 knockout mice. *Heart Rhythm*, **9**, 600-607.

Jiang, M., Boulay, G., Spicher, K., Peyton, M.J., Brabet, P., Birnbaumer, L. & Rudolph, U. (1997) Inactivation of the G alpha i2 and G alpha o genes by homologous recombination. *Receptors Channels*, **5**, 187-192.

D'Errico, J. (2010) Surface Fitting using gridfit. *MATLAB Central File Exchange*,

Kaese, S. & Verheule, S. (2012) Cardiac electrophysiology in mice: a matter of size. *Front Physiol*, **3**,

345.

King, J.H., Huang, C.L. & Fraser, J.A. (2013) Determinants of myocardial conduction velocity: implications for arrhythmogenesis. *Front Physiol*, **4**, 154.

Knollmann, B.C., Schober, T., Petersen, A.O., Sirenko, S.G. & Franz, M.R. (2007) Action potential characterization in intact mouse heart: steady-state cycle length dependence and electrical restitution. *Am J Physiol Heart Circ Physiol*, **292**, H614-21.

Kobayashi, Y., Gotoh, M., Mandel, W.J. & Karagueuzian, H.S. (1992) Increased temporo-spatial dispersion of repolarization during double premature stimulation in the intact ventricle. *Pacing Clin Electrophysiol*, **15**, 2194-2199.

Koenker, R. (2009) Quantreg: quantile regression. *R package version*, **4**,

Krantz, D.S., Quigley, J.F. & O'Callahan, M. (2001) Mental stress as a trigger of acute cardiac events: the role of laboratory studies. *Ital Heart J*, **2**, 895-899.

Kruta, V. & Bravený, P. (1963) Rate of restitution and self-regulation of contractility in mammalian heart muscle.

Kuo, C.S. & Surawicz, B. (1976) Ventricular monophasic action potential changes associated with neurogenic T wave abnormalities and isoproterenol administration in dogs. *American Journal of Cardiology*, **38**, 170-177.

Kurokawa, J., Bankston, J.R., Kaihawa, A., Chen, L., Furukawa, T. & Kass, R.S. (2009) KCNE variants reveal a critical role of the beta subunit carboxyl terminus in PKA-dependent regulation of the IKs potassium channel. *Channels*, **3**, 16-24.

Lambiase, P.D., Ahmed, A.K., Ciaccio, E.J., Brugada, R., Lizotte, E., Chaubey, S., Ben-Simon, R., Chow, A.W., Lowe, M.D. & McKenna, W.J. (2009) High-density substrate mapping in Brugada syndrome: combined role of conduction and repolarization heterogeneities in arrhythmogenesis. *Circulation*, **120**, 106-17, 1-4.

Lambiase, P.D., Rinaldi, A., Hauck, J., Mobb, M., Elliott, D., Mohammad, S., Gill, J.S. & Bucknall, C.A. (2004) Non-contact left ventricular endocardial mapping in cardiac resynchronisation therapy.

Heart, **90**, 44-51.

Lampert, R. (2010) Anger and ventricular arrhythmias. *Current Opinion in Cardiology*, **25**, 46-52.

Lampert, R., Jain, D., Burg, M.M., Batsford, W.P. & McPherson, C.A. (2000) Destabilizing effects of mental stress on ventricular arrhythmias in patients with implantable cardioverter-defibrillators. *Circulation*, **101**, 158-164.

Lampert, R., Rosenfeld, L., Batsford, W., Lee, F. & McPherson, C. (1994) Circadian variation of sustained ventricular tachycardia in patients with coronary artery disease and implantable cardioverter-defibrillators. *Circulation*, **90**, 241-247.

Lampert, R., Shusterman, V., Burg, M., McPherson, C., Batsford, W., Goldberg, A. & Soufer, R. (2009) Anger-induced T-wave alternans predicts future ventricular arrhythmias in patients with implantable cardioverter-defibrillators. *Journal of the American College of Cardiology*, **53**, 774-778.

Lampert, R., Shusterman, V., Burg, M.M., Lee, F.A., Earley, C., Goldberg, A., McPherson, C.A., Batsford, W.P. & Soufer, R. (2005) Effects of psychologic stress on repolarization and relationship to autonomic and hemodynamic factors. *J Cardiovasc Electrophysiol*, **16**, 372-377.

Lampert, R., Soufer, R., McPherson, C.A., Batsford, W.P., Tirado, S., Earley, C., Goldberg, A. & Shusterman, V. (2007) Implantable cardioverter-defibrillator shocks increase T-wave alternans. *J Cardiovasc Electrophysiol*, **18**, 512-517.

Lampert, R., Joska, T., Burg, M.M., Batsford, W.P., McPherson, C.A. & Jain, D. (2002) Emotional and physical precipitants of ventricular arrhythmia. *Circulation*, **106**, 1800-1805.

Langendorff, O. (1895) Investigations on alive mammalian heart. *Pfl√°gers Arch*, **61**, 291-332.

Laurita, K.R., Girouard, S.D. & Rosenbaum, D.S. (1996) Modulation of ventricular repolarization by a premature stimulus. Role of epicardial dispersion of repolarization kinetics demonstrated by optical mapping of the intact guinea pig heart. *Circulation Research*, **79**, 493-503.

Lee, P., Klos, M., Bollensdorff, C., Hou, L., Ewart, P., Kamp, T.J., Zhang, J., Bizy, A., Guerrero-Serna, G. & Kohl, P. (2012) Simultaneous Voltage and Calcium Mapping of Genetically Purified

Human Induced Pluripotent Stem Cell–Derived Cardiac Myocyte Monolayers. *Circulation Research*, **110**, 1556-1563.

Leor, J., Poole, W.K. & Kloner, R.A. (1996) Sudden cardiac death triggered by an earthquake. *New England Journal of Medicine*, **334**, 413-419.

Lester, D. (2009) Voodoo Death. *OMEGA--Journal of Death and Dying*, **59**, 1-18.

Liu, N., Colombi, B., Memmi, M., Zissimopoulos, S., Rizzi, N., Negri, S., Imbriani, M., Napolitano, C., Lai, F.A. & Priori, S.G. (2006) Arrhythmogenesis in catecholaminergic polymorphic ventricular tachycardia: insights from a RyR2 R4496C knock-in mouse model. *Circulation Research*, **99**, 292-298.

Lombardi, R., da Graca Cabreira-Hansen, M., Bell, A., Fromm, R.R., Willerson, J.T. & Marian, A.J. (2011) Nuclear plakoglobin is essential for differentiation of cardiac progenitor cells to adipocytes in arrhythmogenic right ventricular cardiomyopathy. *Circulation Research*, **109**, 1342-1353.

Lown, B. & DeSilva, R.A. (1978) Roles of psychologic stress and autonomic nervous system changes in provocation of ventricular premature complexes. *American Journal of Cardiology*, **41**, 979-985.

Lown, B., Verrier, R.L. & Rabinowitz, S.H. (1977) Neural and psychologic mechanisms and the problem of sudden cardiac death. *American Journal of Cardiology*, **39**, 890-902.

Ma, D., Wei, H., Lu, J., Ho, S., Zhang, G., Sun, X., Oh, Y., Tan, S.H., Ng, M.L., Shim, W., Wong, P. & Liew, R. (2013) Generation of patient-specific induced pluripotent stem cell-derived cardiomyocytes as a cellular model of arrhythmogenic right ventricular cardiomyopathy. *Eur Heart J*, **34**, 1122-1133.

Mantravadi, R., Gabris, B., Liu, T., Choi, B.R., de Groat, W.C., Ng, G.A. & Salama, G. (2007) Autonomic nerve stimulation reverses ventricular repolarization sequence in rabbit hearts. *Circulation Research*, **100**, e72-80.

Marcus, F.I., McKenna, W.J., Sherrill, D., Basso, C., Bauce, B., Bluemke, D.A., Calkins, H., Corrado, D., Cox, M.G., Daubert, J.P., Fontaine, G., Gear, K., Hauer, R., Nava, A., Picard, M.H., Protonotarios, N., Saffitz, J.E., Sanborn, D.M., Steinberg, J.S., Tandri, H., Thiene, G., Towbin,

J.A., Tsatsopoulou, A., Wichter, T. & Zareba, W. (2010) Diagnosis of arrhythmogenic right ventricular cardiomyopathy/dysplasia: proposed modification of the task force criteria. *Circulation*, **121**, 1533-1541.

Finlay, M.C., A Ahmed, J Barr-Amato, G Quarta, L Xu, R Ben-Simon, O Segal, M Lowe, W McKenna, AChow, & Lambiase, P.D. (2012) Dynamic Changes In Activation And Repolarisation Distinguish Early Arrhythmic Right Ventricular Cardiomyopathy From Benign Outflow Tract Tachycardia: Insights From Non-contact Mapping And Computational Analysis. *Heart rhythm : the official journal of the Heart Rhythm Society Heart rhythm : the official journal of the Heart Rhythm Society Heart Rhythm*, **9**, S292-S328.

McKoy, G., Protonotarios, N., Crosby, A., Tsatsopoulou, A., Anastasakis, A., Coonar, A., Norman, M., Baboonian, C., Jeffery, S. & McKenna, W.J. (2000) Identification of a deletion in plakoglobin in arrhythmogenic right ventricular cardiomyopathy with palmoplantar keratoderma and woolly hair (Naxos disease). *Lancet*, **355**, 2119-2124.

Meisel, S.R., Dayan, K.I., Pauzner, H., Chetboun, I., Arbel, Y., David, D. & Kutz, I. (1991) Effect of Iraqi missile war on incidence of acute myocardial infarction and sudden death in Israeli civilians. *The Lancet*, **338**, 660-661.

Merner, N.D., Hodgkinson, K.A., Haywood, A.F., Connors, S., French, V.M., Drenckhahn, J.D., Kupprion, C., Ramadanova, K., Thierfelder, L., McKenna, W., Gallagher, B., Morris-Larkin, L., Bassett, A.S., Parfrey, P.S. & Young, T.L. (2008) Arrhythmogenic right ventricular cardiomyopathy type 5 is a fully penetrant, lethal arrhythmic disorder caused by a missense mutation in the TMEM43 gene. *American Journal of Human Genetics*, **82**, 809-821.

Mines, G.R. (1914) On circulating excitations in heart muscles and their possible relation to tachycardia and fibrillation. *Transactions of the Royal Society of Canada*, **4**, 43-52.

Mironov, S., Jalife, J. & Tolkacheva, E.G. (2008) Role of conduction velocity restitution and short-term memory in the development of action potential duration alternans in isolated rabbit hearts. *Circulation*, **118**, 17-25.

Moore, E.N., Preston, J.B. & Moe, G.K. (1965) Durations of Transmembrane Potentials and Functional Refractory Periods of Canine False Tendon and Ventricular Myocardium: Comparisons in

Single Fibers. *Circulation Research*, **17**, 259-273.

Moore, J.W.r., Barrington, W., Bazaz, R., Jain, S., Nemec, J., Ngwu, O., Schwartzman, D., Shalaby, A. & Saba, S. (2009) Complications of replacing implantable devices in response to advisories: a single center experience. *International Journal of Cardiology*, **134**, 42-46.

Morady, F., Kadish, A.H., DiCarlo, L., Kou, W.H., Winston, S., deBuitlier, M., Calkins, H., Rosenheck, S. & Sousa, J. (1990) Long-term results of catheter ablation of idiopathic right ventricular tachycardia. *Circulation*, **82**, 2093-2099.

Morita, H., Zipes, D.P., Fukushima-Kusano, K., Nagase, S., Nakamura, K., Morita, S.T., Ohe, T. & Wu, J. (2008) Repolarization heterogeneity in the right ventricular outflow tract: correlation with ventricular arrhythmias in Brugada patients and in an in vitro canine Brugada model. *Heart Rhythm*, **5**, 725-733.

Moss, A.J. (1989) Preliminary report: effect of encainide and flecainide on mortality in a randomized trial of arrhythmia suppression after myocardial infarction. The Cardiac Arrhythmia Suppression Trial (CAST) Investigators. *New England Journal of Medicine*, **321**, 406-412.

Moss, A.J., Hall, W.J., Cannom, D.S., Daubert, J.P., Higgins, S.L., Klein, H., Levine, J.H., Saksena, S., Waldo, A.L., Wilber, D., Brown, M.W. & Heo, M. (1996) Improved survival with an implanted defibrillator in patients with coronary disease at high risk for ventricular arrhythmia. Multicenter Automatic Defibrillator Implantation Trial Investigators. *New England Journal of Medicine*, **335**, 1933-1940.

Moss, A.J., Zareba, W., Hall, W.J., Klein, H., Wilber, D.J., Cannom, D.S., Daubert, J.P., Higgins, S.L., Brown, M.W. & Andrews, M.L. (2002) Prophylactic implantation of a defibrillator in patients with myocardial infarction and reduced ejection fraction. *New England Journal of Medicine*, **346**, 877-883.

Myles, R.C., Bernus, O., Burton, F.L., Cobbe, S.M. & Smith, G.L. (2010) Effect of activation sequence on transmural patterns of repolarization and action potential duration in rabbit ventricular myocardium. *Am J Physiol Heart Circ Physiol*, **299**, H1812-22.

Myles, R.C., Burton, F.L., Cobbe, S.M. & Smith, G.L. (2011) Alternans of action potential duration and

amplitude in rabbits with left ventricular dysfunction following myocardial infarction. *J Mol Cell Cardiol*, **50**, 510-521.

Myles, R.C., Wang, L., Kang, C., Bers, D.M. & Ripplinger, C.M. (2012) Local beta-adrenergic stimulation overcomes source-sink mismatch to generate focal arrhythmia. *Circulation Research*, **110**, 1454-1464.

Nam, G.B., Ko, K.H., Kim, J., Park, K.M., Rhee, K.S., Choi, K.J., Kim, Y.H. & Antzelevitch, C. (2010) Mode of onset of ventricular fibrillation in patients with early repolarization pattern vs. Brugada syndrome. *Eur Heart J*, **31**, 330-339.

Nattel, S., Maguy, A., Le Bouter, S. & Yeh, Y.H. (2007) Arrhythmogenic ion-channel remodeling in the heart: heart failure, myocardial infarction, and atrial fibrillation. *Physiological Reviews*, **87**, 425-456.

Nerbonne, J.M. (2004) Studying Cardiac Arrhythmias in the Mouse,ÄîA Reasonable Model for Probing Mechanisms? *Trends in Cardiovascular Medicine*, **14**, 83-93.

Ng, G.A., Brack, K.E., Patel, V.H. & Coote, J.H. (2007) Autonomic modulation of electrical restitution, alternans and ventricular fibrillation initiation in the isolated heart. *Cardiovascular Research*, **73**, 750-760.

Nicolson, W.B., McCann, G.P., Brown, P.D., Sandilands, A.J., Stafford, P.J., Schlindwein, F.S., Samani, N.J. & Ng, G.A. (2012) A novel surface electrocardiogram-based marker of ventricular arrhythmia risk in patients with ischemic cardiomyopathy. *J Am Heart Assoc*, **1**, e001552.

Noble, D. (1962) A modification of the Hodgkin--Huxley equations applicable to Purkinje fibre action and pace-maker potentials. *Journal of Physiology*, **160**, 317-352.

Noble, D. (2007) From the Hodgkin-Huxley axon to the virtual heart. *Journal of Physiology*, **580**, 15-22.

Nolasco, J.B. & Dahlen, R.W. (1968) A graphic method for the study of alternation in cardiac action potentials. *Journal of applied physiology*, **25**, 191-196.

Norgett, E.E., Hatsell, S.J., Carvajal-Huerta, L., Cabezas, J.C., Common, J., Purkis, P.E., Whittock, N., Leigh, I.M., Stevens, H.P. & Kelsell, D.P. (2000) Recessive mutation in desmoplakin disrupts

desmoplakin-intermediate filament interactions and causes dilated cardiomyopathy, woolly hair and keratoderma. *Human Molecular Genetics*, **9**, 2761-2766.

Norman, M., Simpson, M., Mogensen, J., Shaw, A., Hughes, S., Syrris, P., Sen-Chowdhry, S., Rowland, E., Crosby, A. & McKenna, W.J. (2005) Novel mutation in desmoplakin causes arrhythmogenic left ventricular cardiomyopathy. *Circulation*, **112**, 636-642.

O'Hara, T., Virag, L., Varro, A. & Rudy, Y. (2011) Simulation of the undiseased human cardiac ventricular action potential: model formulation and experimental validation. *PLoS Computational Biology*, **7**, e1002061.

Osadchii, O.E., Larsen, A.P. & Olesen, S.P. (2010) Predictive value of electrical restitution in hypokalemia-induced ventricular arrhythmogenicity. *Am J Physiol Heart Circ Physiol*, **298**, H210-20.

Otani, N.F. (2007) Theory of action potential wave block at-a-distance in the heart. *Physical Review E*, **75**, 21910.

Pandit, S.V. (2010) T-wave alternans testing: can it predict arrhythmogenesis? *Heart Rhythm*, **7**, 769-770.

Papadakis, M., Sharma, S., Cox, S., Sheppard, M.N., Panoulas, V.F. & Behr, E.R. (2009) The magnitude of sudden cardiac death in the young: a death certificate-based review in England and Wales. *Europace*, **11**, 1353-1358.

Papadatos, G.A., Wallerstein, P.M., Head, C.E., Ratcliff, R., Brady, P.A., Benndorf, K., Saumarez, R.C., Trezise, A.E., Huang, C.L., Vandenberg, J.I., Colledge, W.H. & Grace, A.A. (2002) Slowed conduction and ventricular tachycardia after targeted disruption of the cardiac sodium channel gene Scn5a. *Proceedings of the National Academy of Sciences of the United States of America*, **99**, 6210-6215.

Parker, G.W., Michael, L.H., Hartley, C.J., Skinner, J.E. & Entman, M.L. (1990) Central beta-adrenergic mechanisms may modulate ischemic ventricular fibrillation in pigs. *Circulation Research*, **66**, 259-270.

Parker, G.W., Michael, L.H. & Entman, M.L. (1987) An animal model to examine the response to environmental stress as a factor in sudden cardiac death. *The American journal of cardiology*,

60, J9-J14.

Paz, O., Zhou, X., Gillberg, J., Tseng, H.J., Gang, E. & Swerdlow, C. (2006) Detection of T-wave alternans using an implantable cardioverter-defibrillator. *Heart Rhythm*, **3**, 791-797.

Pilichou, K., Nava, A., Basso, C., Beffagna, G., Bauce, B., Lorenzon, A., Frigo, G., Vettori, A., Valente, M., Towbin, J., Thiene, G., Danieli, G.A. & Rampazzo, A. (2006) Mutations in desmoglein-2 gene are associated with arrhythmogenic right ventricular cardiomyopathy. *Circulation*, **113**, 1171-1179.

Pillekamp, F., Reppel, M., Dinkelacker, V., Duan, Y., Jazmati, N., Bloch, W., Brockmeier, K., Hescheler, J., Fleischmann, B.K. & Koehling, R. (2005) Establishment and characterization of a mouse embryonic heart slice preparation. *Cell Physiol Biochem*, **16**, 127-132.

Pinheiro, J., Bates, D., DebRoy, S. & Sarkar, D. (2009) the R Core team (2009) nlme: Linear and Nonlinear Mixed Effects Models. R package version 3.1-96. *R Foundation for Statistical Computing, Vienna, Austria*,

Poelzing, S. & Rosenbaum, D.S. (2009) The modulated dispersion hypothesis confirmed in humans. *Circ Arrhythm Electrophysiol*, **2**, 100-101.

Pogwizd, S.M., Schlotthauer, K., Li, L., Yuan, W. & Bers, D.M. (2001) Arrhythmogenesis and Contractile Dysfunction in Heart Failure : Roles of Sodium-Calcium Exchange, Inward Rectifier Potassium Current, and Residual Â -Adrenergic Responsiveness. *Circulation Research*, **88**, 1159-1167.

Pond, A.L. & Nerbonne, J.M. (2001) ERG proteins and functional cardiac I(Kr) channels in rat, mouse, and human heart. *Trends Cardiovasc Med*, **11**, 286-294.

Potse, M., Coronel, R., Opthof, T. & Vinet, A. (2007) The positive T wave. *Anadolu Kardiyol Derg*, **7 Suppl 1**, 164-167.

Potse, M., Vinet, A., Opthof, T. & Coronel, R. (2009) Validation of a simple model for the morphology of the T wave in unipolar electrograms. *Am J Physiol Heart Circ Physiol*, **297**, H792-801.

Qu, Z., Garfinkel, A., Chen, P.S. & Weiss, J.N. (2000) Mechanisms of discordant alternans and induction

of reentry in simulated cardiac tissue. *Circulation*, **102**, 1664-1670.

Qu, Z., Kil, J., Xie, F., Garfinkel, A. & Weiss, J.N. (2000) Scroll wave dynamics in a three-dimensional cardiac tissue model: roles of restitution, thickness, and fiber rotation. *Biophysical Journal*, **78**, 2761-2775.

Quarta, G., Ward, D., Tome Esteban, M.T., Pantazis, A., Elliott, P.M., Volpe, M., Autore, C. & McKenna, W.J. (2010) Dynamic electrocardiographic changes in patients with arrhythmogenic right ventricular cardiomyopathy. *Heart*, **96**, 516-522.

Team, R.C.D. (2010) R: A language and environment for statistical computing. *R Foundation for Statistical Computing Vienna Austria*,

Rampazzo, A., Nava, A., Malacrida, S., Beffagna, G., Bauce, B., Rossi, V., Zimbello, R., Simionati, B., Basso, C., Thiene, G., Towbin, J.A. & Danieli, G.A. (2002) Mutation in human desmoplakin domain binding to plakoglobin causes a dominant form of arrhythmogenic right ventricular cardiomyopathy. *American Journal of Human Genetics*, **71**, 1200-1206.

Rashba, E.J., Cooklin, M., MacMurdy, K., Kavesh, N., Kirk, M., Sarang, S., Peters, R.W., Shorofsky, S.R. & Gold, M.R. (2002) Effects of selective autonomic blockade on T-wave alternans in humans. *Circulation*, **105**, 837-842.

Remme, C.A., Verkerk, A.O., Nuyens, D., van Ginneken, A.C., van Brunschot, S., Belterman, C.N., Wilders, R., van Roon, M.A., Tan, H.L., Wilde, A.A., Carmeliet, P., de Bakker, J.M., Veldkamp, M.W. & Bezzina, C.R. (2006) Overlap syndrome of cardiac sodium channel disease in mice carrying the equivalent mutation of human SCN5A-1795insD. *Circulation*, **114**, 2584-2594.

Rizzo, S., Lodder, E.M., Verkerk, A.O., Wolswinkel, R., Beekman, L., Pilichou, K., Basso, C., Remme, C.A., Thiene, G. & Bezzina, C.R. (2012) Intercalated disc abnormalities, reduced Na+ current density, and conduction slowing in desmoglein-2 mutant mice prior to cardiomyopathic changes. *Cardiovascular Research*, **95**, 409-418.

Rhett, J.M., Ongstad, E.L., Jourdan, J. & Gourdie, R.G. (2012) Cx43 associates with Na(v)1.5 in the cardiomyocyte perinexus. *Journal of Membrane Biology*, **245**, 411-422.

Rudolph, U., Spicher, K. & Birnbaumer, L. (1996) Adenylyl cyclase inhibition and altered G protein

subunit expression and ADP-ribosylation patterns in tissues and cells from Gi2 alpha-/-mice. *Proceedings of the National Academy of Sciences of the United States of America*, **93**, 3209-3214.

Rudy, Y. (2009) Cardiac repolarization: insights from mathematical modeling and electrocardiographic imaging (ECGI). *Heart Rhythm*, **6**, S49-55.

Sabir, I.N., Killeen, M.J., Grace, A.A. & Huang, C.L.H. (2008) Ventricular arrhythmogenesis: insights from murine models. *Progress in biophysics and molecular biology*, **98**, 208-218.

Saffitz, J.E., Asimaki, A. & Huang, H. (2010) Arrhythmogenic right ventricular cardiomyopathy: new insights into mechanisms of disease. *Cardiovasc Pathol*, **19**, 166-170.

Sakhuja, R., Shah, A.J., Keebler, M. & Thakur, R.K. (2009) Atrial fibrillation in patients with implantable defibrillators. *Cardiology Clinics*, **27**, 151-61, ix-x.

Samuels, M.A. (2007) 'Voodoo' death revisited: the modern lessons of neurocardiology. *Cleve Clin J Med*, **74 Suppl 1**, S8-16.

Santangeli, P., Pieroni, M., Dello Russo, A., Casella, M., Pelargonio, G., Macchione, A., Camporeale, A., Smaldone, C., Bartoletti, S., Di Biase, L., Bellocci, F. & Natale, A. (2010) Noninvasive diagnosis of electroanatomic abnormalities in arrhythmogenic right ventricular cardiomyopathy. *Circ Arrhythm Electrophysiol*, **3**, 632-638.

Sato, P.Y., Musa, H., Coombs, W., Guerrero-Serna, G., Patino, G.A., Taffet, S.M., Isom, L.L. & Delmar, M. (2009) Loss of plakophilin-2 expression leads to decreased sodium current and slower conduction velocity in cultured cardiac myocytes. *Circulation Research*, **105**, 523-526.

Saumarez, R.C. (2009) Risk assessment in hypertrophic cardiomyopathy. *Heart*, **95**, 421; author reply 421.

Saumarez, R.C., Chojnowska, L., Derksen, R., Pytkowski, M., Sterlinski, M., Huang, C.L., Sadoul, N., Hauer, R.N., Ruzyllo, W. & Grace, A.A. (2003) Sudden death in noncoronary heart disease is associated with delayed paced ventricular activation. *Circulation*, **107**, 2595-2600.

Saumarez, R.C. & Grace, A.A. (2000) Paced ventricular electrogram fractionation and sudden death in

hypertrophic cardiomyopathy and other non-coronary heart diseases. *Cardiovascular Research*, **47**, 11-22.

Saumarez, R.C., Heald, S., Gill, J., Slade, A.K., de Belder, M., Walczak, F., Rowland, E., Ward, D.E. & Camm, A.J. (1995) Primary ventricular fibrillation is associated with increased paced right ventricular electrogram fractionation. *Circulation*, **92**, 2565-2571.

Saumarez, R.C., Pytkowski, M., Sterlinski, M., Bourke, J.P., Clague, J.R., Cobbe, S.M., Connelly, D.T., Griffith, M.J., McKeown, P.P., McLeod, K., Morgan, J.M., Sadoul, N., Chojnowska, L., Huang, C.L. & Grace, A.A. (2008) Paced ventricular electrogram fractionation predicts sudden cardiac death in hypertrophic cardiomyopathy. *Eur Heart J*, **29**, 1653-1661.

Saumarez, R.C., Slade, A.K., Grace, A.A., Sadoul, N., Camm, A.J. & McKenna, W.J. (1995) The significance of paced electrogram fractionation in hypertrophic cardiomyopathy. A prospective study. *Circulation*, **91**, 2762-2768.

Scherlag, B.J., LAU, S.U.N.H., HELFANT, R.H., BERKOWITZ, W.D., STEIN, E. & DAMATO, A.N. (1969) Catheter technique for recording His bundle activity in man. *Circulation*, **39**, 13-18.

Schilling, R.J., Peters, N.S. & Davies, D.W. (1998) Simultaneous endocardial mapping in the human left ventricle using a noncontact catheter: comparison of contact and reconstructed electrograms during sinus rhythm. *Circulation*, **98**, 887-898.

Schwartz, P.J. & Crotti, L. (2011) QTc behavior during exercise and genetic testing for the long-QT syndrome. *Circulation*, **124**, 2181-2184.

Selvaraj, R.J., Picton, P., Nanthakumar, K. & Chauhan, V.S. (2007) Steeper restitution slopes across right ventricular endocardium in patients with cardiomyopathy at high risk of ventricular arrhythmias. *Am J Physiol Heart Circ Physiol*, **292**, H1262-8.

Sen-Chowdhry, S., Syrris, P., Ward, D., Asimaki, A., Sevdalis, E. & McKenna, W.J. (2007) Clinical and genetic characterization of families with arrhythmogenic right ventricular dysplasia/cardiomyopathy provides novel insights into patterns of disease expression. *Circulation*, **115**, 1710-1720.

Shimizu, S., Kobayashi, Y., Miyauchi, Y., Ohmura, K., Atarashi, H. & Takano, T. (2000) Temporal and

spatial dispersion of repolarization during premature impulse propagation in human intact ventricular muscle: comparison between single vs double premature stimulation. *Europace*, **2**, 201-206.

Shuldiner, A.R. (1996) Transgenic animals. *New England Journal of Medicine*, **334**, 653-655.

Silva, J. & Rudy, Y. (2005) Subunit interaction determines IKs participation in cardiac repolarization and repolarization reserve. *Circulation*, **112**, 1384-1391.

Siso-Nadal, F., Otani, N.F., Gilmour Jr, R.F. & Fox, J.J. (2008) Boundary-induced reentry in homogeneous excitable tissue. *Physical Review E*, **78**, 31925.

Stein, M., van, V.T.A., Hauer, R.N., de, B.J.M. & van, R.H.V. (2011) A 50% reduction of excitability but not of intercellular coupling affects conduction velocity restitution and activation delay in the mouse heart. *PLoS ONE*, **6**, e20310.

Steinhaus, B.M. (1989) Estimating cardiac transmembrane activation and recovery times from unipolar and bipolar extracellular electrograms: a simulation study. *Circulation Research*, **64**, 449-462.

Stopper, M., Joska, T., Burg, M.M., Batsford, W.P., McPherson, C.A., Jain, D. & Lampert, R. (2007) Electrophysiologic characteristics of anger-triggered arrhythmias. *Heart Rhythm*, **4**, 268-273.

Sy, R.W., van der Werf, C., Chattha, I.S., Chockalingam, P., Adler, A., Healey, J.S., Perrin, M., Gollob, M.H., Skanes, A.C., Yee, R., Gula, L.J., Leong-Sit, P., Viskin, S., Klein, G.J., Wilde, A.A. & Krahn, A.D. (2011) Derivation and validation of a simple exercise-based algorithm for prediction of genetic testing in relatives of LQTS probands. *Circulation*, **124**, 2187-2194.

Syrris, P., Ward, D., Asimaki, A., Evans, A., Sen-Chowdhry, S., Hughes, S.E. & McKenna, W.J. (2007) Desmoglein-2 mutations in arrhythmogenic right ventricular cardiomyopathy: a genotype-phenotype characterization of familial disease. *Eur Heart J*, **28**, 581-588.

Syrris, P., Ward, D., Asimaki, A., Sen-Chowdhry, S., Ebrahim, H.Y., Evans, A., Hitomi, N., Norman, M., Pantazis, A., Shaw, A.L., Elliott, P.M. & McKenna, W.J. (2006) Clinical expression of plakophilin-2 mutations in familial arrhythmogenic right ventricular cardiomyopathy. *Circulation*, **113**, 356-364.

Syrris, P., Ward, D., Evans, A., Asimaki, A., Gandjbakhch, E., Sen-Chowdhry, S. & McKenna, W.J. (2006) Arrhythmogenic right ventricular dysplasia/cardiomyopathy associated with mutations in the desmosomal gene desmocollin-2. *American Journal of Human Genetics*, **79**, 978-984.

Taggart, P., Batchvarov, V.N., Sutton, P., Young, G., Young, S. & Patterson, D. (2009) Repolarization changes induced by mental stress in normal subjects and patients with coronary artery disease: effect of nitroglycerine. *Psychosomatic Medicine*, **71**, 23-29.

Taggart, P., Sutton, P., Chalabi, Z., Boyett, M.R., Simon, R., Elliott, D. & Gill, J.S. (2003) Effect of adrenergic stimulation on action potential duration restitution in humans. *Circulation*, **107**, 285-289.

Tandri, H., Asimaki, A., Abraham, T., Dalal, D., Tops, L., Jain, R., Saffitz, J.E., Judge, D.P., Russell, S.D., Halushka, M., Bluemke, D.A., Kass, D.A. & Calkins, H. (2009) Prolonged RV endocardial activation duration: a novel marker of arrhythmogenic right ventricular dysplasia/cardiomyopathy. *Heart Rhythm*, **6**, 769-775.

Taylor, M., Graw, S., Sinagra, G., Barnes, C., Slavov, D., Brun, F., Pinamonti, B., Salcedo, E.E., Sauer, W., Pyxaras, S., Anderson, B., Simon, B., Bogomolovas, J., Labeit, S., Granzier, H. & Mestroni, L. (2011) Genetic Variation in Titin in Arrhythmogenic Right Ventricular Cardiomyopathy-Overlap Syndromes. *Circulation*,

ten Tusscher, K.H., Mourad, A., Nash, M.P., Clayton, R.H., Bradley, C.P., Paterson, D.J., Hren, R., Hayward, M., Panfilov, A.V. & Taggart, P. (2009) Organization of ventricular fibrillation in the human heart: experiments and models. *Exp Physiol*, **94**, 553-562.

ten Tusscher, K.H. & Panfilov, A.V. (2006) Alternans and spiral breakup in a human ventricular tissue model. *Am J Physiol Heart Circ Physiol*, **291**, H1088-100.

investigators, T.A.v.I.D.A.V.I.D.) (1997) A comparison of antiarrhythmic-drug therapy with implantable defibrillators in patients resuscitated from near-fatal ventricular arrhythmias. The Antiarrhythmics versus Implantable Defibrillators (AVID) Investigators. *New England Journal of Medicine*, **337**, 1576-1583.

Therneau, T.M., Atkinson, B. & Ripley, B. (2010) Rpart: recursive partitioning. *R package version*, **3**, 1-

46.

Thiene, G., Nava, A., Corrado, D., Rossi, L. & Pennelli, N. (1988) Right ventricular cardiomyopathy and sudden death in young people. *New England Journal of Medicine*, **318**, 129-133.

Thiene, G., Nava, A., Corrado, D., Rossi, L. & Pennelli, N. (1988) Right ventricular cardiomyopathy and sudden death in young people. *New England Journal of Medicine*, **318**, 129-133.

Tiso, N., Stephan, D.A., Nava, A., Bagattin, A., Devaney, J.M., Stanchi, F., Larderet, G., Brahmbhatt, B., Brown, K., Bauce, B., Muriago, M., Basso, C., Thiene, G., Danieli, G.A. & Rampazzo, A. (2001) Identification of mutations in the cardiac ryanodine receptor gene in families affected with arrhythmogenic right ventricular cardiomyopathy type 2 (ARVD2). *Human Molecular Genetics*, **10**, 189-194.

Tolosana, J.M., Berne, P., Mont, L., Heras, M., Berruezo, A., Monteagudo, J., Tamborero, D., Benito, B. & Brugada, J. (2009) Preparation for pacemaker or implantable cardiac defibrillator implants in patients with high risk of thrombo-embolic events: oral anticoagulation or bridging with intravenous heparin? A prospective randomized trial. *Eur Heart J*, **30**, 1880-1884.

Toyoshima, H., Lux, R.L., Wyatt, R.F., Burgess, M. & Abildskov, J.A. (1981) Sequences of early and late phases of repolarization on dog ventricular epicardium. *Journal of Electrocardiology*, **14**, 143-152.

Trichopoulos, D., Katsouyanni, K., Zavitsanos, X., Tzonou, A. & Dalla-Vorgia, P. (1983) Psychological stress and fatal heart attack: the Athens (1981) earthquake natural experiment. *Lancet*, **1**, 441-444.

Tsai, C.F., Chen, S.A., Tai, C.T., Chiang, C.E., Lee, S.H., Wen, Z.C., Huang, J.L., Ding, Y.A. & Chang, M.S. (1997) Idiopathic monomorphic ventricular tachycardia: clinical outcome, electrophysiologic characteristics and long-term results of catheter ablation. *International Journal of Cardiology*, **62**, 143-150.

van der Avoort, C.J., Filion, K.B., Dendukuri, N. & Brophy, J.M. (2009) Microvolt T-wave alternans as a predictor of mortality and severe arrhythmias in patients with left-ventricular dysfunction: a systematic review and meta-analysis. *BMC Cardiovasc Disord*, **9**, 5.

van der Heyden, M.A., Wijnhoven, T.J. & Opthof, T. (2005) Molecular aspects of adrenergic modulation of cardiac L-type Ca2+ channels. *Cardiovascular Research*, **65**, 28-39.

van der Zwaag, P.A., Jongbloed, J.D., van den Berg, M.P., van der Smagt, J.J., Jongbloed, R., Bikker, H., Hofstra, R.M. & van Tintelen, J.P. (2009) A genetic variants database for arrhythmogenic right ventricular dysplasia/cardiomyopathy. *Hum Mutat*, **30**, 1278-1283.

van Rijen, H.V., Eckardt, D., Degen, J., Theis, M., Ott, T., Willecke, K., Jongsma, H.J., Opthof, T. & de Bakker, J.M. (2004) Slow conduction and enhanced anisotropy increase the propensity for ventricular tachyarrhythmias in adult mice with induced deletion of connexin43. *Circulation*, **109**, 1048-1055.

van Tintelen, J.P., Van Gelder, I.C., Asimaki, A., Suurmeijer, A.J.H., Wiesfeld, A.C.P., Jongbloed, J.D.H., van, d.W., Arthur, Kuks, J.B.M., van Spaendonck-Zwarts, K.Y., Notermans, N., Boven, L., van den Heuvel, F., Veenstra-Knol, H.E., Saffitz, J.E., Hofstra, R.M.W. & van den Berg, M.P. (2009) Severe cardiac phenotype with right ventricular predominance in a large cohort of patients with a single missense mutation in the DES gene. *Heart Rhythm*, **6**, 1574-1583.

van Rijen, H.V., de Bakker, J.M. & van Veen, T.A. (2005) Hypoxia, electrical uncoupling, and conduction slowing: Role of conduction reserve. *Cardiovascular Research*, **66**, 9-11.

Verrier, R.L., Klingenheben, T., Malik, M., El-Sherif, N., Exner, D.V., Hohnloser, S.H., Ikeda, T., Martinez, J.P., Narayan, S.M., Nieminen, T. & Rosenbaum, D.S. (2011) Microvolt T-wave alternans physiological basis, methods of measurement, and clinical utility--consensus guideline by International Society for Holter and Noninvasive Electrocardiology. *Journal of the American College of Cardiology*, **58**, 1309-1324.

Volders, P.G. (2010) Novel insights into the role of the sympathetic nervous system in cardiac arrhythmogenesis. *Heart Rhythm*, **7**, 1900-1906.

Voridis, E.M., Mallios, K.D. & Papantonis, T.M. (1983) Holter monitoring during 1981 Athens earthquakes. *The Lancet*, **321**, 1281-1282.

Vyas, H., Hejlik, J. & Ackerman, M.J. (2006) Epinephrine QT stress testing in the evaluation of congenital long-QT syndrome: diagnostic accuracy of the paradoxical QT response. *Circulation*,

113, 1385-1392.

Waldo, A.L., Camm, A.J., deRuyter, H., Friedman, P.L., MacNeil, D.J., Pauls, J.F., Pitt, B., Pratt, C.M., Schwartz, P.J. & Veltri, E.P. (1996) Effect of d-sotalol on mortality in patients with left ventricular dysfunction after recent and remote myocardial infarction. The SWORD Investigators. Survival With Oral d-Sotalol. *Lancet*, **348**, 7-12.

Wang, Y., Cuculich, P.S., Zhang, J., Desouza, K.A., Vijayakumar, R., Chen, J., Faddis, M.N., Lindsay, B.D., Smith, T.W. & Rudy, Y. (2011) Noninvasive electroanatomic mapping of human ventricular arrhythmias with electrocardiographic imaging. *Sci Transl Med*, **3**, 98ra84.

Watanabe, H., Chopra, N., Laver, D., Hwang, H.S., Davies, S.S., Roach, D.E., Duff, H.J., Roden, D.M., Wilde, A.A. & Knollmann, B.C. (2009) Flecainide prevents catecholaminergic polymorphic ventricular tachycardia in mice and humans. *Nature Medicine*, **15**, 380-383.

Watanabe, M.A., Fenton, F.H., Evans, S.J., Hastings, H.M. & Karma, A. (2001) Mechanisms for discordant alternans. *J Cardiovasc Electrophysiol*, **12**, 196-206.

Weiss, J.N., Chen, P.S., Qu, Z., Karagueuzian, H.S. & Garfinkel, A. (2000) Ventricular fibrillation: how do we stop the waves from breaking? *Circulation Research*, **87**, 1103-1107.

Weiss, J.N., Chen, P.S., Qu, Z., Karagueuzian, H.S., Lin, S.F. & Garfinkel, A. (2002) Electrical restitution and cardiac fibrillation. *J Cardiovasc Electrophysiol*, **13**, 292-295.

Weiss, J.N., Garfinkel, A., Karagueuzian, H.S., Chen, P.S. & Qu, Z. (2010) Early afterdepolarizations and cardiac arrhythmias. *Heart Rhythm*, **7**, 1891-1899.

Weiss, J.N., Qu, Z., Chen, P.S., Lin, S.F., Karagueuzian, H.S., Hayashi, H., Garfinkel, A. & Karma, A. (2005) The dynamics of cardiac fibrillation. *Circulation*, **112**, 1232-1240.

Wilbert-Lampen, U., Leistner, D., Greven, S., Pohl, T., Sper, S., Völker, C., Güthlin, D., Plasse, A., Knez, A. & Küchenhoff, H. (2008) Cardiovascular events during World Cup soccer. *New England Journal of Medicine*, **358**, 475-483.

Witkowski, F.X., Leon, L.J., Penkoske, P.A., Giles, W.R., Spano, M.L., Ditto, W.L. & Winfree, A.T. (1998) Spatiotemporal evolution of ventricular fibrillation. *Nature*, **392**, 78-82.

Wyatt RF, B.M.J., Evans AK, Lux RL, Abildskov JA, Tsutsumi T. (1981) Estimation of ventricular transmembrane action potential durations and repolarization times from unipolar electrograms (Abstract). *American Journal of Cardiology*, **47**, 488.

Xie, F., Qu, Z., Garfinkel, A. & Weiss, J.N. (2002) Electrical refractory period restitution and spiral wave reentry in simulated cardiac tissue. *Am J Physiol Heart Circ Physiol*, **283**, H448-60.

Xie, F., Qu, Z., Yang, J., Baher, A., Weiss, J.N. & Garfinkel, A. (2004) A simulation study of the effects of cardiac anatomy in ventricular fibrillation. *Journal of Clinical Investigation*, **113**, 686-693.

Xie, Y., Sato, D., Garfinkel, A., Qu, Z. & Weiss, J.N. (2010) So little source, so much sink: requirements for afterdepolarizations to propagate in tissue. *Biophysical Journal*, **99**, 1408-1415.

Yanowitz, F., Preston, J.B. & Abildskov, J.A. (1966) Functional Distribution of Right and Left Stellate Innervation to the Ventricles: Production of neuogenic electrrocardiographs changes by unilateral alteration of sympathetic tone. *Circulation Research*, **18**, 416-428.

Yue, A.M. (2006) Letter regarding article by Koller et al, "Altered dynamics of action potential restitution and alternans in humans with structural heart disease" *Circulation*, **113**, e462; author reply e462.

Yue, A.M. (2007) Significant correlation between monophasic action potential (MAP) durations and activation-recovery intervals (ARIs) determined at the maximum positive slope of the positive T wave (conventional method). *Heart Rhythm*, **4**, 120-1; author reply 121.

Yue, A.M., Betts, T.R., Roberts, P.R. & Morgan, J.M. (2005) Global dynamic coupling of activation and repolarization in the human ventricle. *Circulation*, **112**, 2592-2601.

Yue, A.M., Paisey, J.R., Robinson, S., Betts, T.R., Roberts, P.R. & Morgan, J.M. (2004) Determination of human ventricular repolarization by noncontact mapping: validation with monophasic action potential recordings. *Circulation*, **110**, 1343-1350.

Zaitsev, A.V., Guha, P.K., Sarmast, F., Kolli, A., Berenfeld, O., Pertsov, A.M., de Groot, J.R., Coronel, R. & Jalife, J. (2003) Wavebreak formation during ventricular fibrillation in the isolated, regionally ischemic pig heart. *Circulation Research*, **92**, 546-553.

Zaniboni, M., Riva, I., Cacciani, F. & Groppi, M. (2010) How different two almost identical action potentials can be: a model study on cardiac repolarization. *Math Biosci*, **228**, 56-70.

Zhang, J., Wilson, G.F., Soerens, A.G., Koonce, C.H., Yu, J., Palecek, S.P., Thomson, J.A. & Kamp, T.J. (2009) Functional cardiomyocytes derived from human induced pluripotent stem cells. *Circulation Research*, **104**, e30-41.

Zheng, Z.-J., Croft, J.B., Giles, W.H. & Mensah, G.A. (2001) Sudden Cardiac Death in the United States, 1989 to 1998. *Circulation*, **104**, 2158-2163.

Zipes, D.P., Camm, A.J., Borggrefe, M., Buxton, A.E., Chaitman, B., Fromer, M., Gregoratos, G., Klein, G., Moss, A.J., Myerburg, R.J., Priori, S.G., Quinones, M.A., Roden, D.M., Silka, M.J., Tracy, C., Smith, S.C.J., Jacobs, A.K., Adams, C.D., Antman, E.M., Anderson, J.L., Hunt, S.A., Halperin, J.L., Nishimura, R., Ornato, J.P., Page, R.L., Riegel, B., Blanc, J.J., Budaj, A., Dean, V., Deckers, J.W., Despres, C., Dickstein, K., Lekakis, J., McGregor, K., Metra, M., Morais, J., Osterspey, A., Tamargo, J.L. & Zamorano, J.L. (2006) ACC/AHA/ESC 2006 Guidelines for Management of Patients With Ventricular Arrhythmias and the Prevention of Sudden Cardiac Death: a report of the American College of Cardiology/American Heart Association Task Force and the European Society of Cardiology Committee for Practice Guidelines (writing committee to develop Guidelines for Management of Patients With Ventricular Arrhythmias and the Prevention of Sudden Cardiac Death): developed in collaboration with the European Heart Rhythm Association and the Heart Rhythm Society. *Circulation*, **114**, e385-484.

Zuberi, Z., Birnbaumer, L. & Tinker, A. (2008) The role of inhibitory heterotrimeric G proteins in the control of in vivo heart rate dynamics. *Am J Physiol Regul Integr Comp Physiol*, **295**, R1822-30.

Zuberi, Z., Nobles, M., Sebastian, S., Dyson, A., Lim, S.Y., Breckenridge, R., Birnbaumer, L. & Tinker, A. (2010) Absence of the inhibitory G-protein Galphai2 predisposes to ventricular cardiac arrhythmia. *Circ Arrhythm Electrophysiol*, **3**, 391-400.